Early immunomodulatory program triggered by pro-tolerogenic *Bifidobacterium pseudolongum* drives cardiac transplant outcomes

Authors:

Samuel J Gavzy[1,2], Allison Kensiski[1], Vikas Saxena[1], Ram Lakhan[1], Lauren Hittle[3], Jegan Iyyathurai[1], Long Wu[1], Hima Dhakal[1], Zachariah L Lee[1], Lushen Li[1,1], Young Lee[1], Tianshu Zhang[1,2], Hnin W Lwin[3], Marina W Shirkey[1], Christina M Paluskievicz[1,2], Wenji Piao[1], Emmanuel F Mongodin[3], Bing Ma[3,4,*], Jonathan S Bromberg[1,2,4,*]

[1] University of Maryland School of Medicine, Center for Vascular and Inflammatory Diseases, Baltimore, MD, USA
[2]University of Maryland School of Medicine, Department of Surgery, Baltimore, MD, USA
[3]University of Maryland School of Medicine, Institute for Genome Sciences, Baltimore, MD, USA
[4]Departments of Microbiology and Immunology, Baltimore, MD, USA

*** Corresponding Authors:**
Jonathan S. Bromberg, MD, PhD
jbromberg@som.umaryland.edu

Bing Ma, Ph.D.
bma@som.umaryland.edu

Keywords:
Gut microbiota, Bifidobacterium, Immune suppression, Tregs, transplant tolerance, lymph node remodeling

ABSTRACT

Despite ongoing improvements in regimens to prevent allograft rejection, most cardiac and other types of allografts eventually succumb to chronic vasculopathy, interstitial fibrosis, or endothelial changes, and eventually graft failure. Adaptive immune-mediated damage is considered the primary cause of long-term graft failure, though the events leading to chronic rejection are still poorly understood. Gut microbiota is a known driving force in immune dysfunction. We previously showed that gut microbiota dysbiosis profoundly influences the outcome of vascularized cardiac allografts and subsequently identified biomarker species or “bacterial determinants” associated with these differential graft outcomes (anti-inflammatory *Bifidobacterium pseudolongum* (*Bifido*) and pro-inflammatory *Desulfovibrio desulfuricans* (*Desulfo*)). In this study, we further detailed the multifaceted immunomodulatory properties of the pro-tolerogenic bacterial species over time, using our clinically relevant model of allogenic heart transplantation. This model simultaneously accounts for the immunomodulatory properties of antibiotics and tacrolimus immunosuppression, in addition to bacterial determinants. We observed that *Bifido* induced an early anti-inflammatory phenotype within 7 days, while *Desulfo* resulted in a pro-inflammatory phenotype, defined by alterations in leukocyte distribution and lymph node (LN) structure. These effects were further modulated by inhibition of myeloid cell migration by CCR2 inhibition, supporting the notion that bacterial determinants regulate innate immunity which subsequently influences adaptive immunity. Indeed, *in vitro* results showed that *Bifido* and *Desulfo* acted directly on primary innate immune cells. However, by 40 days after treatment, these two bacterial determinants were associated with mixed effects in their impact on LN architecture and immune cell composition. These dynamic effects suggest a critical role for early bacterial determinant-triggered immunological events such as innate immune cell engagement and LN architectural changes in the subsequent modulation of pro-tolerant versus pro-inflammatory immune responses in organ transplant recipients.

Abbreviations:

Abx – antibiotics
APC – antigen presenting cell
Bifido – *Bifidobacterium pseudolongum*
CR – Cortical ridge
DC – Dendritic cell
Desulfo – *Desulfovibrio desulfuricans*
FRC – Fibroblastic reticular cell
HEV – High endothelial venule
IHC – Immunohistochemistry
ILC – Innate lymphoid cell
LN – Lymph node
MΦ - Macrophage
SBT – Single bacterial strain transfer
Treg – Regulatory T cell

INTRODUCTION

One-year survival rates in solid organ transplantation routinely exceed 90-95%, and many well-characterized variables (such as donor organ quality and recipient comorbidities) determine short-term outcomes. However, most cardiac and other types of allografts eventually succumb to chronic vascular, interstitial, or endothelial impairment beyond the first year, despite the many improvements over the past decades in donor organ preservation, recipient selection, immunosuppressive regimens and monitoring, and infection prophylaxis [1-7]. As a result, the long-term rate of decline of allograft function after transplant remain frustratingly high and has not changed in the past 20 years [5, 8]. Though adaptive immune-mediated damage is generally considered the primary cause of the long-term graft failure, the immunological events leading to chronic rejection are still poorly understood, with a resulting dearth of predictive diagnostic tools and interventions. A significant portion of studies have focused on adaptive immunity to alloantigens, yet chronic rejection is only loosely associated with T and B cell immunity [2, 3, 9], necessitating a novel approach.

Numerous studies have shown that the microbiota is a driving force in immune dysfunction and thus a potential diagnostic or therapeutic target [10-12]. Gut microbiota was shown to trigger pro- or anti-inflammatory signals that regulate local and systemic innate and adaptive immune homeostasis [13]. Cell surface and secreted microbial components such as cell walls, nucleic acids, and metabolites interact with innate and adaptive immunity through receptors on endothelial cells, innate lymphoid cells (ILC), dendritic cells (DC), and lymphocytes [14-16]. Conversely, regulatory T cells (Tregs) influence the microbiota composition and directly recognize the microbiota through antigen-specific receptors [17], while the microbiota directly instructs Foxp3+ Tregs [18, 19]. While changes in the microbiota following organ and bone marrow transplant have been well documented [20-31], these studies, as well as those focused on different diseases, have been largely associative. Together, these observations emphasize the

99 challenges while also providing the rationale for characterizing the microbiota and determining
100 the precise mechanisms it employs to modulate inflammation and immunity, that consequently
101 affect chronic organ damage.

102 Given the myriad therapeutic interventions during the transplant process, defining the
103 specific mechanisms through which the gut microbiota interacts with the host immune system
104 remains elusive. The immune system and microbiota have bidirectional interactions, and in
105 transplantation, immunosuppression alters the immune system, while antibiotic (abx) and
106 immunosuppression administration both alter the microbiota [32-34]. Disruption of the microbiota,
107 for example through abx treatment, has been shown to impact graft survival. Lei et al. [22] showed
108 that abx alone improved graft survival. We observed significant changes in LN stromal structures
109 defined by laminin α4:α5 ratios in mice treated with abx and single bacterial strain transfer (SBT)
110 [35], consistent with other studies showing that abx have long-term effects on microbiota structure
111 [15, 32, 36-38], and immune events initiated by the microbiota persist as changes in LN structure
112 and function [39]. While studies have previously demonstrated associations of bacteria such as
113 *Bifidobacterium* species with anti-inflammatory activities [40, 41], or *Desulfovibrio* species with
114 pro-inflammatory consequences [42, 43], the host pathways leading to these inflammatory
115 outcomes have not been fully characterized, as most studies have focused on the early and local
116 gut host responses to these bacteria, and few studies have investigated distal or systemic and
117 long-term consequences of these bacterial stimuli.

118 We previously demonstrated that both the gut microbiota as a whole or the responsible
119 single species can profoundly influence the outcomes of vascularized cardiac allografts [35]. Oral
120 gavage with a single anti-inflammatory strain of *Bifidobacterium pseudolongum* (*Bifido*) resulted
121 in similarly significant improvement in long-term allograft survival and the prevention of
122 inflammation and fibrosis in the grafts as did gavage with the whole feces of pregnant mice
123 (immune suppression) [35]. On the other hand, the single pro-inflammatory strain of
124 *Desulfovibrio desulfuricans* (*Desulfo*) triggered higher inflammation, similar to using the whole

125 feces of colitic mice (immune inflammation) [35]. These findings implicated these single bacterial
126 strains as major microbial drivers of the overall immunomodulatory effects and allograft outcomes
127 from the pregnant and colic mouse microbiomes. Further characterization of the *Bifido*-induced
128 innate immune response revealed a balanced anti-inflammatory and homeostatic cytokine
129 response from DCs and macrophages (MΦ). *Bifido* also induced changes in LN structure,
130 resulting in an increased ratio of laminin α4:α5 in the cortical ridge (CR), a microdomain structure
131 mechanistically associated with immunologic suppression and tolerance [35]. In comparison,
132 *Desulfo* was associated with inflammation and induced diametrical effects with reduced laminin
133 α4:α5 ratios [35]. These initial observations demonstrated that single bacterial species influence
134 inflammation and fibrosis, and ultimately affect allograft outcomes and alloimmunity, through
135 broad effects on the local, regional, and systemic innate and adaptive immune systems.

136 This study expanded on our initial findings [35] by further dissecting the molecular
137 pathways involved in the interactions among specific immune cell populations, LNs, and selected
138 members of the gut microbiota (i.e., *Bifido* and *Desulfo* species). Using our *in vivo* model
139 combining SBT, allogenic heart transplant, abx and immunosuppression drug treatment, we
140 further detailed the dynamic immunomodulatory properties of pro-tolerogenic and pro-
141 inflammatory bacteria on graft outcome. We specifically investigated the immunologic changes
142 that take place over time in order to understand the onset, progression, and durability of SBT-
143 induced immunomodulatory effects. Similar to our previous findings [44], different strains of *Bifido*
144 exerted unique immunomodulatory effects both *in vivo* and *in vitro.* Furthermore, *Bifido* and
145 *Desulfo* directly acted on innate immune cells *in vitro*. In addition to charactering the individual
146 immunomodulatory properties of abx and tacrolimus immunosuppression, we also showed that
147 *Bifido* induced an anti-inflammatory phenotype while *Desulfo* resulted in a pro-inflammatory
148 phenotype *in vivo*. Most outstandingly and unique to this study, the *Bifido* effect on LN architecture
149 and immune cell composition was most pronounced within 7 days of treatment, with the bacteria-
150 driven effects becoming attenuated over time, so that pro- and anti-inflammatory effects of both

151 bacteria were observed. These dynamic changes highlight the importance of early innate immune
152 cell engagement and LN architectural changes in the modulation of pro-tolerant versus pro-
153 inflammatory immune responses in organ transplant recipients.

154 **RESULTS**

155 ***Bifido* and *Desulfo* result in changes in long term graft health and LN laminin α4:α5 ratios**

156 Mice were treated with the antibiotics (abx) cocktail to deplete their normal microbiota,
157 after which gavage was performed using WT mouse whole stool samples (control) or single
158 bacterial strains of *B. pseudolongum* ATCC27774 (*Bifido* ATCC), *B. pseudolongum* UMB-MBP-
159 001 (*Bifido* MD), or *D. desulfuricans* (*Desulfo*) for SBT. Cardiac transplants were then performed
160 with low dose tacrolimus immunosuppression that was administered daily. Allografts were
161 assessed for inflammation and fibrosis 40 days after transplant along with LNs for architectural
162 changes characterized by the ratio of laminin α4:α5 via immunohistochemistry (IHC).

163 Mice that received *Bifido* ATCC SBT had lower cardiac allograft inflammation scores than
164 mice gavaged with *Desulfo* or treated with control gavage (**Fig. 1a**), consistent with our previous
165 results [35]. Histology revealed more CD4+ helper and CD8+ cytotoxic T lymphocytes in the grafts
166 of *Desulfo* treated mice (**Fig. 1b**), compatible with increased cytotoxicity, rejection, and
167 inflammation. The LN laminin α4:α5 ratio in the CR and the high endothelial venules (HEV) was
168 significantly higher in *Bifido* ATCC gavaged mice compared to WT stool control mice (**Fig. 1c**),
169 consistent with a more suppressive and tolerogenic immune environment.

170 We previously demonstrated that porcine-derived *Bifido* ATCC and murine-derived *Bifido*
171 MD elicited strain-specific patterns of immune changes both *in vitro* and *in vivo* [44]. To examine
172 whether these differences extended to allograft inflammation and long-term changes in LN
173 architecture and immune cell homing, we performed allogeneic cardiac transplants comparing
174 both *Bifido* ATCC *and Bifido* MD SBT as well as *Desulfo* and control PBS gavage. There were no
175 episodes of early rejection and animals were sacrificed at day 40. Analysis of their LNs, spleen,
176 and intestine revealed the following:

177 <u>*Flow cytometry:*</u> By flow cytometry, there were increased CD11c+ DCs within pLN of *Bifido* ATCC
178 treated compared to control and other SBT groups (**Fig. 1d)**. Otherwise, no differences were

179 observed between treatment groups for CD4 or CD8+ T cells, Foxp3+ Tregs, CD11c+ DCs, or
180 F4/80+ MΦ populations in mLN, pLN, or spleen.
181 *Mesenteric LN immunohistochemistry cell analysis:* By IHC, there were increased Foxp3+ Tregs
182 around HEV of mLN in *Desulfo* treated mice **(Fig. 1e)**.
183 *Peripheral LN immunohistochemistry cell analysis:* In the pLN, *Bifido* MD and *Desulfo* treated
184 mice had decreased Foxp3+ Tregs around HEVs (**Fig. 1f)**. *Bifido* ATCC treated mice had
185 increased F4/80+ MΦ compared to control and *Desulfo*, and decreased CD11c+ DCs in pLN CR
186 **(Fig. 1f)**. *Bifido* MD also displayed decreased CD11c+ DCs around pLN HEV (**Fig. 1f)**.
187 *LN laminin ratios:* *Bifido* and *Desulfo* treated mice had decreased laminin $\alpha4$:$\alpha5$ ratios around the
188 mLN CR, consistent with a more inflammatory immune environment **(Fig. 1g)**.
189 *Intestine immunohistochemistry:* In the intestine, *Bifido* ATCC treated mice had increased Foxp3+
190 Tregs, decreased F4/80+ MΦ, and increased CD11c+ DCs compared to control. While *Desulfo*
191 treated mice had decreased F4/80 MΦ compared to control and decreased Foxp3+ Tregs and
192 CD11c+ DCs compared to *Bifido* ATCC **(Fig 1h)**. Overall, *Desulfo* had mixed effects in mLN with
193 anti-inflammatory Foxp3+ Treg increases as well as pro-inflammatory decreased laminin ratios.
194 While in the pLN and intestine, *Desulfo* had pro-inflammatory effects with decreased Foxp3+
195 Tregs. *Bifido* MD showed pro-inflammatory changes as well with decreased pLN Foxp3+ Tregs
196 and decreased mLN laminin ratios. *Bifido* ATCC showed anti-inflammatory effects with increased
197 intestine Foxp3+ Tregs. Both *Bifido* MD and ATCC showed decreased CD11c+ DCs in the pLN.
198 *Bifido* ATCC showed increased pLN F4/80+ MΦ. In contrast to pLN, *Bifido* ATCC showed an
199 increase in intestinal CD11c+ DCs and decreased F4/80+ MΦ.
200 We next investigated whether these changes persisted 60 days after transplant and SBT.
201 Analysis of their LNs and spleen revealed the following:
202 *Flow cytometry:* By flow cytometry, splenic CD4 and CD8+ T cells were decreased in *Bifido* MD
203 treated mice compared to control. B220+ B cells were increased in spleens of *Bifido* MD treated

204 mice **(Fig. 1i)**. In the mLN, B220+ B cells were increased with *Bifido* MD treatment **(Fig. 1j)**. In
205 the pLN of *Bifido* MD treated animals, F4/80+ MΦ were decreased compared to control **(Fig. 1j)**.
206 *Mesenteric LN immunohistochemistry cell analysis:* By IHC, *Bifido* MD treated mice had
207 decreased Foxp3+ Tregs in the CR, increased F4/80+ MΦ around HEV and CR, and decreased
208 CD11c+ DCs around HEV and CR **(Fig. 1k)**. *Desulfo* treated animals had decreased Foxp3+
209 Tregs in CR, increased F4/80+ MΦ in CR, and decreased CD11c+ DCs around both HEV and
210 CR **(Fig. 1k)**.
211 *Peripheral LN immunohistochemistry cell analysis:* In the pLN, *Bifido* MD treated mice had
212 decreased Foxp3+ Tregs in the CR and increased CD11c+ DCs around HEV and CR **(Fig. 1l)**.
213 *Desulfo* treated mice also had decreased CD11c+ DCs in CR compared to *Bifido* **(Fig. 1l)**.
214 *LN laminin ratios:* In the pLN CR, *Desulfo* treated mice showed increased ratios compared to both
215 control and *Bifido* **(Fig. 1m)**. Laminin ratios were also increased with *Desulfo* compared to *Bifido*
216 in pLN HEV and mLN HEV **(Fig. 1m)**.
217 *Intestine immunohistochemistry:* In the intestine, *Bifido* MD treated mice had decreased Foxp3+
218 Tregs compared to control and *Desulfo* and increased CD11c+ DCs compared to control and
219 *Desulfo* **(Fig. 1n)**. Overall, on day 60, *Bifido* MD mice showed decreased splenic T cells and
220 increased B cells along with increased mLN B cells and decreased pLN F4/80+ MΦ by flow
221 cytometry. By IHC, *Bifido* MD showed pro-inflammatory effects with decreased Foxp3+ Tregs in
222 mLN, pLN, and intestine, similar to day 40. *Desulfo* resulted in mixed effects with pro-inflammatory
223 mLN changes with decreased Foxp3+ Tregs and anti-inflammatory laminin ratios in both mLN
224 and pLN in contrast to its effects at day 40. *Bifido* MD and *Desulfo* showed increased mLN F4/80+
225 MΦ and decreased mLN CD11c+ DCs.
226 Single dose administration of *Bifido MD, Bifido ATCC*, and *Desulfo* each elicited significant
227 differences in LN architecture and immune cell homing compared to one another. Based on gut
228 microbiota and IHC data from 40 and 60 days post-SBT, we hypothesized that the systemic

229 effects of SBT take place early and attenuate over time, as the immune system re-equilibrates
230 and as the microbiota reverts over time.
231
232 **Early changes in intestinal and LN immune compartment structure due to *Bifido* and**
233 ***Desulfo***
234 The above results suggested that the microbiota regulated global immune states, with
235 functional consequences for alloimmunity. To assess the initial immune changes that set the
236 stage for this immunomodulation, we focused on early changes in LN and intestine T cell and
237 myeloid cell content and distribution as well as LN laminin α4:α5 ratios. Given the complex and
238 multidirectional interactions of abx, SBT, and tacrolimus treatments on the gut microbiome and
239 immune system, we assessed these components individually by treating mice with abx alone for
240 7 days, tacrolimus alone for 3 days, or both treatments together (7 days of abx followed by 3 days
241 of tacrolimus). By flow cytometry, tacrolimus reduced overall cellularity of CD4+ T cells, CD8+ T
242 cells, Foxp3+ Tregs, and B220+ B cells in mLN. However, there were no significant differences
243 in the pLN **(Fig. 2a)**. By IHC, Foxp3+ Tregs were decreased in mLN HEV by abx, tacrolimus, and
244 the two together compared to untreated control **(Fig. 2b)**. In the mLN CR, Foxp3+ Tregs
245 decreased with tacrolimus alone and tacrolimus with abx **(Fig. 2b)**. CD11c+ DCs decreased with
246 tacrolimus treatment compared to control **(Fig. 2b)**. In the pLN, Foxp3+ Tregs were decreased
247 with abx treatment only **(Fig. 2c)**. CD11c+ DCs were decreased by tacrolimus and abx alone in
248 pLN CR (**Fig. 2c**). In the mLN HEV, laminin α4:α5 ratios were decreased by abx alone (**Fig. 2d**).
249 In the intestine, Foxp3+ Tregs were decreased by either abx or tacrolimus, but not the two
250 together in intestine **(Fig. 2b)**. Conversely, intestine F4/80+ MΦ were increased by either abx or
251 tacrolimus, but not the two together **(Fig. 2c)**. CD11c+ DCs were only increased by tacrolimus in
252 intestine **(Fig. 2d)**. In the intestine tacrolimus increased Foxp3+ Tregs, F4/80+ MΦ, and CD11c+
253 DCs **(Fig. 2e)**. Overall, tacrolimus alone decreased mLN cellularity by flow cytometry. Tacrolimus,

254 abx, and the two together were pro-inflammatory, as shown by decreased Foxp3+ Tregs in mLN
255 and pLN as well as decreased laminin ratios in mLN. It was only in intestine that tacrolimus alone
256 had anti-inflammatory effects by increasing Foxp3+ Tregs. These findings reinforce the notion
257 that abx and immunosuppression, alone and in concert, exert distinct pro-inflammatory LN
258 perturbations, prior to addition of SBT.

259 Building on these early immune changes due to these single or combined variables, mice
260 were next treated with abx (6 days), SBT (PBS, *Bifido* MD, *Bifido* ATCC, or *Desulfo)* at day 0 and
261 then tissues obtained for analysis at day 3. The results are as follows:

262 *Flow cytometry analysis:* By flow cytometry, in the mLN, *Bifido* ATCC resulted in decreased CD4+
263 T cells. *Desulfo* resulted in increased CD11c+ DCs compared to *Bifido* MD. F4/80+ MΦ were also
264 increased with *Desulfo* compared to *Bifido* MD **(Fig 3a)**. In pLN, *Bifido* ATCC resulted in increased
265 CD8+ T cells compared to control. CD11c+ DCs were decreased in the pLN of all treatment
266 groups compared to control. B220+ B cells were increased in the pLN of *Desulfo* treated animals
267 compared to *Bifido* MD. In the spleen, there were increased F4/80+ MΦ with *Bifido* MD treatment
268 compared to *Desulfo* and control **(Fig. 3a)**.

269 *Mesenteric LN immunohistochemistry:* Foxp3+ Tregs were increased in mLN CR with *Bifido* and
270 *Desulfo* treatments. F4/80+ MΦ were decreased in CR by *Bifido* ATCC and in CR and HEV by
271 *Bifido* MD and *Desulfo* **(Fig. 3b)**.

272 *Peripheral LN immunohistochemistry:* In pLN CR, *Bifido* ATCC resulted in decreased Foxp3+
273 Tregs compared to control. CD11c+ DCs were increased compared to control with *Bifido MD* in
274 pLN CR. F4/80+ MΦ were increased in pLN CR with *Bifido* MD compared to control **(Fig. 3c)**.

275 *LN laminin ratios:* In the mLN HEV and CR, *Bifido* ATCC resulted in increased laminin $\alpha 4{:}\alpha 5$ ratios
276 compared to control, *Desulfo*, and *Bifido* MD. There were no changes in pLN laminin $\alpha 4{:}\alpha 5$ ratios
277 **(Fig. 3d)**.

278 *Intestine immunohistochemistry cell analysis:* In the intestine, *Desulfo* treated mice showed
279 increased Foxp3+ Tregs compared to *Bifido* and control **(Fig 3e)**. *Bifido* MD mice had decreased
280 CD11c+ DCs compared to *Desulfo, Bifido* ATCC, and control. F4/80+ MΦ were decreased in all
281 SBT treatment groups compared to control **(Fig. 3e)**. Overall, despite pro-inflammatory decreased
282 pLN Foxp3+ Tregs with *Bifido* ATCC, there were also anti-inflammatory mLN architectural and
283 Foxp3+ Treg changes. *Bifido* MD had a smaller anti-inflammatory effect with increased Foxp3+
284 Tregs in the mLN. *Desulfo* treated mice showed anti-inflammatory changes in the intestine with
285 increased Foxp3+ Tregs. Since both *Bifido* strains differentially modulated immune responses
286 and since *Bifido MD* is murine-tropic with improved anti-inflammatory capacity *in vitro* [44], further
287 transplant experiments were carried out using the *Bifido MD* strain.

288 We then sought to incorporate immunosuppression at this early time point. Mice were next
289 treated with abx (6 days), single bacterial SBT at day 0, daily tacrolimus starting on day 0, and
290 then tissues obtained for analysis at day 3.

291 *Flow cytometry analysis:* By flow cytometry, there were no changes observed in mLN or pLN
292 numbers or relative percentages of CD4+ T cells, CD8+ T cells, Foxp3+ Tregs, or B220+ B cells.
293 There were also minimal changes observed in numbers and percentages of CD11c+ DCs or
294 F4/80+ MΦ, or their subsets defined by CD11b, CD103, and/or CX3CR1 surface receptors
295 **(Suppl. Fig. S1)**. Our data indicated that the addition of tacrolimus to the above treatment protocol
296 eliminated the minor changes observed by flow cytometry in mLN, pLN, and spleen after 3 days.

297 *Mesenteric LN immunohistochemistry:* Foxp3+ Tregs and CD11c+ DCs were increased and
298 F4/80+ MΦ decreased in the CR in both *Bifido* and *Desulfo* treated groups. Thus, while the
299 absolute numbers and ratios of cell content did not change as assessed by flow cytometry, the
300 microanatomic distribution of these cells around the CR, the region where Foxp3+ Tregs are
301 induced and activated, did change **(Fig. 4a)**.

302 *Peripheral LN immunohistochemistry:* In the pLN, *Desulfo* resulted in increased F4/80+ MΦ in the
303 HEV **(Fig. 4b)**. There were otherwise no significant changes in Foxp3+ Tregs, CD11c+ DCs, or
304 F4/80+ MΦ in the pLN HEV or CR.
305 *LN laminin ratios:* Analysis of LNs for stromal fiber remodeling in regional mLN showed increased
306 laminin $\alpha4$:$\alpha5$ ratios, suggestive of a more suppressive environment, in the CR with *Bifido* MD
307 treatment as compared to *Desulfo* and *Bifido* ATCC **(Fig. 4c)**. In the systemic pLN, there were
308 decreased laminin $\alpha4$:$\alpha5$ ratios in the HEV and CR with *Desulfo* compared to control **(Fig. 4c)**. In
309 the pLN HEV, both *Bifido* treatments also resulted in decreased laminin ratios compared to
310 control.
311 *Intestine immunohistochemistry:* IHC of intestinal segments showed a decrease in Foxp3+ Tregs
312 cells in *Bifido* and *Desulfo* treated groups compared to control (**Fig. 4d)**. There were no changes
313 in F4/80+ MΦ and CD11c+ DCs. These observations suggested that the addition of
314 immunosuppressant may inhibit early intestinal changes between animals treated with abx and
315 SBT only. Overall, *Bifido* resulted in anti-inflammatory changes in the mLN with increased Foxp3+
316 Tregs and laminin ratios, similar to the prior treatment regimen without tacrolimus. However, *Bifido*
317 also caused pro-inflammatory changes in pLN and intestine with decreased laminin ratios and
318 Foxp3+ Tregs, respectively. *Desulfo* displayed a largely pro-inflammatory phenotype with
319 decreased pLN laminin ratios and decreased Foxp3+ Tregs in the intestine despite increased
320 mLN Foxp3+ Tregs, in contrast with a *Desulfo* anti-inflammatory effect with the prior treatment
321 regimen lacking tacrolimus. These results showed that the early microbiota induced changes in
322 immune content and structure of LNs and subsequent suppressive or inflammatory
323 responsiveness was further modulated by the addition of immunosuppressant tacrolimus.
324 We next studied the capability of tacrolimus to modulate the alloimmune response to abx
325 and SBT. C57BL/6 mice were treated with abx, followed by SBT using PBS, or gavage with either
326 *Bifido* MD or *Desulfo*, cardiac transplantation, and tacrolimus (3 mg/kg/d) on the day of transplant.

327 The tacrolimus was continued daily for 7 days, and the recipients were euthanized on day 8 after
328 transplant to assess changes in immune cell content and LN architecture between treatment
329 groups. The results are as follows:
330 *Mesenteric LN immunohistochemistry:* *Desulfo* treatment resulted in decreased mLN Foxp3+
331 Tregs compared to control and *Bifido* and decreased mLN CR CD11c+ DCs compared to *Bifido*
332 (**Fig. 5a)**.
333 *Peripheral LN immunohistochemistry:* *Desulfo* resulted in decreased pLN Foxp3+ Tregs and
334 CD11c+ DCs compared to control and *Bifido* (**Fig. 5b)** consistent with a more pro-inflammatory
335 environment.
336 *LN laminin ratios:* *Bifido* resulted in a pro-tolerant phenotype, with increased laminin α4:α5 ratios
337 in the mLN CR compared to control (**Fig. 5c),** whereas *Desulfo* resulted in increased ratios in the
338 pLN HEV compared to control and *Bifido*.
339 *Intestine immunohistochemistry:* Both *Desulfo* and *Bifido* treated mice had decreased CD11c+
340 DCs compared to control **(Fig. 5d)***.* Overall, *Bifido* resulted in pro-tolerant mLN laminin changes
341 while *Desulfo* resulted in pro-inflammatory changes with decreased mLN and pLN Foxp3+ Tregs
342 at day 7.
343 We further assessed this immunomodulatory effect after a longer period of time. C57BL/6
344 mice were treated with abx, followed by gavage with PBS, or SBT with either *Bifido* MD or *Desulfo*,
345 cardiac transplantation, tacrolimus daily for 14 days, and the recipients were euthanized on day
346 15 after transplant to assess changes in immune cell content and LN architecture between
347 treatment groups. The results are as follows:
348 *Mesenteric LN immunohistochemistry:* There were no changes in Foxp3+ Tregs, CD11c+ DCs,
349 or F4/80+ MΦ in pLN HEV or CR (**Fig. 5e)**.
350 *Peripheral LN immunohistochemistry:* *Bifido* treatment resulted in increased Foxp3+ Tregs in HEV
351 compared to control and CR compared to both *Desulfo* and control. *Desulfo* had increased
352 CD11c+ DCs in CR and around HEV compared to control (**Fig. 5f)**.

353 <u>*LN laminin ratios:*</u> *Bifido* resulted in increased laminin α4:α5 ratios around mLN HEV compared
354 to control and *Desulfo* (**Fig. 5g)**. However, there were no differences in the ratios of laminin
355 expression with *Bifido* treatment in pLN.
356 <u>*Intestine immunohistochemistry:*</u> In the intestine, *Desulfo* treated mice had decreased F4/80 MΦ
357 compared to control **(Fig. 5h)***.* Overall, *Bifido* resulted in pro-tolerogenic changes in pLN with
358 increased Foxp3+ Tregs and mLN with increased laminin ratios, whereas *Desulfo* appeared to
359 have a neutral effect at day 14.
360
361 ***Bifido* and Desulfo induced early changes in T cell responses**
362 To characterize T cell trafficking in response to the gut microbiota, C57BL/6 mice were
363 treated with abx, followed by gavage with PBS, or SBT with either *Bifido* MD or *Desulfo*, and
364 cardiac transplantation. Mice also received adoptive transfer of alloantigen specific, T cell receptor
365 transgenic TEa T cells (2 x 10^5) along with tacrolimus on the day of transplant. The tacrolimus
366 was continued daily for 7 days, and the gut microbiota characterized over this time. The recipients
367 were euthanized on day 8 after transplant to assess migration and differentiation of the alloantigen
368 specific T cells to mesenteric and systemic LNs, spleens and grafts as assessed by both IHC and
369 flow cytometry. Analysis of their LNs revealed the following:
370 <u>*Flow cytometry analysis:*</u> After 7 days, the proportion of transferred TEa cells in mLN or pLN did
371 not differ between treatment groups. However, very few transferred cells were detected in spleen
372 of *Desulfo* treated animals compared to *Bifido* and control (**Fig. 6a**). Transferred TEa cells
373 differentiated into more Foxp3+ Tregs in the pLNs of *Desulfo* treated groups compared to control
374 (**Fig. 6a**). However, there were fewer effector CD4 CD44+CD69- T cells (Teff) in *Bifido* mLNs and
375 pLNs compared to the *Desulfo* and control groups (**Fig. 6a**). These changes in the *Bifido* group
376 were consistent with an increased suppressive mLN environment and the increased suppressive
377 environment observed by IHC above **(Fig 5a)**.

378 Graft inflammation and fibrosis were similar across the 3 study groups, as expected for
379 this very early post-transplant time point (**Suppl. Fig. S2**). Importantly, the gavage treatments did
380 not affect serum tacrolimus levels across study groups (**Suppl. Fig. S3**), showing that these
381 immunologic effects were not due to microbiota induced alterations in exposure to
382 immunosuppression.

383 Given the small differences in allograft outcomes at 7 days post-transplant between
384 treatment groups, we next sought to characterize T cell trafficking, LN occupancy and structure,
385 and allograft outcomes after additional time had passed (14 days post-transplant). Mice were
386 treated as above and euthanized after 14 days. Analysis of their LNs revealed the following:

387 *Flow cytometry analysis:* After 14 days, the proportion of transferred TEa cells in pLN and spleen
388 was greater in *Bifido* treated animals compared to control and *Desulfo*. There was no difference
389 between groups in the mLN **(Fig. 6b)**. Contrary to 7 days, after 14 days, transferred TEa cells
390 differentiated into the greatest percentage of Foxp3+ Tregs in the pLN and spleen of control
391 animals with *Desulfo* treated animals also having a greater percentage than *Bifido MD* in spleen
392 **(Fig.6c)**. Furthermore, there was a greater percentage of Teff cells in *Bifido* mLN compared to
393 control and *Desulfo*. In the pLN, there was a decreased percentage of Teff cells in *Desulfo* treated
394 animals compared to control **(Fig. 6d)**. The ratio of Treg:Teff was greatest in *Desulfo* compared
395 to *Bifido* in mLN, pLN, and spleen **(Fig. 6e)**. Overall, these data show a reversal of the trend of
396 increased mLN Treg:Teff seen in the 7 day treatment group. This may suggest that despite
397 decreased LN Foxp3+ Tregs in the *Bifido* group compared to *Desulfo* at 14 days, the increased
398 Foxp3+ Tregs seen at 7 days may have been redeployed to the allograft by this timepoint,
399 explaining the decreased fibrosis in *Bifido* allografts at day 14. It is also important to note that
400 fewer overall TEa cells survived in *Desulfo* treated animals compared to *Bifido* and control, and
401 thus it is difficult to strictly compare the percentages of individual cell types in *Desulfo* treated
402 mice to the other two treatment groups. Lastly, as noted above, the early tolerogenic versus pro-

403 inflammatory effects of *Bifido* and *Desulfo*, respectively, became mixed and less distinct at later
404 time points.

405 Graft inflammation was similar across the 3 study groups, as expected for this very early
406 post-transplant time point (**Suppl. Fig. S2**). However, there was greater fibrosis in *Desulfo* treated
407 animals compared to *Bifido* or control after 14 days **(Fig. 6f)** consistent with our previous findings
408 [45].

409

410 **Myeloid response involved in LN remodeling**

411 The results above demonstrated that anti- and pro-inflammatory signals from the gut
412 microbiome were transmitted to the LN, resulting in remodeling of the laminin α4:α5 fiber ratios
413 and subsequent graft acceptance or graft inflammation and fibrosis. Since the gut is the largest
414 immune organ and functions as a physical barrier against luminal microbes and also a critical
415 interface between commensal microbiota and innate immune cell populations [46], we sought to
416 investigate the role of myeloid cell homing in transducing signals between the gut and LN. To
417 understand the sequence of immunologic events that lead to these alterations, we characterized
418 the requirement for CCR2-dependent myeloid cell mobilization and responses in LN remodeling.
419 The CCR2 antagonist RS504393 was administered for 7 days to inhibit monocyte and MΦ
420 recruitment. Mesenteric and systemic LNs were harvested and laminin α4:α5 ratios evaluated by
421 IHC, and lymphoid and myeloid cells by IHC and flow cytometry. Transplantation and graft survival
422 were also evaluated in mice treated with the CCR2 antagonist.

423 RS504393 administration alone decreased the expression of both laminin α4 and α5 in
424 the pLN CR and HEV, however the α4:α5 ratios remained unchanged (**Fig. 7**). RS504393
425 treatment showed a minor, but significant (p=0.02) prolongation in graft survival, median survival
426 time (MST) of 15.3 days, compared to control, MST of 6.7 days.

427 Next, mice received combinations of abx (6 days), gavage with *Bifido* MD or *Desulfo* single
428 bacterial species or PBS (day 0), and RS504393 (7 days). Assessing LN and spleen by flow
429 cytometry, the *Bifido* group had decreased mLN Foxp3+ Tregs, but otherwise revealed no major
430 effects on the overall numbers or percentages of CD4+ and CD8+ T cells, B220+ B cells, CD11c+
431 DCs, or F4/80+ MΦ (**Fig. 8a**).

432 By IHC in the mLN CR, Foxp3+ Tregs decreased after *Desulfo* treatment compared to
433 *Bifido* and control **(Fig. 8b)**. Both *Desulfo* and *Bifido* decreased CD11c+ DCs in mLN CR **(Fig.**
434 **8b)**. F4/80+ MΦ were decreased in the mLN HEV and CR with both *Desulfo* and *Bifido* (**Fig 8b**).
435 In the pLN, there were minimal changes apart from *Desulfo* treatment resulted in increased
436 F4/80+ MΦ compared to *Bifido* in CR **(Fig. 8c)**.

437 *Bifido* and *Desulfo* caused increased laminin α4:α5 ratios compared to control, with *Bifido*
438 causing greater ratios than *Desulfo* in mLN **(Fig. 8d**). In the pLN, *Desulfo* resulted in increased
439 laminin ratios compared to *Bifido* and control **(Fig. 8d**). Since SBT with both bacterial species and
440 RS504393 increased laminin ratios in mLN compared to abx alone which decreased the ratios
441 **(Fig. 2d)**, this suggests that CCR2 inhibition abrogated these pro-inflammatory LN changes.

442 In the intestine, by IHC, CD11c+ DCs decreased with *Desulfo* and F4/80+ MΦ were
443 decreased with *Bifido*, compared to control **(Fig. 8e)**. Overall, *Bifido* resulted in anti-inflammatory
444 mLN laminin ratios while *Desulfo* resulted in a mixed effect with decreased Foxp3+ Tregs in the
445 mLN as well as increased laminin ratios in mLN and pLN. Notably, both *Bifido* and *Desulfo*
446 resulted in decreased mLN F4/80+ MΦ and CD11c+ DCs. These effects suggest that CCR2
447 inhibition may abrogate some of the pro-inflammatory effects of *Desulfo*, but not *Bifido.*

448 To assess the impact of CCR2-mediated myeloid migration on allograft outcomes, mice
449 were transplanted with allogeneic hearts along with combinations of abx (6 days), gavage with
450 *Bifido* or *Desulfo* single bacterial species or PBS (day 0), and RS504393 (7 days). Consistent with
451 previously shown differences in graft inflammation scores between *Bifido* MD and *Desulfo groups*,

452 *Desulfo* treated mice rejected allografts earlier than PBS and *Bifido* treated mice (MSTs 12.5, 16,
453 and 19 days, respectively, $p<0.004$) (**Fig. 8f)**.

454 As noted above, abx (6 days), SBT, allogeneic cardiac transplant, and tacrolimus (7 days)
455 showed that *Bifido* resulted in pro-tolerant mLN laminin changes while *Desulfo* resulted in pro-
456 inflammatory pLN laminin changes as well as decreased Foxp3+ Tregs. *Desulfo* treatment also
457 resulted in decreased pLN CD11c+ DCs compared to control. Both *Desulfo* and *Bifido* treated
458 mice had decreased CD11c+ DCs compared to control. Compared to RS504393 treatment,
459 tacrolimus did not disturb the pro-tolerant or pro-inflammatory effects of *Bifido* or *Desulfo*,
460 respectively.

461 To further understand whether CCR2-mediated myeloid homing was required for
462 mediating immunomodulatory effects of microbiota during pharmacologic immunosuppression,
463 combinations of abx (6 days); SBT with *Bifido* MD, *Desulfo*, or PBS (day 0); and tacrolimus plus
464 RS504393 (7 days) were administered. Intestinal tissues, LN, and spleens were then obtained.
465 Flow cytometry for CD4+ and CD8+ T cells, B220+ B cells, CD11c+ DCs, and F4/80+ MΦ showed
466 no major effects on the overall numbers or percentages (**Suppl. Fig. S4**). By IHC in the mLN,
467 *Desulfo* resulted in increased Foxp3+ Tregs and CD11c+ DCs in HEV and CR **(Fig. 9a)**. In the
468 mLN CR, *Bifido* also resulted in increased Foxp3+ Tregs. In pLN, *Desulfo* resulted in decreased
469 Foxp3+ Tregs in pLN HEV **(Fig. 9b)**. Both *Desulfo* and *Bifido* resulted in decreased CD11c+ DCs
470 in pLN HEV and CR. In the pLN HEV, *Desulfo* resulted in decreased and F4/80+ MΦ **(Fig. 9b)**.
471 There were no changes in LN laminin $\alpha4$:$\alpha5$ ratios in mLN or pLN **(Fig. 9c)**.

472 In the intestine, there was also no difference in immune cell populations **(Fig. 9d)**. Overall,
473 *Bifido* resulted in minor anti-inflammatory changes in mLN with increased Foxp3+ Tregs while
474 *Desulfo* resulted in pro-inflammatory decreases in Foxp3+ Tregs in mLN and pLN. Neither *Bifido*
475 nor *Desulfo* resulted in LN architectural changes. Together, these observations suggest that

476 RS504393 and tacrolimus together inhibit at least some of the immunomodulatory capabilities of
477 *Bifido* and *Desulfo*.
478
479 ***Bifido* and *Desulfo* impact the activation programming of myeloid cells *in vitro***
480 We further sought to characterize the nature of gut microbiota-myeloid cell interactions.
481 We previously demonstrated that *Bifido* induced more balanced anti-inflammatory and
482 homeostatic cytokine responses in the JAWS DC and RAWS MΦ cell lines, compared to *Desulfo*.
483 We extended these initial observations by using the different strains of *Bifido* against primary bone
484 marrow derived DCs (BMDCs) and peritoneal MΦ. These isolated myeloid cells were then
485 stimulated in culture with UV-killed *Bifido* ATCC, *Bifido* MD, or *Desulfo*. After 24 hours of
486 stimulation, the myeloid cells were harvested, and supernatants tested for IL-6, IL-10 and TNFα
487 by ELISA. BMDC and MΦ were analyzed by flow cytometry for activation markers MHC II, CD40,
488 CD80, and CD86. BMDCs displayed increased MHC II in response to *Desulfo* and *Bifido* ATCC.
489 *Bifido* ATCC, *Bifido* MD, and *Desulfo* all increased CD40 expression, with *Desulfo* stimulating the
490 greatest increase. Both *Bifido* MD and *Desulfo* increased CD80 expression, whereas only *Desulfo*
491 increased CD86 **(Fig. 10a)**. Amongst cultured peritoneal MΦ, the proportion of M1 phenotype
492 (F4/80+ MHC II+) was not affected by treatment **(Fig. 10b)**. However, *Bifido* MD treatment led to
493 an increased proportion of M2 (F4/80+ CD206+) compared to control, *Desulfo* leading to more
494 M2 than *Bifido* MD, and *Bifido* ATCC with the greatest proportion of M2. CD40 expression
495 increased with any bacteria treatment compared to control amongst the M1 subset (**Fig. 10b)**.
496 Although not surprising that bacteria directly activate antigen presenting cells (APCs), each
497 bacteria triggers a unique activation pattern suggesting that APCs may contribute to mediating
498 microbiota-specific signals from the gut.
499 Furthermore, examining the concentration of cytokine in the supernatant of each of these
500 cultures also revealed unique patterns. In BMDCs, TNFα was elevated with *Desulfo* and *Bifido*

501 ATCC, but not *Bifido* MD **(Fig. 10c)**. IL-6 was elevated in all groups with progressively higher
502 levels from *Bifido* MD to ATCC to *Desulfo*, respectively. While IL-10 was elevated in all treatment
503 groups, levels were highest with *Bifido* ATCC **(Fig. 9c)**. BMDC responses to *Bifido* co-culture was
504 consistent with relative anti-inflammatory phenotype (decreased TNFα and IL-6 with increased
505 IL-10) compared to *Desulfo.* In peritoneal MΦ, TNFα was elevated by *Desulfo* **(Fig. 10d)**. Both
506 *Bifido* ATCC and *Desulfo* led to increased IL-6. While both *Bifido* ATCC and *Bifido* MD led to
507 increased IL-10, and *Desulfo* treated MΦ expressed an even higher level **(Fig. 10d).** While
508 *Desulfo* treatment also seemed to stimulate a pro-inflammatory phenotype in MΦ with elevated
509 IL-6 and TNFα, the bacteria also stimulated more IL-10 compared to *Bifido*. However, in keeping
510 with flow cytometry data and prior cell line findings, *Bifido* and *Desulfo* were able to stimulate
511 distinctive activation patterning in APCs as evidenced by surface marker expression and cytokine
512 production.
513
514 **Early changes in intestinal barrier function due to tacrolimus and bacterial gavage**
515 Intestinal epithelial barrier function is critical for normal gut homeostasis, whereas its
516 dysfunction and associated microbial dysbiosis have been associated with both gastrointestinal
517 and neuroinflammatory diseases [47-49]. Changes in intestinal permeability therefore are
518 reflective of the gut epithelial barrier response to luminal environmental cues. Given the
519 differential impact of *Desulfo* and *Bifido* on allograft outcomes and LN architecture, as well as the
520 modulatory effect of abx (7 days) and tacrolimus (3 days), we sought to assess changes in
521 intestinal permeability in response to these treatments. We observed that tacrolimus induced
522 decreased permeability compared to no treatment, whereas abx did not significantly change
523 permeability **(Fig. 11a)**. Mice that received abx pre-treatment followed by SBT and tacrolimus
524 showed decreased intestinal permeability with both *Bifido* and *Desulfo* compared with control after
525 3 days; and *Bifido* showed less of a decrease compared to *Desulfo* **(Fig. 11b)**. These results

526 indicate tacrolimus alone significantly reduced intestinal permeability, likely via induced anti-
527 inflammatory intestinal changes [50]. However, with addition of abx to tacrolimus, this effect was
528 abolished.

529 However, in mice receiving SBT, tacrolimus, and heart transplants, *Desulfo* treated
530 animals displayed elevated permeability compared to controls at day 7 **(Fig. 11c)**. At day 14,
531 although the *Desulfo* group still demonstrated significantly higher permeability compared to
532 control, this difference was less prominent than at day 7 **(Fig. 11d)**. These results suggest that
533 the pro-inflammatory *Desulfo* exerted a profound impact on the intestinal epithelium compared to
534 *Bifido* after 7 days, while this effect became attenuated by 14 days.

535

536 **Early profound impact of bacterial gavage on microbiota with equilibration at later time**
537 **points**

538 We next sought to address the stability of bacterial determinant colonization and its
539 relationship with the host microbiome in a clinically relevant murine model following cardiac
540 transplant [35]. In brief, C57BL/6 mice were treated with abx, followed by SBT with either *Bifido*
541 MD or *Desulfo* or gavage with control WT stool, and cardiac transplantation. Mice also received
542 tacrolimus daily for 40 days, and the gut microbiota was characterized longitudinally over this time
543 using 16S rRNA gene amplicon sequencing. The among-sample diversity of the microbial
544 community, as measured by Shannon diversity index, showed that overall microbial diversity
545 decreased within the first 2 weeks after *Bifido* and *Desulfo* SBT, with restoration of diversity at
546 later time points **(Fig. 12a)**. The between-sample diversity of the microbial community, calculated
547 using Jensen–Shannon divergence distance, demonstrated distinct separation of *Bifido* and
548 *Desulfo* after SBT, while the gut microbiota composition profiles of all 3 treatment groups
549 converged by week 2 **(Fig. 12b**). These results indicate the profound, yet transient impact of both
550 *Bifido* and *Desulfo* on the gut microbiota.

551 Further taxonomic analysis revealed the major species responsible for the altered gut
552 microbiota composition and structure following SBT **(Fig. 12c-j)**. The change in relative
553 abundance of all taxonomic groups is shown in **Suppl. Fig. S4**. Most outstandingly, we observed
554 *Bifidobacterium*, *Bacteroides*, and *Clostridiales* were among the groups most responsive to SBT.
555 Notably, *Bifidobacterium pseudolongum* was most abundant after SBT with *Bifido*, although it was
556 present at lower levels in *Desulfo* and control groups, but sharply decreased within 2 weeks in
557 the *Bifido* group **(Fig. 12c)**. This decrease in *B. pseudolongum* was accompanied by a steep
558 increase in *Bifidobacterium animalis*, a murine gut commensal that cohabitates with *B.*
559 *pseudolongum,* which likely became more abundant due to their complementary carbohydrate
560 assimilation capabilities of luminal substrates **(Fig. 12d)**. *Bacteroidales* family S24-7, a group of
561 fermentative anaerobic commensals that often predominate murine gut microbiota [51], sharply
562 decreased after SBT and was restored from week 2 onward **(Fig. 12e)**. Further, *Akkermansia*
563 *muciniphila*, a human and murine commensal known for its anti-inflammatory and mucin-
564 degrading properties [52], sharply increased only in response to *Bifido* gavage **(Fig. 12f)**. *A.*
565 *muciniphila* reached peak abundance at week 2, followed by a stable, reduced level through week
566 6. In our previous study [44], *A. muciniphila* was shown to be enriched in the gut microbiota in
567 *Bifido* MD gavaged mice, despite its overall low abundance. Further, *Lachnospiraceae* and
568 *Ruminococcus*, obligate anaerobes within *Clostridiales* with diverse fermentative capabilities,
569 were highly variable following SBT, potentially due to shifting luminal substrates **(Fig. 12g-j)**.
570 Overall, these results indicate the drastic and dynamic changes in gut microbiota composition and
571 structure brought on by single bacterial gavage. The significant, yet transient impact of bacterial
572 determinants on the host microbiome further implicates the profound influence these strains exert
573 on the gut microbiome as well as their critical role in host immunomodulation.

574 **DISCUSSION**

575 This study recapitulated our initial findings of the deterministic role that single bacterial
576 strains play in pro- and anti-inflammatory host immune modulation [35] and further elucidated the
577 cellular and molecular pathways involved over time in the multifaceted interactions among
578 different immune cell populations in response to bacterial determinants. Not only were specific
579 bacterial strains able to skew alloimmune responses toward tolerance or rejection, but we also
580 showed that abx, immunosuppression, and transplantation each modified this process. Most
581 outstandingly, we demonstrated the time-dependent effect of pro-tolerogenic and pro-
582 inflammatory bacterial strains (*Bifido* and *Desulfo*, respectively) on immunological events and
583 graft outcome. These results emphasize a critical holistic understanding of these variables
584 including timing of SBT administration, as transplant recipients are exposed to all of these agents
585 over the course of their medical care.

586 We previously showed that *Bifido* and *Desulfo* gavage were able to exert pro-tolerant and
587 pro-inflammatory LN effects after 14 days, respectively [35]. In this study, we expanded on these
588 findings to show that *Bifido* and *Desulfo* affected LN architecture and immune cell content and
589 distribution as early as 3 days following gavage and was stable at the cellular level up to 7 days.
590 Improved allograft fibrosis with pro-tolerant bacteria was stable up to 14 days. These bacterial
591 effects, which were most pronounced at early time points became obscured over time, as
592 evidenced by both pro and anti-inflammatory changes in LN architecture and immune cell content
593 and distribution beyond 14 days of treatment. We speculate that these kinetic changes may be
594 the result of complex interactions among the multiple treatments each mouse received. First, long-
595 term immunosuppression can lead to dysbiosis in human transplant recipients [53]. Preliminary
596 work by our group has confirmed that treatment with immunosuppression alone significantly alters
597 the gut microbiome after 30 days [54] and that the host metabolome is altered by SBT after 7
598 days [55]. Second, abx can significantly impede the colonization of specific bacterial strains due
599 to increased colonization by antimicrobial drug resistance strains, resulting in blooms of

600 pathogenic bacteria [56, 57]. Third, the availability of nutrient niches within the host microbiota
601 strongly influences the colonizing potential and stability of individual administered bacteria [57].
602 Our data showed that both abx and tacrolimus exerted pro-inflammatory mLN architectural
603 changes and decreased Foxp3+ Treg content in both mLN and pLN, although tacrolimus also
604 showed anti-inflammatory effects in the intestine by increasing Foxp3+ Tregs and decreased
605 intestinal permeability. Our results confirmed our earlier findings that *Bifido* exerts pro-tolerant
606 changes and *Desulfo* exerts pro-inflammatory LN changes early on, while suggesting that LN
607 architecture and lymphocyte content changes are dynamic over longer treatment periods, as in
608 the case of this study, at 40 to 60 days. These observations strongly suggest that immune
609 analyses require a detailed appreciation of several major variables and an assessment of both
610 short and long-term changes. In particular, for microbiota-informed interventions, longitudinal
611 monitoring of bacteria colonization and consideration of repeated administration may be critical
612 to ensure a long term biotherapeutic effect [53, 58].

613 We previously showed that *Bifido* MD and ATCC elicited strain-specific differential effects
614 on innate immune cell activation, tolerogenic LN architecture, and host transcriptome profiles [44].
615 In this study, when mice were treated with abx and SBT, murine-isolated *Bifido* MD elicited early
616 pro-tolerant immune changes after 3 days while porcine-isolated *Bifido* ATCC demonstrated
617 mixed pro and anti-inflammatory effects. We speculate that these strain-specific
618 immunomodulatory effects may be rooted in adaption to the mammalian gut microenvironments
619 from which they were derived. This is in agreement with other studies showing that bacteria-
620 induced immune modulation is not dictated by bacterial phylogeny [59, 60]. Though the specific
621 mechanisms of bacterial immunomodulatory effects vary among strains and remain largely
622 unclear, the modulation of endogenous gut microbiome with consequent effects on intestinal
623 metabolism and immunity is critically involved in this process [61]. The various taxonomic groups
624 that were shown to respond to SBT in this study demonstrate the major involvement of
625 endogenous gut microbiota as intermediate variables between the bacterial determinant and host

626 immune response. For example, S24-7, one of the major responders to both *Bifido* and *Desulfo*,
627 can be considered an innate immune system target due to their degree of IgA-labeling [62, 63].
628 Furthermore, the observed decrease in *B. pseudolongum* with concomitant increase in
629 *Bifidobacterium animalis* following SBT, highlights the complex dynamic nature of the gut
630 microbiota as well as the phenomenon of "functional redundancy", describing that physiologic
631 processes, such as anti-inflammatory signals, can be carried out by different bacterial species of
632 the microbiome at different times. In fact, recent studies redefine the "microbiome core" as the
633 "ecological core" that presents components of the microbiome, keystone species or metabolic
634 pathways, that are disproportionally important for shaping community physiological properties
635 [64]. *Bifido* SBT therefore affects the ecological core, potentially through alterations to pivotal
636 metabolic activities of keystone species. When mice were treated with abx, SBT, and
637 immunosuppression, *Bifido* MD also showed increased anti-inflammatory activity in mLN with
638 increased laminin ratios; however, both strains displayed pro-inflammatory effects in pLN with
639 decreased laminin ratios. These data confirm that *Bifido* MD and ATCC possess strain-specific
640 immunomodulatory properties *in vivo* and that these effects were likely due to the gut
641 microenvironment, which was further modulated by the addition of immunosuppressant
642 tacrolimus.

643 Having observed LN changes in architecture and Treg content, we next showed that mice
644 receiving abx, SBT, heart transplant, and donor specific TEa cell infusion developed fewer CD4
645 Teff in mLN and pLN with *Bifido* treatment after 7 days compared to *Desulfo* and control groups,
646 consistent with a suppressive environment. IHC data matched this in showing more anti-
647 inflammatory changes with *Bifido* and pro-inflammatory changes with *Desulfo*. In similarly treated
648 mice followed for 14 days, *Bifido* mice continued to show anti-inflammatory LN architecture
649 changes by IHC, but relatively fewer TEa Treg compared to *Bifido* treatment after 7 days,
650 suggesting that these cells may have been redeployed to the allograft. In fact, *Bifido* treated mice
651 had decreased allograft fibrosis scores after 14 days compared to *Desulfo* and control. In a recent

652 study of mouse model of spontaneous tolerance, by 2-3 weeks post-transplant, accepted renal
653 allografts develop peri-arterial Treg-rich organized lymphoid structures [65], suggesting that Treg
654 deployment to the graft is important. In keeping with 16S rRNA data above, the pro-tolerant
655 immunomodulatory effects of *Bifido* SBT were stable for at least 14 days following gavage.

656 We also focused on the roles of innate immune cells in the mechanisms of gut microbiota
657 induced immunomodulation. CCR2 is necessary for MΦ migration, and blocking CCR2 modified
658 the immunomodulatory properties of *Bifido* and *Desulfo.* In particular, RS504393 abrogated the
659 pro-inflammatory effects of *Desulfo* more than *Bifido*. Despite this effect, when mice were treated
660 with abx, SBT, heart transplant, and RS504393, *Desulfo* treated mice still rejected faster than the
661 *Bifido* treated group. This further supports that while CCR2 may play a role in mediating the
662 immunomodulatory effects of *Bifido* and *Desulfo*, there are additional mechanisms at play.
663 Furthermore, when tacrolimus was added to abx, SBT, and RS504393, pro-tolerant LN laminin
664 architectural changes in mLN and pLN seen with abx, SBT, and RS504393 were eliminated.
665 Using an in vitro culture system of primary DC and MΦ to specifically study the effect of microbiota
666 on innate immune cells, we also showed that *Bifido* and *Desulfo* act directly on innate immune
667 cells. Furthermore, different strains of *Bifido* exerted unique immunomodulatory effects. Similar
668 to *in vivo* data, porcine derived *Bifido* ATCC yielded more pro-inflammatory effects compared to
669 murine derived *Bifido* MD. *Desulfo* was even more pro-inflammatory compared to *Bifido* ATCC.
670 Overall, these observations demonstrated that DC and MΦ were likely critical for transducing
671 microbiota induced changes in the intestine to adaptive immune cells in the gut and further
672 downstream to mLN and pLN.

673 The gut microbiota is intimately involved with innate immunity through cells such as MΦ
674 and DC, and their subsequent effects on the host adaptive immune response. Intestinal MΦ form
675 an interdigitated network with the entire mucosal lamina propria vasculature; these connections
676 are disrupted in the absence of microbiota, which also correlates with increased bacterial

677 translocation across the lamina propria [66]. Sensing of mucosal-associated bacteria is triggered
678 by the Mincle-Syk (and not MyD88) signaling pathway in lysozyme-expressing DCs, inducing IL-
679 6 and IL-23 which in turn stimulate intestinal Th17 and IL-17-secreting ILCs to produce IL-17 and
680 IL-22 [67]. In addition to their well-known roles in antigen presentation, myeloid cells have major
681 roles in regulating secondary lymphoid organ structure and function. Chyou *et al.* [68] and Kumar
682 et al. [69] showed the importance of DCs in regulating the structure of LN vasculature and stromal
683 cells in response to and resolution of immune responses. Matozaki and colleagues identified
684 important roles for SIRPα+ DCs in determining the growth and differentiation of LN stromal
685 fibroblastic reticular cells (FRC) [70, 71]. FRCs in turn are responsible for constructing the laminin
686 α-chain scaffold that promotes immunogenic or tolerogenic niches within the LN to regulate
687 immune responses [72-74]. Together, these investigations suggest an essential mechanism
688 whereby the microbiota stimulates gut myeloid responses, which in turn regulate regional or
689 systemic responses via soluble mediators or migration to the LN. The LN responses include
690 functional alterations in FRC and vascular stromal cells that determine microdomain structures in
691 the LN that regulate adaptive immune responses. Future studies may assess the axis of
692 communication between microbiota, APCs homing between gut and LN, and FRCs.

693 Our results emphasize that abx and immunosuppression alone and in concert modulate
694 LN architecture and immune cell composition. Within this network, SBT with *Bifido* induced an
695 early anti-inflammatory phenotype while *Desulfo* resulted in a pro-inflammatory phenotype using
696 both the in vivo transplant model and primary cell culture. This is effect is likely related to the
697 transient stability of each gavaged bacterial determinant within the host microbiota, as evidenced
698 by our longitudinal 16S RNA data. The gut microbiota can act directly on MΦ and DC, and the
699 immunomodulatory effect of *Desulfo* is mediated at least partially through CCR2, as receptor
700 blockade abrogated bacterial pro-inflammatory effects *in vivo*. At later times, both bacteria were
701 associated with mixed effects in their impact on LN architecture and immune cell composition.

702 However, *Bifido* and *Desulfo* likely act through several other mechanisms. Future studies are
703 warranted to assess the stability of *Bifido* and *Desulfo* colonization following bacterial gavage
704 using longitudinal high resolution metagenome analysis, the ideal timing and dosing regimen of
705 bacterial determinants to achieve long lasting immune modulation, and probe bacteria-secreted
706 mediators that exert critical immunomodulatory effects over time. These dynamic effects highlight
707 the importance of early innate immune cell engagement and LN architectural changes in the
708 modulation of pro-tolerant versus pro-inflammatory immune responses in organ transplant
709 recipients.

710

711

712 **METHODS AND MATERIALS**

713 **Study approval**

714 All the procedures involving mice were performed in accordance with the guidelines and
715 regulations set by the Office of Animal Welfare Assurance of the University of Maryland School
716 of Medicine, under the approved IACUC protocol nos. 1518004 and 0121001.

717
718 **Mice**

719 Female C57BL/6 mice were used as cardiac transplant recipients, normal stool donors, and
720 pregnant stool donors. C57BL/6 mice were from the University of Maryland School of Medicine
721 Veterinary Resources breeding colony. Cardiac donors were female BALB/c mice, purchased
722 from The Jackson Laboratory (Bar Harbor, ME). C57BL/6 and BALB/c mice were used between
723 8 and 14 weeks of age. TEa T cell receptor transgenic mice [75] on a C57BL/6 background that
724 spontaneously develop colitis, due to a lack of Tregs, were used as the source for colitic stool and
725 were a gift from Alexander Rudensky (Memorial Sloan Kettering Cancer Center, New York, NY,
726 USA) [76, 77].

727
728 **Bacterial strain cultivation**

729 We previously described *B. pseudolongum* isolation methods from mouse feces [78] , from which
730 the *B. pseudolongum* UMB-MBP-01 (*Bifido* MD) strain was isolated. The *B. pseudolongum*
731 *subsp*. *pseudolongum Mitsuoka* ATCC25526 (*Bifido* ATCC) isolate was purchased from the
732 American Type Culture Collection (ATCC, Manassas, VA). Both *B. pseudolongum* UMB-MBP-01
733 and ATCC25526 isolates were used in cell stimulation and cytokine assays, after being initially
734 grown anaerobically at 37°C for 3–5 days on Bifidus Selective Media (BSM) agar plates (Millipore
735 Sigma, Burlington, MA), from which a single colony was selected and grown in BSM broth
736 (Millipore Sigma, 90273-500G-F) until stationary phase (up to 3 days). *Desulfovibrio desulfuricans*
737 *subsp. desulfuricans* (ATCC 27774) was purchased from ATCC (Manassas, VA) and grown in
738 ATCC 1249 Modified Baar's Medium (MBM) for sulfate reducers, which was made according to

739 the ATCC protocol. Cultures were initially incubated under anaerobic conditions for 5 days on
740 MBM agar plates, after which single colonies were chosen, transferred to liquid media, and
741 incubated for up to 3 weeks.
742
743 **Cell culture**
744 Murine bone marrow (BM) derived dendritic cells (BMDC) were generated using a previously
745 published protocol [79]. Briefly, the marrows from femurs and tibiae of female C57BL/6 mice were
746 flushed with PBS. The single cell suspension was cultured in a 100 mm petri dish in cell culture
747 medium RPMI-1640 supplemented with penicillin (100 U/ml), streptomycin (100 µg/ml), L-
748 glutamine (2 mM), 2-mercaptoethanol (50 µM), heat inactivated FCS (10%) (Sigma-Aldrich, St.
749 Louis, MO). The medium was supplemented with rmGM-CSF (10 ng/ml, R&D Systems,
750 Minneapolis, MN), refreshed every 3 days. After 10 days, loosely attached cells were collected
751 as immature BMDC and stimulated as described below. Peritoneal MΦ were harvested using a
752 previously published protocol [80]. Briefly, elicited MΦ were harvested from C57BL/6 mice which
753 received 3 ml of 3% Brewer Modified Thioglycolate Medium (Becton Dickinson, Sparks, MD) i.p.
754 Four days later, MΦ were harvested by injecting 5 ml of ice-cold PBS, three times, into the
755 peritoneal cavity. Cells were resuspended in complete medium and stimulated as described
756 below.
757
758 **Cell stimulation, cytokine and chemokine assays**
759 *D. desulfuricans* ATCC 27774 or *B. pseudolongum* cultures were spun down, the supernatant
760 collected, and bacterial cells killed by UV exposure at 100 µJ/cm^2 for four 15-minute cycles with
761 a UV CrossLinker (Fisher Scientific, Hampton, NH). BMDC and peritoneal MΦ (1 x 10^6) were
762 seeded into duplicate 12-well plates in 1 ml complete medium. The following day, myeloid cells
763 were stimulated with UV-killed *B. pseudolongum* MD, *B. pseudolongum* ATCC,
764 or *D. desulfuricans* bacteria at a multiplicity of infection (MOI) of 5 for 24 hours. Culture

765 supernatants were collected for ELISA. ELISAs for TNFα, IL-6, and IL-10 were purchased from
766 BioLegend (San Diego, CA) and CCL19 from Boster Biological Technology (Pleasanton, CA).
767
768 **Source stool collection and SBT**
769 Stool was collected from normal female C57BL/6 mice between 8 and 14 weeks of age, pregnant
770 C57BL/6 mice at approximately days 8–14 of pregnancy, and colitic TEa mice after the onset of
771 colitis (usually 3 months of age). Pregnant mice were timed using a combination of vaginal plug
772 monitoring, mouse weight tracking, and back-calculation from day of mouse pup birth (C57BL/6
773 gestation is 19.25 days). Pellets were weighed, homogenized in PBS at 200 mg/ml, and frozen at
774 –80°C until use. Cultured *B. pseudolongum* ATCC25526 bacteria were suspended at 1 ×
775 10^8 CFU/ml in PBS and used fresh. For SBT, mice were fed abx (kanamycin, gentamicin, colistin,
776 metronidazole, and vancomycin) ad libitum in drinking water on days –6 to –1 before transplant.
777 On day 0, C57BL/6 mice received BALB/c hearts. Fecal samples (200 µl, 200 mg/ml) or
778 cultured *B. pseudolongum* ATCC25526 (200 µl, 1 × 10^7 CFU/ml) were also transferred on day 0
779 by oral gavage. Mice received daily immunosuppression of tacrolimus (3 mg/kg/d s.c.) starting on
780 day 0 [81, 82]. Fecal pellets and intestinal tissue were collected from transplanted mice and
781 analyzed via 16S rRNA gene sequencing.
782
783 **Reagents**
784 Antibiotics were USP grade or pharmaceutical secondary standard: kanamycin sulfate (0.4 mg/ml,
785 MilliporeSigma), gentamicin sulfate (0.035 mg/ml, MilliporeSigma), colistin sulfate (850 U/ml,
786 MilliporeSigma), metronidazole (0.215 mg/ml, MilliporeSigma), and vancomycin hydrochloride
787 (0.045 mg/ml, MilliporeSigma) were dissolved in vivarium drinking water and administered ad
788 libitum. Tacrolimus (USP grade, MilliporeSigma) was reconstituted in DMSO (USP grade,
789 MilliporeSigma) at 20 mg/ml. DMSO stock was diluted to 2–3 mg/kg with absolute ethanol (USP
790 grade, Decon Labs). DMSO/ethanol stock was diluted 1:5 in sterile PBS for s.c. injection and
791 injected at 10 µl/g. Anti-CD40L mAb (clone MR1) grown in serum-free medium was obtain from

792 BioXCell (Lebanon, NH). The CCR2 antagonist RS504393 (Tocris Bioscience, Bristol, UK) by
793 resuspending to 10 mM in DMSO and then further diluting in PBS for administration at 2 mg/kg/d
794 s.c. for 7 days to inhibit monocyte and MΦ recruitment.

795
796 **Histology**

797 Cardiac allografts were assessed for survival by abdominal palpation; harvested at day 40, day
798 60, or time of rejection defined by two consecutive days without palpable heart beats; fixed for 2
799 days in 10% buffered formalin (ThermoFisher Scientific, Waltham, MA); and transferred to 70%
800 ethanol. Samples were embedded in paraffin, processed and stained with H&E or Masson's
801 trichrome. H&E samples were evaluated for parenchymal rejection score (from 0–4) using
802 previously published criteria [83]. Trichrome samples were scored 1–4, with 1 as minimal (<10%
803 area), 2 as mild (10%–30%), 3 as moderate (30%–50%), and 4 as severe (>50%). Slides were
804 read by multiple individuals blinded to the treatment group of the specimen. Scores for each slide
805 were averaged.

806
807 **Immunohistochemistry**

808 Mesenteric and peripheral LN, and segments of intestine between the duodenum and jejunum
809 were separately excised and immediately submerged in OCT compound (Sakura Finetek,
810 Torrance, CA) or fixed using paraformaldehyde. Sections (6 μm) were cut in triplicate using a
811 Microm HM 550 cryostat (ThermoFisher Scientific) and fixed in cold 1:1 acetone:methanol, for 5
812 minutes, washed in PBS, or left unfixed for fluorescent microscopy. Primary antibodies were
813 diluted between 1:20 and 1:200 in PBS and incubated for 1 hour in a humidified chamber. The
814 antibodies are listed in Supplemental Table 1. Sections were then washed with PBS, and the
815 secondary antibody was applied at a 1:50–1:400 dilution for 30 minutes (Supplemental Table 1).
816 Slides were washed in PBS for 5 minutes, coverslipped, and imaged using an Accu-Scope EXC-
817 500 fluorescent microscope (Nikon, Tokyo, Japan) and the images analyzed with Volocity
818 software (PerkinElmer, Waltham, MA). Three mice/group, 3-4 mesenteric LN or peripheral LN or

819 pieces of intestine, 3-6 sections/tissue sample, and 10-15 fields/tissue samples were analyzed.
820 Mean of mean fluorescence intensity (MFI) was calculated within demarcated high endothelial
821 venules (HEV) and cortical ridge (CR) regions of mLN and pLN as well as of whole intestinal
822 images. Percent area was calculated by dividing the sum area of demarcated regions with marker
823 fluorescence greater than a given threshold divided by total area analyzed. Treatment groups
824 were compared using quantitation of MFI multiplied by percent area to express both area and
825 intensity of cell and ECM markers.

826

827 **Intestinal permeability assay**

828 Intestinal permeability was assessed as described previously [84]. Briefly, mice were gavaged
829 with FITC-dextran (Catalog# 46944, MW: 4000; Sigma, St. Louis, MO) at a dose of 60 mg/100g
830 body weight at a 120 mg/mL concentration. Four hours later, after euthanasia, blood was collected
831 via cardiac puncture and allowed to clot at room temperature for 2 hours in the dark. Tubes
832 containing blood were centrifuged at 10,000xg for 10 minutes at 4°C and supernatant serum
833 collected. FITC-dextran serum concentration (µg/ml) was measured in duplicates using a black,
834 flat-bottom, 96-well plate (Greiner bio-one, Frickenhausen, Germany) on a FlexStation 3
835 Microplate Reader (Molecular Devices, San Jose, CA) using an excitation wavelength of 490 nm
836 and emission wavelength of 530 nm.

837

838 **Statistics**

839 Datasets were analyzed using GraphPad Prism 9.3.1 (San Diego, CA) with statistical significance
840 defined for $P < 0.05$. For comparisons of fluorescent markers (including laminin $\alpha4$:$\alpha5$ ratios),
841 serum markers, and inflammation scores, Turkey's multiple comparisons tests of one-way
842 ANOVA were used to test for significance.

843

844 **Stool specimen collection and DNA extraction**

845 Stool pellets were collected fresh from cardiac transplant recipients at weekly or biweekly intervals
846 until graft rejection or termination of the experiment. Stool samples were placed in RNAse-free
847 1.7-ml tubes (Denville Scientific, Holliston, MA), stored at 4°C overnight, and then frozen at –80°C
848 until analyzed. DNA extraction from mouse stool pellets was adapted from procedures developed
849 at the Institute for Genome Sciences and previously published [35]. In brief, 0.15-0.25 grams of
850 fecal samples were extracted using the MagAttract PowerMicrobiome DNA/RNA kit (Qiagen,
851 Hilden, Germany) implemented on a Hamilton STAR robotic platform and after a bead-beating
852 step on a TissueLyzer II (Qiagen) in 96-deep well plates. Negative extraction controls were
853 included to ensure that no exogenous DNA contaminated the samples during extraction. DNA
854 quality control/quality assurance was performed using spectrophotometric measurements on a
855 NanoDrop (ThermoFisher Scientific) and gel electrophoresis.

856

857 **16S rRNA gene amplicon sequencing**

858 Using a dual-indexing strategy for multiplexed sequencing developed at the Institute for Genome
859 Sciences and described in detail elsewhere [85, 86], the V3-V4 hypervariable region of the 16S
860 rRNA gene was PCR amplified and sequenced on the Illumina MiSeq (Illumina, San Diego, CA).
861 PCR reactions were set up in 96-well microtiter plates using 319F (5′ -
862 ACTCCTACGGGAGGCAGCAG - 3′) and 806R (5′ - GGACTACHVGGGTWTCTAAT - 3′) as
863 universal primers, each with a linker sequence required for Illumina MiSeq 300bp paired-end
864 sequencing, and a 12-bp heterogeneity-spacer index sequence to minimize biases associated
865 with low-diversity amplicon sequencing [85, 86]. Reactions were performed using Phusion High-
866 Fidelity DNA polymerase (ThermoFisher Scientific) and 50 ng of template DNA in a total reaction
867 volume of 25 µl. PCR-negative controls without DNA template were performed for each primer
868 pair. The following cycling parameters were used: 30 seconds at 98°C, followed by 30 cycles of
869 10 seconds at 98°C, 15 seconds at 66°C, and 15 seconds at 72 °C, with a final step of 10 minutes

870 at 72 °C. Successful amplification was confirmed using gel electrophoresis, after which amplicon
871 cleanup and normalization was performed using the SequalPrep Normalization Plate kit
872 (Invitrogen). A total of 25 ng of 16S PCR amplicons from each sample was pooled, and
873 sequencing was performed using the Illumina MiSeq (Illumina) according to the manufacturer's
874 protocol.

875

876 **Microbiota analysis**

877 After screening 16S rRNA gene reads for low-quality bases and short read lengths [85, 86],
878 paired-end read pairs were assembled using PANDAseq [87], demultiplexed, trimmed of artificial
879 barcodes and primers, and assessed for chimeras using UCHIME in *de novo* mode implemented
880 in Quantitative Insights Into Microbial Ecology (QIIME; release v. 1.9.1) [88]. The resulting quality
881 trimmed sequences were then clustered *de novo* into OTUs with the GreenGenes 16S database
882 (v. 13.8) in QIIME, with a minimum confidence threshold of 0.97. Taxonomic ranks were assigned
883 to each sequence using the Ribosomal Database Project [89] Naïve Bayesian Classifier v.2.2 [90]
884 trained on the Greengenes database (Aug 2013 version) [91], using a confidence value cutoff of
885 0.8. To account for uneven sampling depth and to ensure less biases than the standard approach
886 (total sum normalization), data were normalized with metagenomeSeq's cumulative sum scaling
887 (CSS) [92] when appropriate. Sequencing analyses includes denoising, *de novo*, and reference-
888 based chimera detection were conducted with UCHIME v5.1 [93]. R packages of Vegan [94],
889 Phyloseq [95], Bioconductor [96], metagenomeSeq [92] and ggplot2 [97] were used for the
890 following analyses. The α diversity (within-sample diversity) was estimated using the Shannon
891 diversity index [98]. β-Diversity (between-sample diversity) was determined through
892 multidimensional scaling (MDS) plots using Jensen–Shannon divergence distance to visualize
893 the level of divergence at the different sampling times. Jensen-Shannon divergence is a
894 measurement of dissimilarity between probability distribution, and the Jensen-Shannon metric is
895 the square root of the normalized Jensen-Shannon divergence value [99, 100].

896

REFERENCES

1. Gago M, Cornell LD, Kremers WK, Stegall MD, Cosio FG: **Kidney allograft inflammation and fibrosis, causes and consequences.** *Am J Transplant* 2012, **12:**1199-1207.

2. Israni AK, Leduc R, Jacobson PA, Wildebush W, Guan W, Schladt D, Matas AJ, Oetting WS, De KAFGI: **Inflammation in the setting of chronic allograft dysfunction post-kidney transplant: phenotype and genotype.** *Clin Transplant* 2013, **27:**348-358.

3. Moreso F, Seron D, O'Valle F, Ibernon M, Goma M, Hueso M, Cruzado JM, Bestard O, Duarte V, del Moral RG, Grinyo JM: **Immunephenotype of glomerular and interstitial infiltrating cells in protocol renal allograft biopsies and histological diagnosis.** *Am J Transplant* 2007, **7:**2739-2747.

4. Asleh R, Briasoulis A, Pereira NL, Edwards BS, Frantz RP, Daly RC, Lerman A, Kushwaha SS: **Hypercholesterolemia after conversion to sirolimus as primary immunosuppression and cardiac allograft vasculopathy in heart transplant recipients.** *J Heart Lung Transplant* 2018.

5. Jansen MA, Otten HG, de Weger RA, Huibers MM: **Immunological and Fibrotic Mechanisms in Cardiac Allograft Vasculopathy.** *Transplantation* 2015, **99:**2467-2475.

6. Kim M, Bergmark BA, Zelniker TA, Mehra MR, Stewart GC, Page DS, Woodcome EL, Smallwood JA, Gabardi S, Givertz MM: **Early aspirin use and the development of cardiac allograft vasculopathy.** *J Heart Lung Transplant* 2017, **36:**1344-1349.

7. Mehra MR: **The scourge and enigmatic journey of cardiac allograft vasculopathy.** *J Heart Lung Transplant* 2017, **36:**1291-1293.

8. Lamb KE, Lodhi S, Meier-Kriesche HU: **Long-term renal allograft survival in the United States: a critical reappraisal.** *Am J Transplant* 2011, **11:**450-462.

9. Sellares J, de Freitas DG, Mengel M, Sis B, Hidalgo LG, Matas AJ, Kaplan B, Halloran PF: **Inflammation lesions in kidney transplant biopsies: association with survival is due to the underlying diseases.** *Am J Transplant* 2011, **11:**489-499.

10. Koren O, Spor A, Felin J, Fak F, Stombaugh J, Tremaroli V, Behre CJ, Knight R, Fagerberg B, Ley RE, Backhed F: **Human oral, gut, and plaque microbiota in patients with atherosclerosis.** *Proc Natl Acad Sci U S A* 2011, **108 Suppl 1:**4592-4598.

11. Wang D, Xia M, Yan X, Li D, Wang L, Xu Y, Jin T, Ling W: **Gut microbiota metabolism of anthocyanin promotes reverse cholesterol transport in mice via repressing miRNA-10b.** *Circ Res* 2012, **111:**967-981.

12. Atkinson MA, Chervonsky A: **Does the gut microbiota have a role in type 1 diabetes? Early evidence from humans and animal models of the disease.** *Diabetologia* 2012, **55:**2868-2877.

13. Hooper LV, Littman DR, Macpherson AJ: **Interactions between the microbiota and the immune system.** *Science* 2012, **336:**1268-1273.

934 14. Sonnenberg GF, Monticelli LA, Alenghat T, Fung TC, Hutnick NA, Kunisawa J, Shibata N,
935 Grunberg S, Sinha R, Zahm AM, et al: **Innate lymphoid cells promote anatomical**
936 **containment of lymphoid-resident commensal bacteria.** *Science* 2012, **336:**1321-1325.

937 15. Abt MC, Osborne LC, Monticelli LA, Doering TA, Alenghat T, Sonnenberg GF, Paley MA,
938 Antenus M, Williams KL, Erikson J, et al: **Commensal bacteria calibrate the activation**
939 **threshold of innate antiviral immunity.** *Immunity* 2012, **37:**158-170.

940 16. Chung H, Pamp SJ, Hill JA, Surana NK, Edelman SM, Troy EB, Reading NC, Villablanca
941 EJ, Wang S, Mora JR, et al: **Gut immune maturation depends on colonization with a**
942 **host-specific microbiota.** *Cell* 2012, **149:**1578-1593.

943 17. Josefowicz SZ, Niec RE, Kim HY, Treuting P, Chinen T, Zheng Y, Umetsu DT, Rudensky
944 AY: **Extrathymically generated regulatory T cells control mucosal TH2 inflammation.**
945 *Nature* 2012, **482:**395-399.

946 18. Atarashi K, Tanoue T, Shima T, Imaoka A, Kuwahara T, Momose Y, Cheng G, Yamasaki S,
947 Saito T, Ohba Y, et al: **Induction of colonic regulatory T cells by indigenous**
948 **Clostridium species.** *Science* 2011, **331:**337-341.

949 19. Geuking MB, Cahenzli J, Lawson MA, Ng DC, Slack E, Hapfelmeier S, McCoy KD,
950 Macpherson AJ: **Intestinal bacterial colonization induces mutualistic regulatory T cell**
951 **responses.** *Immunity* 2011, **34:**794-806.

952 20. Shankar J, Nguyen MH, Crespo MM, Kwak EJ, Lucas SK, McHugh KJ, Mounaud S, Alcorn
953 JF, Pilewski JM, Shigemura N, et al: **Looking Beyond Respiratory Cultures:**
954 **Microbiome-Cytokine Signatures of Bacterial Pneumonia and Tracheobronchitis in**
955 **Lung Transplant Recipients.** *Am J Transplant* 2016, **16:**1766-1778.

956 21. Kakihana K, Fujioka Y, Suda W, Najima Y, Kuwata G, Sasajima S, Mimura I, Morita H,
957 Sugiyama D, Nishikawa H, et al: **Fecal microbiota transplantation for patients with**
958 **steroid-resistant acute graft-versus-host disease of the gut.** *Blood* 2016, **128:**2083-
959 2088.

960 22. Lei YM, Chen L, Wang Y, Stefka AT, Molinero LL, Theriault B, Aquino-Michaels K, Sivan
961 AS, Nagler CR, Gajewski TF, et al: **The composition of the microbiota modulates**
962 **allograft rejection.** *J Clin Invest* 2016, **126:**2736-2744.

963 23. Hossain MS, Jaye DL, Pollack BP, Farris AB, Tselanyane ML, David E, Roback JD, Gewirtz
964 AT, Waller EK: **Flagellin, a TLR5 agonist, reduces graft-versus-host disease in**
965 **allogeneic hematopoietic stem cell transplantation recipients while enhancing**
966 **antiviral immunity.** *J Immunol* 2011, **187:**5130-5140.

967 24. Jenq RR, Ubeda C, Taur Y, Menezes CC, Khanin R, Dudakov JA, Liu C, West ML, Singer
968 NV, Equinda MJ, et al: **Regulation of intestinal inflammation by microbiota following**
969 **allogeneic bone marrow transplantation.** *J Exp Med* 2012, **209:**903-911.

970 25. Oh PL, Martinez I, Sun Y, Walter J, Peterson DA, Mercer DF: **Characterization of the ileal**
971 **microbiota in rejecting and nonrejecting recipients of small bowel transplants.** *Am J*
972 *Transplant* 2012, **12:**753-762.

973 26. Fricke WF, Maddox C, Song Y, Bromberg JS: **Human microbiota characterization in the**
974 **course of renal transplantation.** *Am J Transplant* 2014, **14:**416-427.

975 27. Dickson RP, Erb-Downward JR, Freeman CM, Walker N, Scales BS, Beck JM, Martinez FJ,
976 Curtis JL, Lama VN, Huffnagle GB: **Changes in the lung microbiome following lung**
977 **transplantation include the emergence of two distinct Pseudomonas species with**
978 **distinct clinical associations.** *PLoS One* 2014, **9:**e97214.

979 28. Lee JR, Muthukumar T, Dadhania D, Taur Y, Jenq RR, Toussaint NC, Ling L, Pamer E,
980 Suthanthiran M: **Gut microbiota and tacrolimus dosing in kidney transplantation.** *PLoS*
981 *One* 2015, **10:**e0122399.

982 29. Lee JR, Muthukumar T, Dadhania D, Toussaint NC, Ling L, Pamer E, Suthanthiran M: **Gut**
983 **microbial community structure and complications after kidney transplantation: a**
984 **pilot study.** *Transplantation* 2014, **98:**697-705.

985 30. Lemahieu W, Maes B, Verbeke K, Rutgeerts P, Geboes K, Vanrenterghem Y: **Cytochrome**
986 **P450 3A4 and P-glycoprotein activity and assimilation of tacrolimus in transplant**
987 **patients with persistent diarrhea.** *Am J Transplant* 2005, **5:**1383-1391.

988 31. Willner DL, Hugenholtz P, Yerkovich ST, Tan ME, Daly JN, Lachner N, Hopkins PM,
989 Chambers DC: **Reestablishment of recipient-associated microbiota in the lung**
990 **allograft is linked to reduced risk of bronchiolitis obliterans syndrome.** *Am J Respir*
991 *Crit Care Med* 2013, **187:**640-647.

992 32. Dethlefsen L, Relman DA: **Incomplete recovery and individualized responses of the**
993 **human distal gut microbiota to repeated antibiotic perturbation.** *Proc Natl Acad Sci U*
994 *S A* 2011, **108 Suppl 1:**4554-4561.

995 33. von Rosenvinge EC, Song Y, White JR, Maddox C, Blanchard T, Fricke WF: **Immune**
996 **status, antibiotic medication and pH are associated with changes in the stomach**
997 **fluid microbiota.** *ISME J* 2013, **7:**1354-1366.

998 34. Vrbanac A, Patras KA, Jarmusch AK, Mills RH, Shing SR, Quinn RA, Vargas F, Gonzalez
999 DJ, Dorrestein PC, Knight R, Nizet V: **Evaluating Organism-Wide Changes in the**
1000 **Metabolome and Microbiome following a Single Dose of Antibiotic.** *mSystems* 2020, **5**.

1001 35. Bromberg JS, Hittle LE, Xiong Y, Saxena V, Smyth EM, Li L, Zhang T, Wagner C, Fricke
1002 WF, Simon T, et al: **Gut microbiota–dependent modulation of innate immunity and**
1003 **lymph node remodeling affects cardiac allograft outcomes.** *JCI Insight* 2018, **3**.

1004 36. Falony G, Joossens M, Vieira-Silva S, Wang J, Darzi Y, Faust K, Kurilshikov A, Bonder MJ,
1005 Valles-Colomer M, Vandeputte D, et al: **Population-level analysis of gut microbiome**
1006 **variation.** *Science* 2016, **352:**560-564.

1007 37. Manichanh C, Reeder J, Gibert P, Varela E, Llopis M, Antolin M, Guigo R, Knight R,
1008 Guarner F: **Reshaping the gut microbiome with bacterial transplantation and**
1009 **antibiotic intake.** *Genome Res* 2010, **20:**1411-1419.

1010 38. Zhernakova A, Kurilshikov A, Bonder MJ, Tigchelaar EF, Schirmer M, Vatanen T, Mujagic
1011 Z, Vila AV, Falony G, Vieira-Silva S, et al: **Population-based metagenomics analysis**

1012 **reveals markers for gut microbiome composition and diversity.** *Science* 2016,
1013 **352:**565-569.

1014 39. Fonseca DM, Hand TW, Han SJ, Gerner MY, Glatman Zaretsky A, Byrd AL, Harrison OJ,
1015 Ortiz AM, Quinones M, Trinchieri G, et al: **Microbiota-Dependent Sequelae of Acute**
1016 **Infection Compromise Tissue-Specific Immunity.** *Cell* 2015, **163:**354-366.

1017 40. Ruiz L, Delgado S, Ruas-Madiedo P, Sanchez B, Margolles A: **Bifidobacteria and Their**
1018 **Molecular Communication with the Immune System.** *Front Microbiol* 2017, **8:**2345.

1019 41. Fanning S, Hall LJ, Cronin M, Zomer A, MacSharry J, Goulding D, Motherway MO,
1020 Shanahan F, Nally K, Dougan G, van Sinderen D: **Bifidobacterial surface-**
1021 **exopolysaccharide facilitates commensal-host interaction through immune**
1022 **modulation and pathogen protection.** *Proc Natl Acad Sci U S A* 2012, **109:**2108-2113.

1023 42. Yan Y, Drew DA, Markowitz A, Lloyd-Price J, Abu-Ali G, Nguyen LH, Tran C, Chung DC,
1024 Gilpin KK, Meixell D, et al: **Structure of the Mucosal and Stool Microbiome in Lynch**
1025 **Syndrome.** *Cell Host Microbe* 2020, **27:**585-600 e584.

1026 43. Rooks MG, Veiga P, Wardwell-Scott LH, Tickle T, Segata N, Michaud M, Gallini CA, Beal
1027 C, van Hylckama-Vlieg JE, Ballal SA, et al: **Gut microbiome composition and function in**
1028 **experimental colitis during active disease and treatment-induced remission.** *ISME J*
1029 2014, **8:**1403-1417.

1030 44. Ma B, Gavzy SJ, Saxena V, Song Y, Piao W, Lwin HW, Lakhan R, Lyyathurai J, Li L,
1031 France M, et al: **Strain-specific alterations in gut microbiome and host immune**
1032 **responses elicited by Bifidobacterium pseudolongum.** *bioRxiv*
1033 2022**:**2022.2003.2016.484607.

1034 45. Bromberg JS, Hittle L, Xiong Y, Saxena V, Smyth EM, Li L, Zhang T, Wagner C, Fricke WF,
1035 Simon T, et al: **Gut microbiota-dependent modulation of innate immunity and lymph**
1036 **node remodeling affects cardiac allograft outcomes.** *JCI Insight* 2018, **3**.

1037 46. Peterson LW, Artis D: **Intestinal epithelial cells: regulators of barrier function and**
1038 **immune homeostasis.** *Nat Rev Immunol* 2014, **14:**141-153.

1039 47. Vancamelbeke M, Vermeire S: **The intestinal barrier: a fundamental role in health and**
1040 **disease.** *Expert Rev Gastroenterol Hepatol* 2017, **11:**821-834.

1041 48. Cantoni C, Lin Q, Dorsett Y, Ghezzi L, Liu Z, Pan Y, Chen K, Han Y, Li Z, Xiao H, et al:
1042 **Alterations of host-gut microbiome interactions in multiple sclerosis.** *EBioMedicine*
1043 2022, **76:**103798.

1044 49. Lloyd-Price J, Arze C, Ananthakrishnan AN, Schirmer M, Avila-Pacheco J, Poon TW,
1045 Andrews E, Ajami NJ, Bonham KS, Brislawn CJ, et al: **Multi-omics of the gut microbial**
1046 **ecosystem in inflammatory bowel diseases.** *Nature* 2019, **569:**655-662.

1047 50. van Dieren JM, Lambers ME, Kuipers EJ, Samsom JN, van der Woude CJ, Nieuwenhuis
1048 EE: **Local immune regulation of mucosal inflammation by tacrolimus.** *Dig Dis Sci*
1049 2010, **55:**2514-2519.

1050 51. Ormerod KL, Wood DL, Lachner N, Gellatly SL, Daly JN, Parsons JD, Dal'Molin CG,
1051 Palfreyman RW, Nielsen LK, Cooper MA, et al: **Genomic characterization of the**
1052 **uncultured Bacteroidales family S24-7 inhabiting the guts of homeothermic animals.**
1053 *Microbiome* 2016, **4:**36.

1054 52. Everard A, Belzer C, Geurts L, Ouwerkerk JP, Druart C, Bindels LB, Guiot Y, Derrien M,
1055 Muccioli GG, Delzenne NM, et al: **Cross-talk between Akkermansia muciniphila and**
1056 **intestinal epithelium controls diet-induced obesity.** *Proc Natl Acad Sci U S A* 2013,
1057 **110:**9066-9071.

1058 53. Swarte JC, Li Y, Hu S, Bjork JR, Gacesa R, Vich Vila A, Douwes RM, Collij V, Kurilshikov
1059 A, Post A, et al: **Gut microbiome dysbiosis is associated with increased mortality after**
1060 **solid organ transplantation.** *Sci Transl Med* 2022, **14:**eabn7566.

1061 54. Gavzy SJ, Lakhan R, Iyyathurai J, Saxena V, Li L, Ma B, Mongodin E, Bromberg JS:
1062 **Immunosuppressants Alter Lymph Node Architecture and Create Distinct**
1063 **Microbiome Footprints [abstract].** *Am J Transplant* 2022, **22**.

1064 55. Gavzy S, Lakhan R, Iyyathurai J, Saxena V, Lee ZL, Ma B, Mongodin E, Bromberg JS: **Pro-**
1065 **and Anti-Tolerogenic Microbiota Contribute to Distinct Gut Metabolomes and**
1066 **Downstream Immune Responses.** *Am J Transplant* 2022, **22**.

1067 56. Sorbara MT, Pamer EG: **Interbacterial mechanisms of colonization resistance and the**
1068 **strategies pathogens use to overcome them.** *Mucosal Immunol* 2019, **12:**1-9.

1069 57. Maldonado-Gomez MX, Martinez I, Bottacini F, O'Callaghan A, Ventura M, van Sinderen D,
1070 Hillmann B, Vangay P, Knights D, Hutkins RW, Walter J: **Stable Engraftment of**
1071 **Bifidobacterium longum AH1206 in the Human Gut Depends on Individualized**
1072 **Features of the Resident Microbiome.** *Cell Host Microbe* 2016, **20:**515-526.

1073 58. Gabarre P, Loens C, Tamzali Y, Barrou B, Jaisser F, Tourret J: **Immunosuppressive**
1074 **therapy after solid organ transplantation and the gut microbiota: Bidirectional**
1075 **interactions with clinical consequences.** *Am J Transplant* 2022, **22:**1014-1030.

1076 59. Medina M, Izquierdo E, Ennahar S, Sanz Y: **Differential immunomodulatory properties**
1077 **of Bifidobacterium logum strains: relevance to probiotic selection and clinical**
1078 **applications.** *Clin Exp Immunol* 2007, **150:**531-538.

1079 60. Yang C, Mogno I, Contijoch EJ, Borgerding JN, Aggarwala V, Li Z, Siu S, Grasset EK,
1080 Helmus DS, Dubinsky MC, et al: **Fecal IgA Levels Are Determined by Strain-Level**
1081 **Differences in Bacteroides ovatus and Are Modifiable by Gut Microbiota**
1082 **Manipulation.** *Cell Host Microbe* 2020, **27:**467-475 e466.

1083 61. Reid G, Younes JA, Van der Mei HC, Gloor GB, Knight R, Busscher HJ: **Microbiota**
1084 **restoration: natural and supplemented recovery of human microbial communities.**
1085 *Nat Rev Microbiol* 2011, **9:**27-38.

1086 62. Palm NW, de Zoete MR, Cullen TW, Barry NA, Stefanowski J, Hao L, Degnan PH, Hu J,
1087 Peter I, Zhang W, et al: **Immunoglobulin A coating identifies colitogenic bacteria in**
1088 **inflammatory bowel disease.** *Cell* 2014, **158:**1000-1010.

1089 63. Bunker JJ, Flynn TM, Koval JC, Shaw DG, Meisel M, McDonald BD, Ishizuka IE, Dent AL,
1090 Wilson PC, Jabri B, et al: **Innate and Adaptive Humoral Responses Coat Distinct**
1091 **Commensal Bacteria with Immunoglobulin A.** *Immunity* 2015, **43:**541-553.

1092 64. Risely A: **Applying the core microbiome to understand host-microbe systems.** *J Anim*
1093 *Ecol* 2020, **89:**1549-1558.

1094 65. Rosales IA, Yang C, Farkash EA, Ashry T, Ge J, Aljabban I, Ayyar A, Ndishabandi D, White
1095 R, Gildner E, et al: **Novel intragraft regulatory lymphoid structures in kidney allograft**
1096 **tolerance.** *Am J Transplant* 2022, **22:**705-716.

1097 66. Honda M, Surewaard BGJ, Watanabe M, Hedrick CC, Lee WY, Brown K, McCoy KD,
1098 Kubes P: **Perivascular localization of macrophages in the intestinal mucosa is**
1099 **regulated by Nr4a1 and the microbiome.** *Nat Commun* 2020, **11:**1329.

1100 67. Martinez-Lopez M, Iborra S, Conde-Garrosa R, Mastrangelo A, Danne C, Mann ER, Reid
1101 DM, Gaboriau-Routhiau V, Chaparro M, Lorenzo MP, et al: **Microbiota Sensing by**
1102 **Mincle-Syk Axis in Dendritic Cells Regulates Interleukin-17 and -22 Production and**
1103 **Promotes Intestinal Barrier Integrity.** *Immunity* 2019, **50:**446-461 e449.

1104 68. Chyou S, Benahmed F, Chen J, Kumar V, Tian S, Lipp M, Lu TT: **Coordinated regulation**
1105 **of lymph node vascular-stromal growth first by CD11c+ cells and then by T and B**
1106 **cells.** *J Immunol* 2011, **187:**5558-5567.

1107 69. Kumar V, Dasoveanu DC, Chyou S, Tzeng TC, Rozo C, Liang Y, Stohl W, Fu YX, Ruddle
1108 NH, Lu TT: **A dendritic-cell-stromal axis maintains immune responses in lymph**
1109 **nodes.** *Immunity* 2015, **42:**719-730.

1110 70. Saito Y, Respatika D, Komori S, Washio K, Nishimura T, Kotani T, Murata Y, Okazawa H,
1111 Ohnishi H, Kaneko Y, et al: **SIRPalpha(+) dendritic cells regulate homeostasis of**
1112 **fibroblastic reticular cells via TNF receptor ligands in the adult spleen.** *Proc Natl Acad*
1113 *Sci U S A* 2017, **114:**E10151-E10160.

1114 71. Komori S, Saito Y, Respatika D, Nishimura T, Kotani T, Murata Y, Matozaki T:
1115 **SIRPalpha(+) dendritic cells promote the development of fibroblastic reticular cells in**
1116 **murine peripheral lymph nodes.** *Eur J Immunol* 2019, **49:**1364-1371.

1117 72. Warren KJ, Iwami D, Harris DG, Bromberg JS, Burrell BE: **Laminins affect T cell**
1118 **trafficking and allograft fate.** *J Clin Invest* 2014, **124:**2204-2218.

1119 73. Li L, Shirkey MW, Zhang T, Xiong Y, Piao W, Saxena V, Paluskievicz C, Lee Y, Toney N,
1120 Cerel BM, et al: **The lymph node stromal laminin alpha5 shapes alloimmunity.** *J Clin*
1121 *Invest* 2020, **130:**2602-2619.

1122 74. Simon T, Li L, Wagner C, Zhang T, Saxena V, Brinkman CC, Tostanoski LH, Ostrand-
1123 Rosenberg S, Jewell C, Shea-Donohue T, et al: **Differential Regulation of T-cell**
1124 **Immunity and Tolerance by Stromal Laminin Expressed in the Lymph Node.**
1125 *Transplantation* 2019, **103:**2075-2089.

1126 75. Grubin CE, Kovats S, deRoos P, Rudensky AY: **Deficient positive selection of CD4 T**
1127 **cells in mice displaying altered repertoires of MHC class II-bound self-peptides.**
1128 *Immunity* 1997, **7:**197-208.

1129 76. Bhan AK, Mizoguchi E, Smith RN, Mizoguchi A: **Colitis in transgenic and knockout**
1130 **animals as models of human inflammatory bowel disease.** *Immunol Rev* 1999,
1131 **169:**195-207.

1132 77. Prinz I, Klemm U, Kaufmann SH, Steinhoff U: **Exacerbated colitis associated with**
1133 **elevated levels of activated CD4+ T cells in TCRalpha chain transgenic mice.**
1134 *Gastroenterology* 2004, **126:**170-181.

1135 78. Mongodin EF, Hittle LL, Nadendla S, Brinkman CC, Xiong Y, Bromberg JS: **Complete**
1136 **Genome Sequence of a Strain of Bifidobacterium pseudolongum Isolated from**
1137 **Mouse Feces and Associated with Improved Organ Transplant Outcome.** *Genome*
1138 *Announc* 2017, **5**.

1139 79. Lutz MB, Kukutsch N, Ogilvie ALJ, Rößner S, Koch F, Romani N, Schuler G: **An advanced**
1140 **culture method for generating large quantities of highly pure dendritic cells from**
1141 **mouse bone marrow.** *Journal of Immunological Methods* 1999, **223:**77-92.

1142 80. Zhang X, Goncalves R, Mosser DM: **The isolation and characterization of murine**
1143 **macrophages.** *Curr Protoc Immunol* 2008, **Chapter 14:**Unit 14 11.

1144 81. Murase N, Todo S, Lee PH, Lai HS, Chapman F, Nalesnik MA, Makowka L, Starzl TE:
1145 **Heterotopic heart transplantation in the rat receiving FK-506 alone or with**
1146 **cyclosporine.** *Transplant Proc* 1987, **19:**71-75.

1147 82. Ochiai T, Sakamoto K, Nagata M, Nakajima K, Goto T, Hori S, Kenmochi T, Nakagori T,
1148 Asano T, Isono K: **Studies on FK506 in experimental organ transplantation.** *Transplant*
1149 *Proc* 1988, **20:**209-214.

1150 83. Nagano H, Mitchell RN, Taylor MK, Hasegawa S, Tilney NL, Libby P: **Interferon-gamma**
1151 **deficiency prevents coronary arteriosclerosis but not myocardial rejection in**
1152 **transplanted mouse hearts.** *J Clin Invest* 1997, **100:**550-557.

1153 84. Napolitano LM, Koruda MJ, Meyer AA, Baker CC: **The impact of femur fracture with**
1154 **associated soft tissue injury on immune function and intestinal permeability.** *Shock*
1155 1996, **5:**202-207.

1156 85. Fadrosh DW, Ma B, Gajer P, Sengamalay N, Ott S, Brotman RM, Ravel J: **An improved**
1157 **dual-indexing approach for multiplexed 16S rRNA gene sequencing on the Illumina**
1158 **MiSeq platform.** *Microbiome* 2014, **2:**1-7.

1159 86. Holm JB, Humphrys MS, Robinson CK, Settles ML, Ott S, Fu L, Yang H, Gajer P, He X,
1160 McComb E, et al: **Ultrahigh-Throughput Multiplexing and Sequencing of >500-Base-**
1161 **Pair Amplicon Regions on the Illumina HiSeq 2500 Platform.** *mSystems* 2019, **4**.

1162 87. Masella AP, Bartram AK, Truszkowski JM, Brown DG, Neufeld JD: **PANDAseq: paired-**
1163 **end assembler for illumina sequences.** *BMC Bioinformatics* 2012, **13:**31.

1164 88. Caporaso JG, Kuczynski J, Stombaugh J, Bittinger K, Bushman FD, Costello EK, Fierer N,
1165 Pena AG, Goodrich JK, Gordon JI: **QIIME allows analysis of high-throughput**
1166 **community sequencing data.** *Nature methods* 2010, **7:**335-336.

1167 89. Cole JR, Wang Q, Cardenas E, Fish J, Chai B, Farris RJ, Kulam-Syed-Mohideen AS,
1168 McGarrell DM, Marsh T, Garrity GM, Tiedje JM: **The Ribosomal Database Project:**
1169 **improved alignments and new tools for rRNA analysis.** *Nucleic Acids Res* 2009,
1170 **37:**D141-145.

1171 90. Wang Q, Garrity GM, Tiedje JM, Cole JR: **Naive Bayesian classifier for rapid**
1172 **assignment of rRNA sequences into the new bacterial taxonomy.** *Appl Environ*
1173 *Microbiol* 2007, **73:**5261-5267.

1174 91. McDonald D, Price MN, Goodrich J, Nawrocki EP, DeSantis TZ, Probst A, Andersen GL,
1175 Knight R, Hugenholtz P: **An improved Greengenes taxonomy with explicit ranks for**
1176 **ecological and evolutionary analyses of bacteria and archaea.** *The ISME journal* 2012,
1177 **6:**610-618.

1178 92. Paulson JN, Pop M, Bravo HC, Paulson MJN, OTU TU, biocViews Bioinformatics D:
1179 **Package 'metagenomeSeq'.** 2013.

1180 93. Edgar RC, Haas BJ, Clemente JC, Quince C, Knight R: **UCHIME improves sensitivity and**
1181 **speed of chimera detection.** *Bioinformatics* 2011, **27:**2194-2200.

1182 94. Oksanen J, Kindt R, Legendre P, O'Hara B, Stevens MHH, Oksanen MJ, Suggests M: **The**
1183 **vegan package.** *Community ecology package* 2007**:**631-637.

1184 95. McMurdie PJ, Holmes S: **phyloseq: an R package for reproducible interactive analysis**
1185 **and graphics of microbiome census data.** 2013.

1186 96. Huber W, Carey VJ, Gentleman R, Anders S, Carlson M, Carvalho BS, Bravo HC, Davis S,
1187 Gatto L, Girke T: **Orchestrating high-throughput genomic analysis with Bioconductor.**
1188 *Nature methods* 2015, **12:**115-121.

1189 97. Wickham H: *ggplot2: elegant graphics for data analysis.* Springer Science & Business
1190 Media; 2009.

1191 98. Shannon CE: **A mathematical theory of communication.** *ACM SIGMOBILE Mobile*
1192 *Computing and Communications Review* 2001, **5:**3-55.

1193 99. Gajer P, Brotman RM, Bai G, Sakamoto J, Schutte UM, Zhong X, Koenig SS, Fu L, Ma ZS,
1194 Zhou X, et al: **Temporal dynamics of the human vaginal microbiota.** *Science*
1195 *translational medicine* 2012, **4:**132ra152.

1196 100. Lin J: **Divergence measures based on the Shannon entropy.** *IEEE Transctions on*
1197 *Information Theory* 1991, **37:**145-151.
1198

CONTRIBUTIONS

B.M., E.F.M, J.S.B, S.J.G, and V.S. designed the experiments. S.J.G, A.K., V.S., R.L., J.I., L.W., H.D., Z.L.L., L.L., M.W.S., C.M.P., W.P., and Y.L conducted and analyzed the *in vitro* and *in vivo* experiments. T.Z. performed mouse microsurgery. L. H., H.W.L. performed bacteria cultivation and verification. B.M., E.M., J.S.B, S.J.G., and V.S. wrote the manuscript.

ACKNOWLEDGEMENTS

This work was supported by National Institute of Health (NIH) National Heart, Lung and Blood Institute award R01HL148672 (J.S.B./B.M.), U01AI170050 (B.M./J.S.B.), and NIH National Institute of Allergy and Infectious Diseases training grant T32AI95190-10 (S.J.G.). This manuscript has been released as a pre-print at bioRxiv XX. Emmanuel Mongodin, PhD, contributed to this work as an employee of the University of Maryland School of Medicine. The views expressed in this manuscript are his own and do not necessarily represent the views of the National Institutes of Health or the United States Government.

Data availability

The 16S rRNA gene sequencing data generated in this study was deposited to Genbank under BioProject PRJNA809764 (https://www.ncbi.nlm.nih.gov/bioproject/809764).

CONFLICT OF INTEREST STATEMENT

The authors have declared that no conflict of interest exists.

1220 **FIGURES**

1221

1222 **Figure 1. Effect of *Bifido* and *Desulfo* compared to normal SBT on cardiac graft**
1223 **inflammation and LN remodeling.** Mice given abx (6 days), then SBT (WT stool, *Bifido ATCC,*
1224 or *Desulfo*) on the day of heart transplant, followed by tacrolimus for 40 days. **(a)** Graft
1225 inflammation scores. **(b)** Foxp3+ Tregs, CD4, and CD8 T cells in the cardiac grafts. **(c)** Laminin
1226 α4, α5, and ratios in pLNs. **(d)** Flow cytometry for CD11c+ DC in pLN. IHC for **(e)** Foxp3+ Tregs,
1227 CD11c+ DC, and F4/80+ MΦ around HEV and in CR of mLN, **(f)** Foxp3+ Tregs, CD11c+ DC, and
1228 F4/80+ MΦ around HEV and in CR of pLN, **(g)** laminin α4 and α5 ratios in pLN and mLN; **(h)**
1229 intestine for F4/80+ MΦ, CD11c+ DC, and Foxp3+ Tregs. Mice given abx (6 days), SBT (WT stool,
1230 *Bifido MD,* or *Desulfo*) on the day of heart transplant, followed by tacrolimus for 60 days. Flow
1231 cytometry for **(i)** CD4+ T cells, CD8+ T cells, and B220+ B cells in spleen; **(j)** mLN B220+ B cells,
1232 and pLN F4/80+ MΦ. IHC of **(k)** Foxp3+ Tregs, F4/80+ MΦ, and CD11c+ DC in mLN; **(l)** Foxp3+
1233 Tregs, F4/80+ MΦ, and CD11c+ DC in pLN; **(m)** laminin α4:α5 ratios in mLN and pLN; and **(n)**
1234 Foxp3+ Tregs, CD11c+ DC, and F4/80+ MΦ in intestine. Three mice per group, at least 2 mLN,
1235 pLN, and sections of intestine at duodenal-jejunal junction per mouse, 3 sections/LN/staining
1236 panel. Ordinary one-way ANOVA with Tukey's multiple comparisons test. * $p < 0.05$; ** $p < 0.01$,
1237 *** $p < 0.001$, **** $p < 0.0001$.

1238

1239 **Figure 2. Changes in the distribution of lymphocytes and myeloid cells and LN structure**
1240 **due to abx and tacrolimus.** Mice given abx (6 days) with or without 2 days of tacrolimus. **(a)**
1241 Flow cytometry for mLN CD4+ T cells, CD8+ T cells, Foxp3+ Tregs, and B220+ B cells. IHC for
1242 **(b)** mLN Foxp3+ Tregs, CD11c+ DC, and F4/80+ MΦ around HEV and in CR; **(c)** pLN Foxp3+
1243 Tregs, CD11c+ DC, and F4/80+ MΦ around HEV and in CR; **(d)** laminin α4 and α5 and ratios in
1244 mLN and pLN; **(e)** intestine Foxp3+ Tregs, F4/80+ MΦ, and CD11c+ DC. Statistical analysis as
1245 in **Fig. 1**.

1246
1247 **Figure 3. Early changes in LN architecture and immune cell distribution due to SBT.** Mice
1248 given abx (6 days), then SBT (*PBS, Bifido ATCC, Bifido MD, or Desulfo*). After 3 days, LN, spleen,
1249 and intestinal segments harvested. **(a)** Flow cytometry of mLN CD4+ T cells, CD11c+ DCs, and
1250 F4/80+ MΦ; pLN CD8+ T cells, B220+ B cells, and CD11c+ DC; spleen F4/80+ MΦ. IHC for **(b)**
1251 mLN Foxp3+ Tregs, CD11c+ DC, and F4/80+ MΦ; **(c)** pLN Foxp3+ Tregs, CD11c+ DC, and
1252 F4/80+ MΦ; **(d)** laminin α4 and α5 and ratios in mLN and pLN; **(e)** intestine Foxp3+ Tregs,
1253 CD11c+ DC, and F4/80+ MΦ. Statistical analysis as in **Fig. 1**.

1254
1255 **Figure 4. Early changes in LN architecture and immune cell distribution due to SBT and**
1256 **tacrolimus.** Mice treated with abx (6 days), then SBT (*PBS, Bifido ATCC, Bifido MD, or Desulfo*),
1257 followed by tacrolimus for 2 days. After 3 days, LN and intestinal segments harvested for IHC.
1258 IHC for **(a)** mLN CR Foxp3+ Tregs, CD11c+ DC, and F4/80+ MΦ; **(b)** pLN Foxp3+ Tregs, CD11c+
1259 DC, and F4/80+ MΦ; **(c)** laminin α4 and α5 and ratios in mLN and pLN; (d) intestine Foxp3+
1260 Tregs, CD11c+ DC, and F4/80+ MΦ. Statistics as in **Fig. 1**.

1261

1262 **Figure 5. Changes in LN structure and immune cell distribution due to abx, SBT, heart**
1263 **transplant, and tacrolimus at 7 and 14 days. (a-d)** Mice given abx (6 days), then SBT
1264 (PBS/*Bifido*/*Desulfo*) on the day of heart transplant with injection of TEa T cells (2 x 10^5 cells i.v.),
1265 followed by tacrolimus for 7 days. IHC for **(a)** mLN Foxp3+ Tregs, CD11c+ DC, and F4/80+ MΦ;
1266 **(b)** pLN Foxp3+ Tregs, CD11c+ DC, and F4/80+ MΦ; **(c)** laminin α4 and α5 and ratios in mLN
1267 and pLN; **(d)** intestine Foxp3+ Tregs, CD11c+ DC, and F4/80+ MΦ. **(e-h)** Mice given abx (6 days),
1268 then SBT (PBS/*Bifido*/*Desulfo*) on the day of heart transplant with injection of TEa T cells (2 x 105
1269 cells i.v.), followed by tacrolimus for 14 days. IHC for **(e)** mLN Foxp3+ Tregs, CD11c+ DC, and
1270 F4/80+ MΦ; **(f)** pLN Foxp3+ Tregs, CD11c+ DC, and F4/80+ MΦ; **(g)** laminin α4 and α5 and ratios

1271 in mLN and pLN; **(h)** intestine Foxp3+ Tregs, CD11c+ DC, and F4/80+ MΦ. Statistics as in **Fig.**
1272 **1**.
1273
1274 **Figure 6. Early changes in T cell and allograft responses due to abx, SBT, heart transplant,**
1275 **and tacrolimus at 7 and 14 days.** Mice given abx (6 days), then SBT (PBS/*Bifido*/*Desulfo*) on
1276 the day of heart transplant with injection of TEa T cells (2 x 10^5 cells i.v.), followed by tacrolimus
1277 for 7 days. **(a)** Flow cytometry of mLN, pLN, and spleen for CD4, TEa TCR, Foxp3, CD44, and
1278 CD69. **(b-f)** Mice given abx (6 days), then SBT (PBS/*Bifido/Desulfo*) on the day of heart transplant
1279 with injection of TEa T cells (2 x 105 cells i.v.), followed by tacrolimus for 14 days. Flow cytometry
1280 of TEa cells in mLN, pLN, and spleen for **(b)** % of overall cells, **(c)** Foxp3+ Tregs, **(d)** CD44 and
1281 CD69 markers, and **(e)** Treg:Teff ratio. **(f)** Cardiac allograft fibrosis by trichrome stain. Statistics
1282 for IHC as in **Fig. 1**.
1283
1284 **Figure 7. Effect of CCR2 antagonist RS504393 on LN remodeling and graft survival. Mice**
1285 **received heart transplant followed by RSS504393 or IgG control for 7 days**. **(a)** IHC of pLN
1286 laminin expression. **(b)** Kaplan Meier Survival Curves. RS504393 (MST 15.3 +/- 5.1; n=3), Control
1287 IgG (MST 6.7 +/- 0.5; n=5). Statistics for IHC as in **Fig. 1**.
1288
1289 **Figure 8. Changes in the distribution of lymphocytes and myeloid cells and LN structure**
1290 **due to abx, SBT and RS504393.** Mice received abx (6 days), then SBT (PBS, *Bifido*, or *Desulfo*),
1291 followed by RS504393 days for 7 days. **(a)** Flow cytometry of mLN Foxp3+ Tregs. IHC for **(b)**
1292 mLN Foxp3+ Tregs, CD11c+ DC, and F4/80+ MΦ; **(c)** pLN F4/80+ MΦ; **(d)** laminin α4 and α5
1293 and ratios in mLN and pLN; **(e)** intestine CD11c+ DC and F4/80+ MΦ. Statistics for IHC as in **Fig.**
1294 **1**. **(f)** Allograft survival in mice given abx (6 days), then SBT (PBS, *Bifido*, or *Desulfo*) on the day

1295 of heart transplant, followed by RS504393 for 7 days . Kaplan-Meier analysis with Log Rank
1296 Mantel-Cox test. (p=0.0033).
1297
1298 **Figure 9. Changes in the distribution of lymphocytes and myeloid cells and LN structure**
1299 **due to abx, SBT, tacrolimus and RS504393.** Mice received abx (6 days), then SBT, followed
1300 by tacrolimus and RS504393 for 7 days. IHC for **(a)** mLN Foxp3+ Tregs, CD11c+ DC, and F4/80+
1301 MΦ; **(b)** pLN Foxp3+ Tregs, CD11c+ DC, and F4/80+ MΦ; **(c)** laminin α4 and α5 and ratios in
1302 mLN and pLN; **(d)** intestine Foxp3+ Tregs, CD11c+ DC and F4/80+ MΦ. Statistics for IHC as in
1303 **Fig. 1**.
1304
1305 **Figure 10. Microbiota directly modulate activity of innate immune cells *in vitro*.** Bone
1306 marrow derived DCs (BMDCs) and freshly isolated peritoneal MΦ stimulated with UV-killed *Bifido*
1307 ATCC, *Bifido* MD, *Desulfo*, or media alone. After 24 hours **(a)** BMDC and **(b)** MΦ were analyzed
1308 by flow cytometry for MHC II, CD40, CD80, and CD86. **(c)** BMDC and **(d)** MΦ culture supernatants
1309 tested for IL-6, IL-10 and TNFα by ELISA. One-way ANOVA. * $p < 0.05$; ** $p < 0.01$, *** $p < 0.001$,
1310 **** $p < 0.0001$. Data representative of two separate experiments.
1311
1312 **Figure 11. Early changes in intestinal permeability are associated with abx, SBT, cardiac**
1313 **transplant, and tacrolimus. (a)** Mice given abx (6 days) or tacrolimus (2 days). **(b)** Mice given
1314 abx (6 days), then SBT (PBS/*Bifido/Desulfo*), followed by tacrolimus for 3 days. **(c-d)** Mice given
1315 abx (6 days), then SBT (PBS/*Bifido/Desulfo*) on the day of heart transplant with injection of TEa
1316 T cells (2 x 10^5 cells i.v.), followed by tacrolimus for **(c)** 7 or **(d)** 14 days post-transplant. 3
1317 mice/group. Serum samples analyzed in duplicate. Ordinary one-way ANOVA. * $p < 0.05$; ** $p <$
1318 0.01, *** $p < 0.001$, **** $p < 0.0001$.

1319 **Figure 12. Profound early influence of SBT on gut microbiota with subsequent loss of**
1320 **colonization and distinctive gut microbiota features after 2 weeks .** Mice given abx (6 days),
1321 then SBT (*Bifido* MD/*Desulfo*) or gavage with WT stool on the day of heart transplant, followed by
1322 tacrolimus for 40 days post-transplant. 3 mice/group. Stool pellets collected longitudinally through
1323 day 40. **(a)** The α diversity (within-sample diversity) was estimated using the Shannon diversity
1324 index [98]. **(b)** β-Diversity (between-sample diversity) was determined through multidimensional
1325 scaling plots using Jensen–Shannon divergence distance to visualize the level of divergence at
1326 the different sampling times.
1327
1328
1329
1330

1331

Figure 1

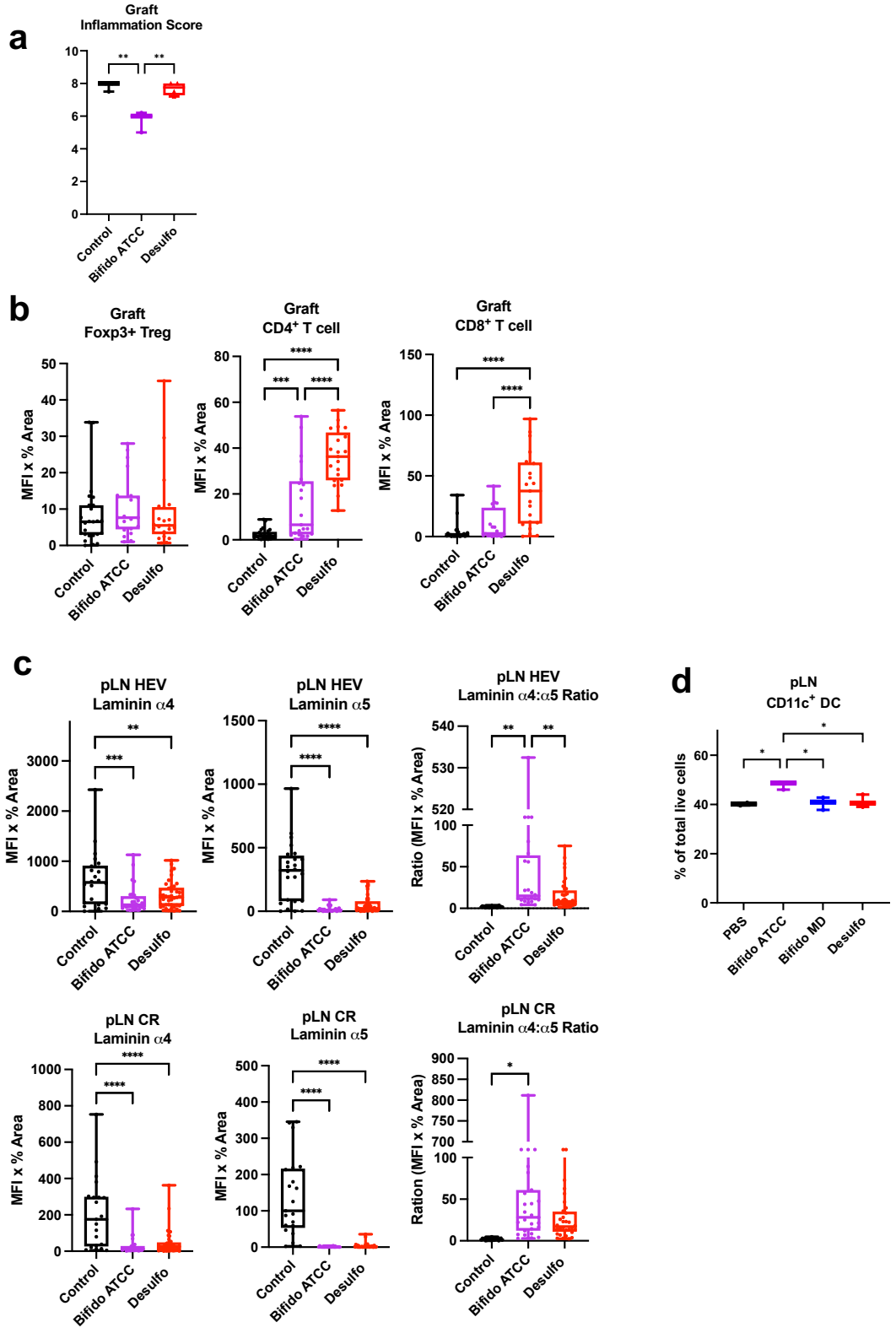

1332

Figure 1

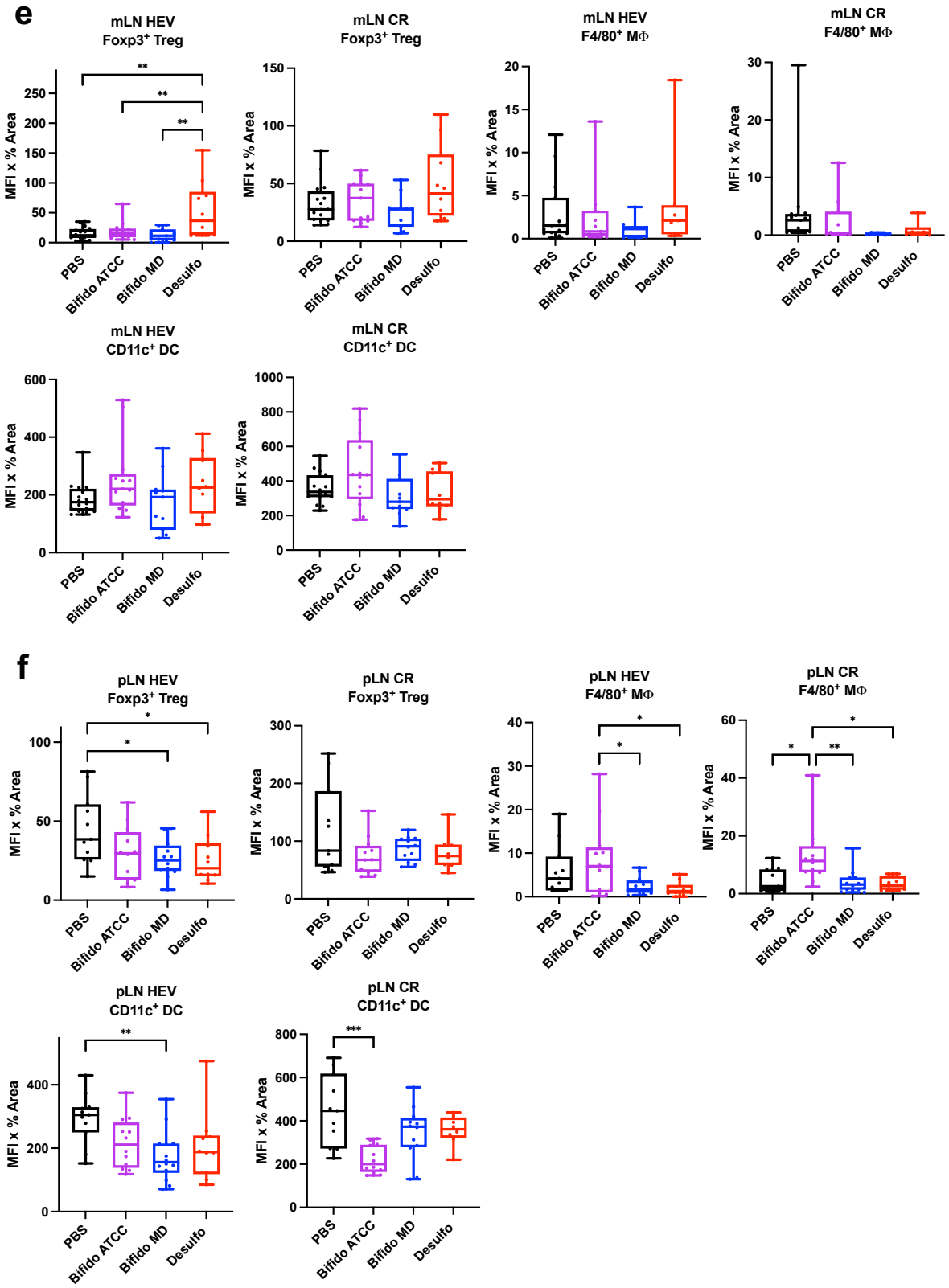

1333

Figure 1

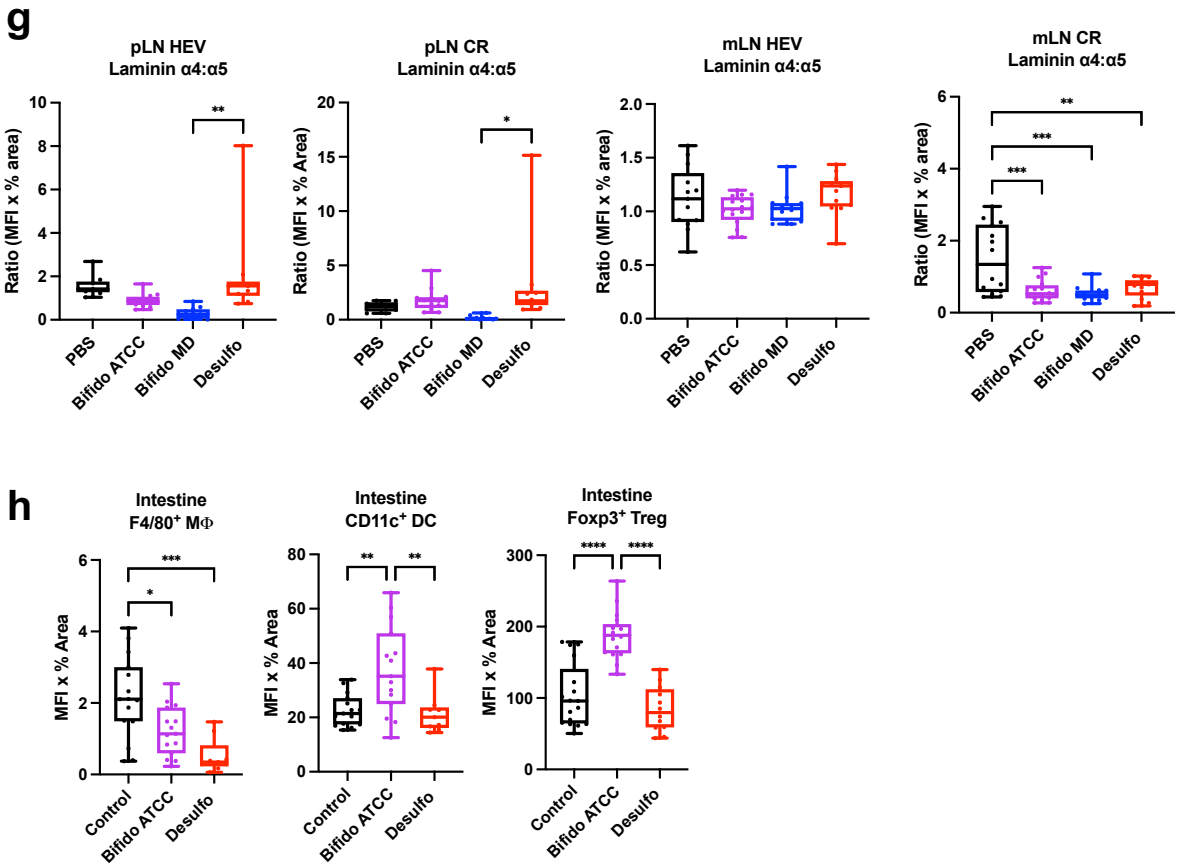

1334

Figure 1

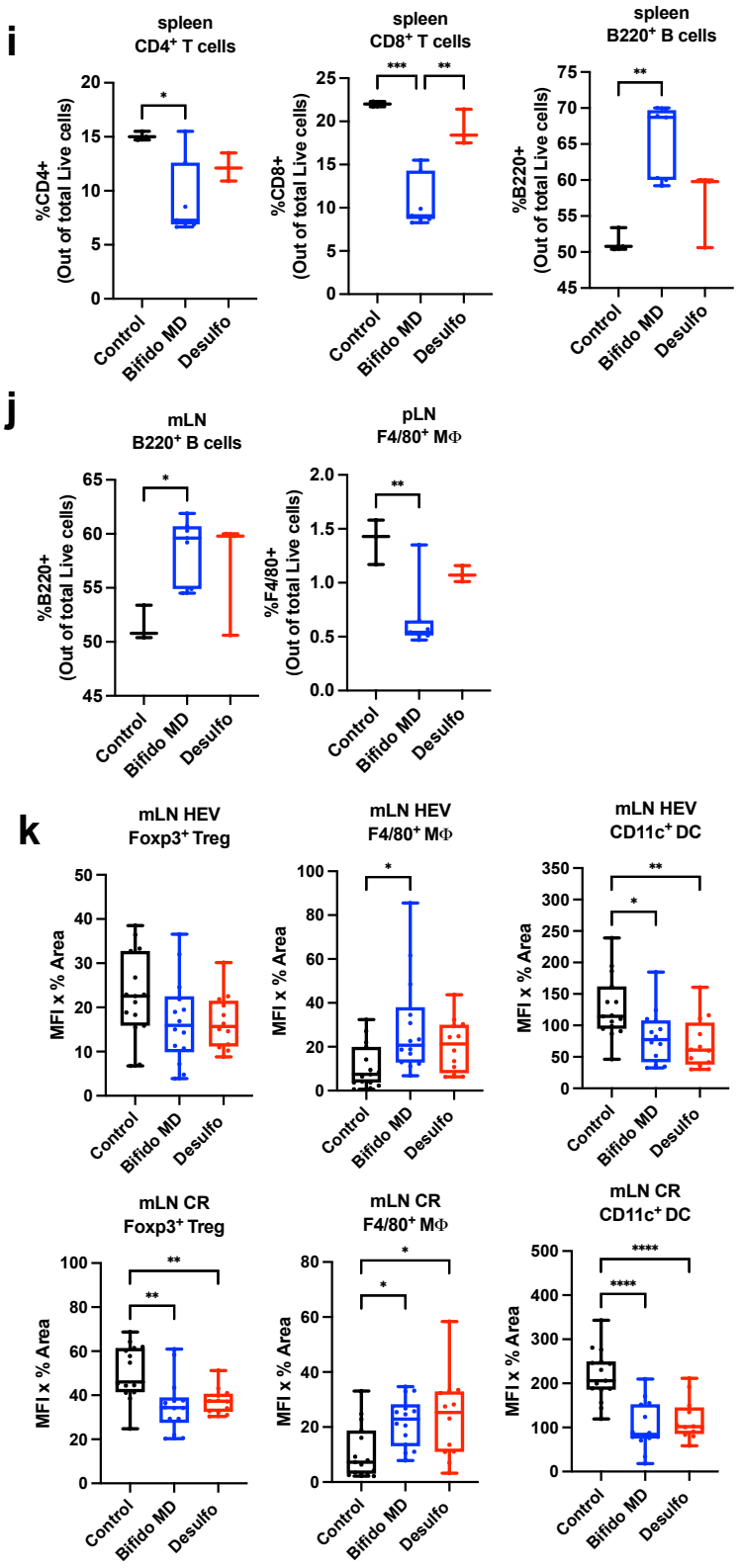

1335

Figure 1

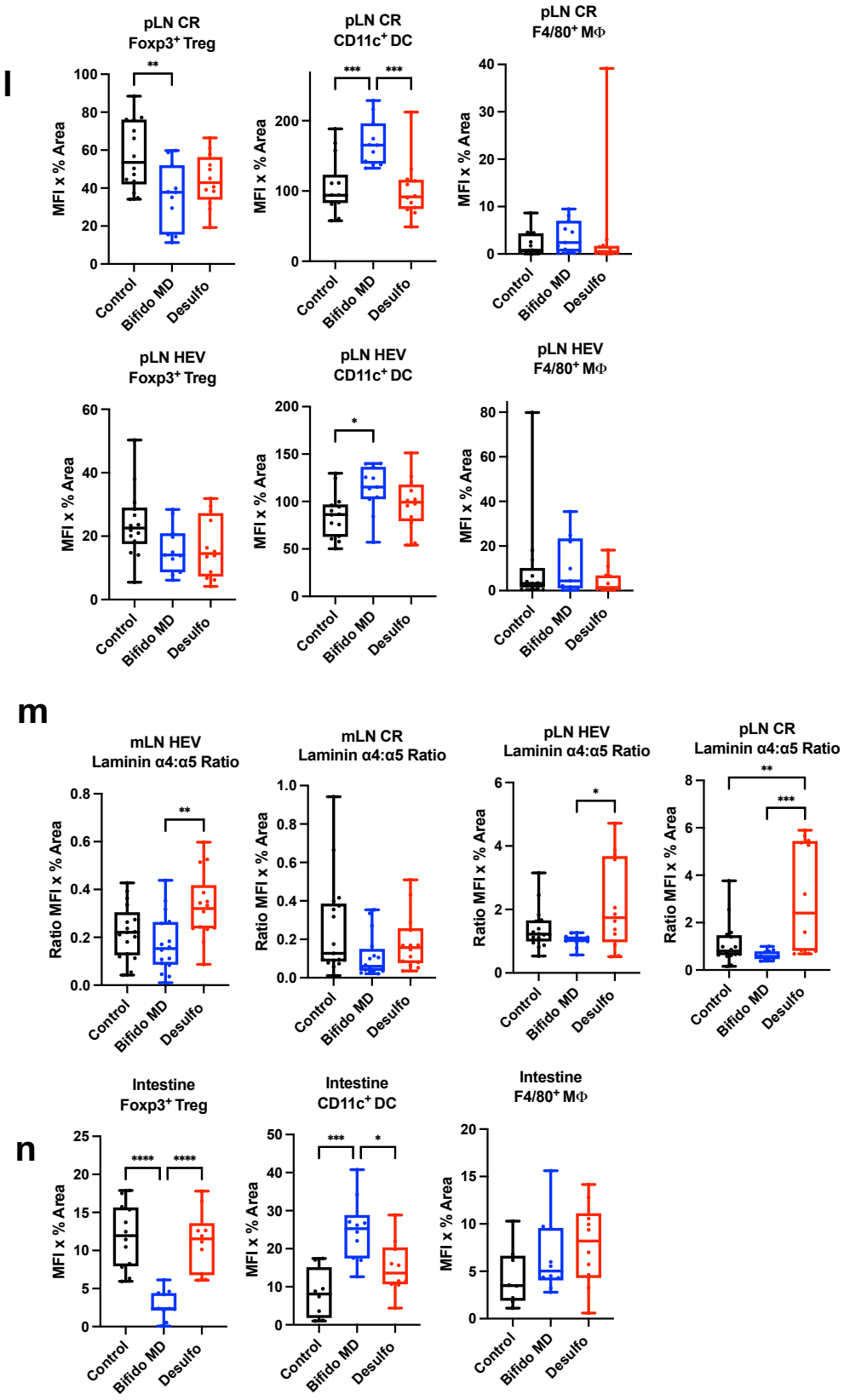

1336

Fig. 2

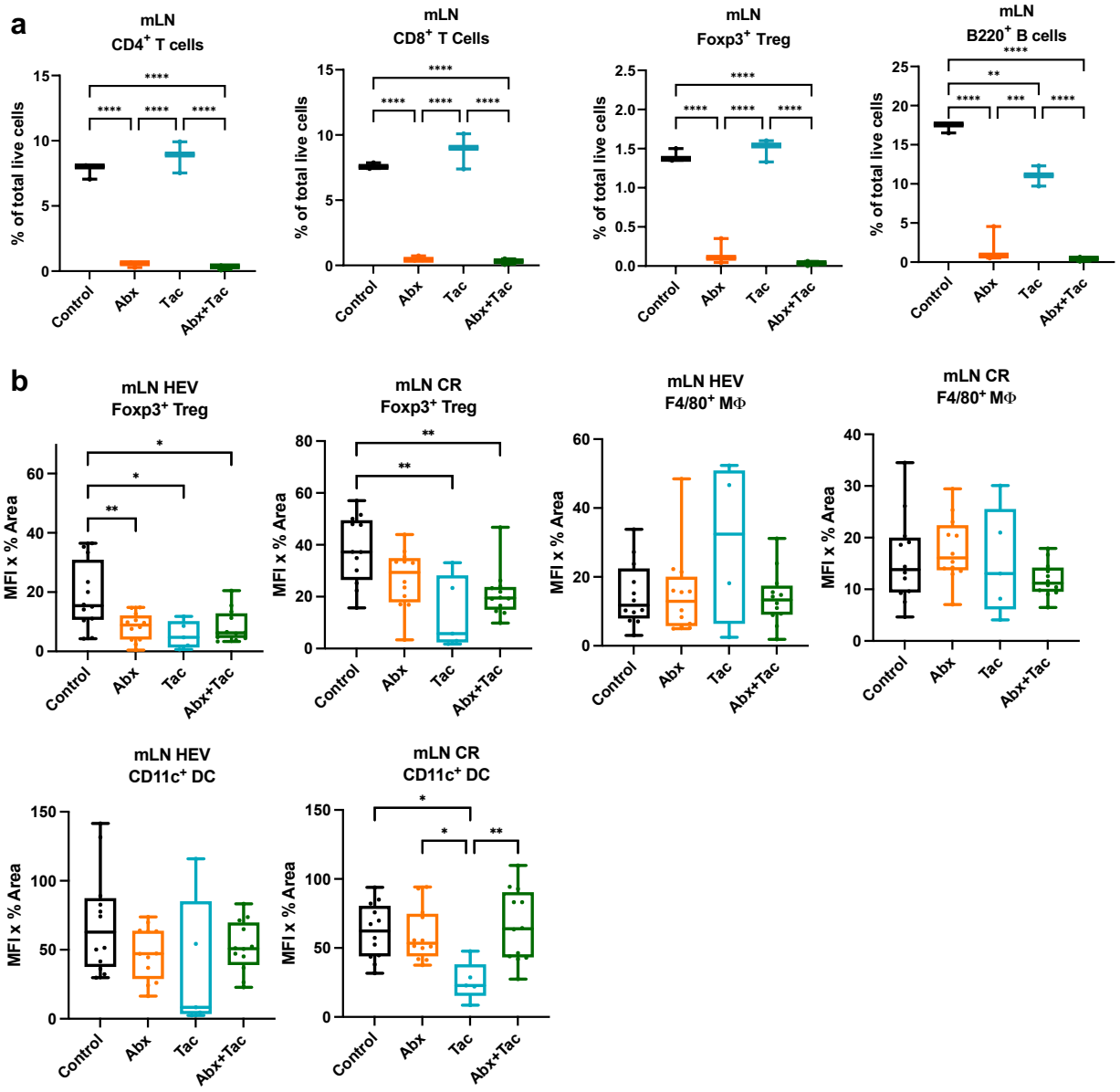
a
mLN
CD4+ T cells
mLN
CD8+ T Cells
mLN
Foxp3+ Treg
mLN
B220+ B cells
% of total live cells
Control
Abx
Tac
Abx+Tac
b
mLN HEV
Foxp3+ Treg
mLN CR
Foxp3+ Treg
mLN HEV
F4/80+ MΦ
mLN CR
F4/80+ MΦ
mLN HEV
CD11c+ DC
mLN CR
CD11c+ DC
MFI x % Area

1337

Fig. 2

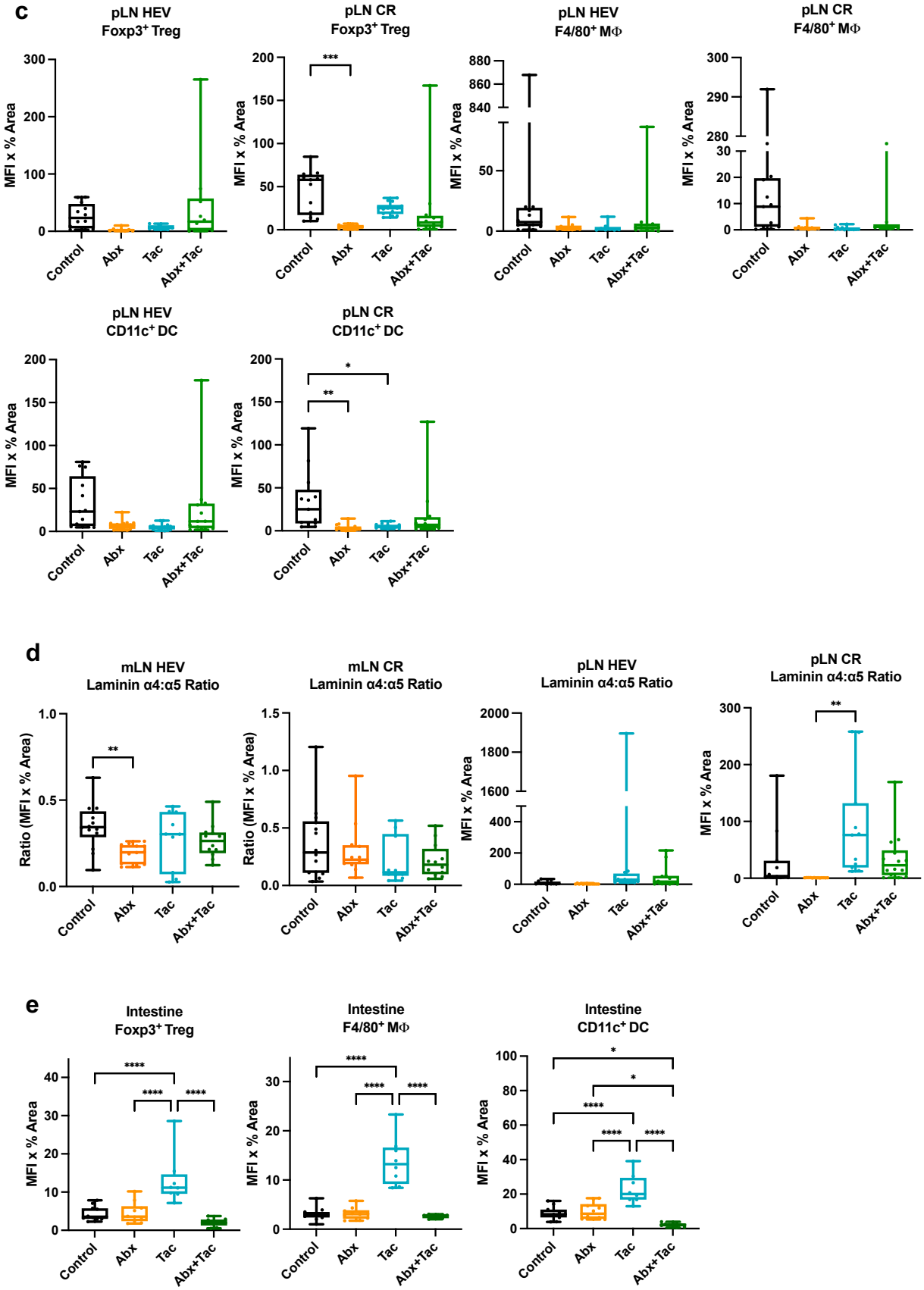
c
pLN HEV
Foxp3+ Treg
pLN CR
Foxp3+ Treg
pLN HEV
F4/80+ MΦ
pLN CR
F4/80+ MΦ
pLN HEV
CD11c+ DC
pLN CR
CD11c+ DC
MFI x % Area
Control
Abx
Tac
Abx+Tac
d
mLN HEV
Laminin α4:α5 Ratio
mLN CR
Laminin α4:α5 Ratio
pLN HEV
Laminin α4:α5 Ratio
pLN CR
Laminin α4:α5 Ratio
Ratio (MFI x % Area)
e
Intestine
Foxp3+ Treg
Intestine
F4/80+ MΦ
Intestine
CD11c+ DC

1338

Fig. 3

a

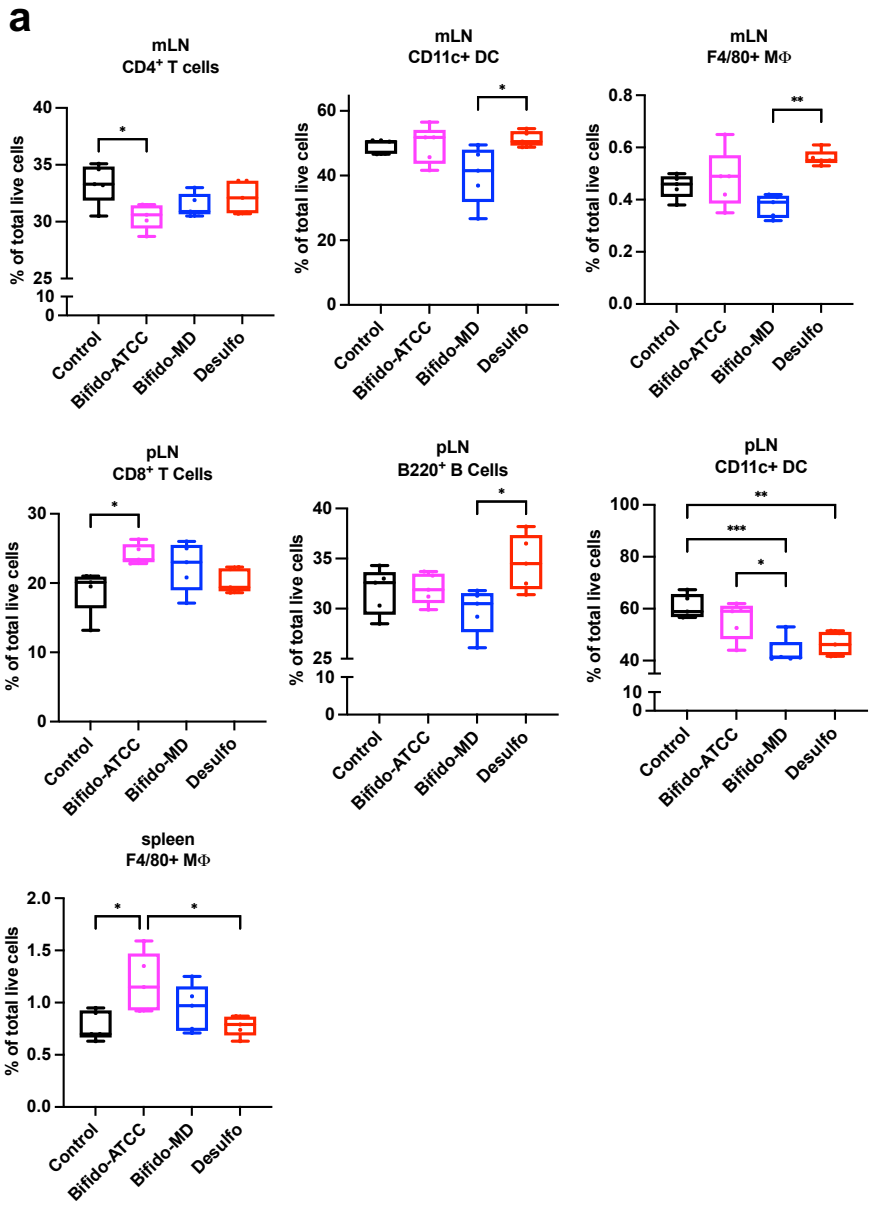
mLN
CD4+ T cells
mLN
CD11c+ DC
mLN
F4/80+ MΦ
pLN
CD8+ T Cells
pLN
B220+ B Cells
pLN
CD11c+ DC
spleen
F4/80+ MΦ
% of total live cells
Control
Bifido-ATCC
Bifido-MD
Desulfo

1339

Fig. 3

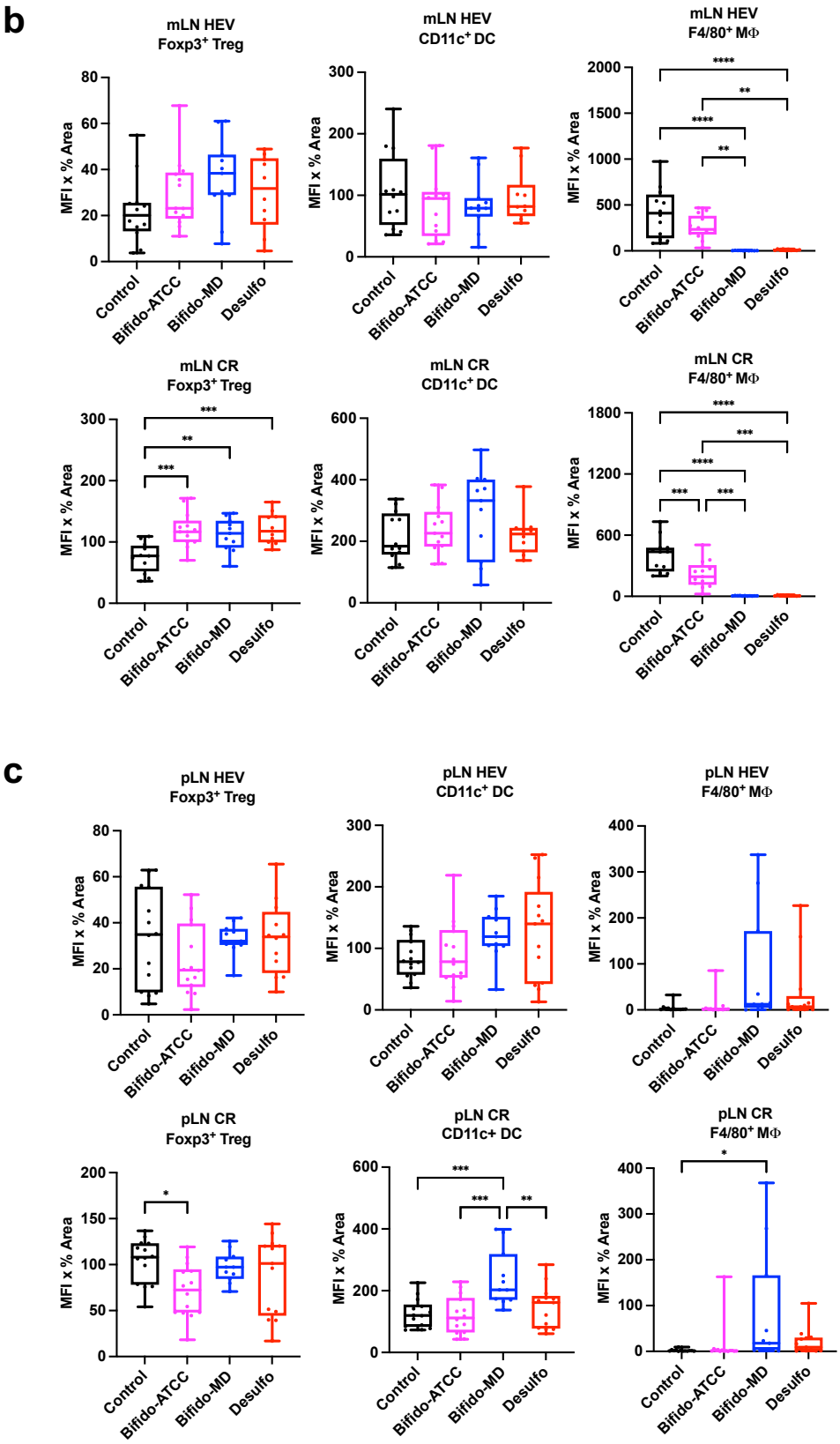
b
mLN HEV
Foxp3+ Treg
mLN HEV
CD11c+ DC
mLN HEV
F4/80+ MΦ
mLN CR
Foxp3+ Treg
mLN CR
CD11c+ DC
mLN CR
F4/80+ MΦ
c
pLN HEV
Foxp3+ Treg
pLN HEV
CD11c+ DC
pLN HEV
F4/80+ MΦ
pLN CR
Foxp3+ Treg
pLN CR
CD11c+ DC
pLN CR
F4/80+ MΦ
MFI x % Area
Control
Bifido-ATCC
Bifido-MD
Desulfo

1340

Fig. 3

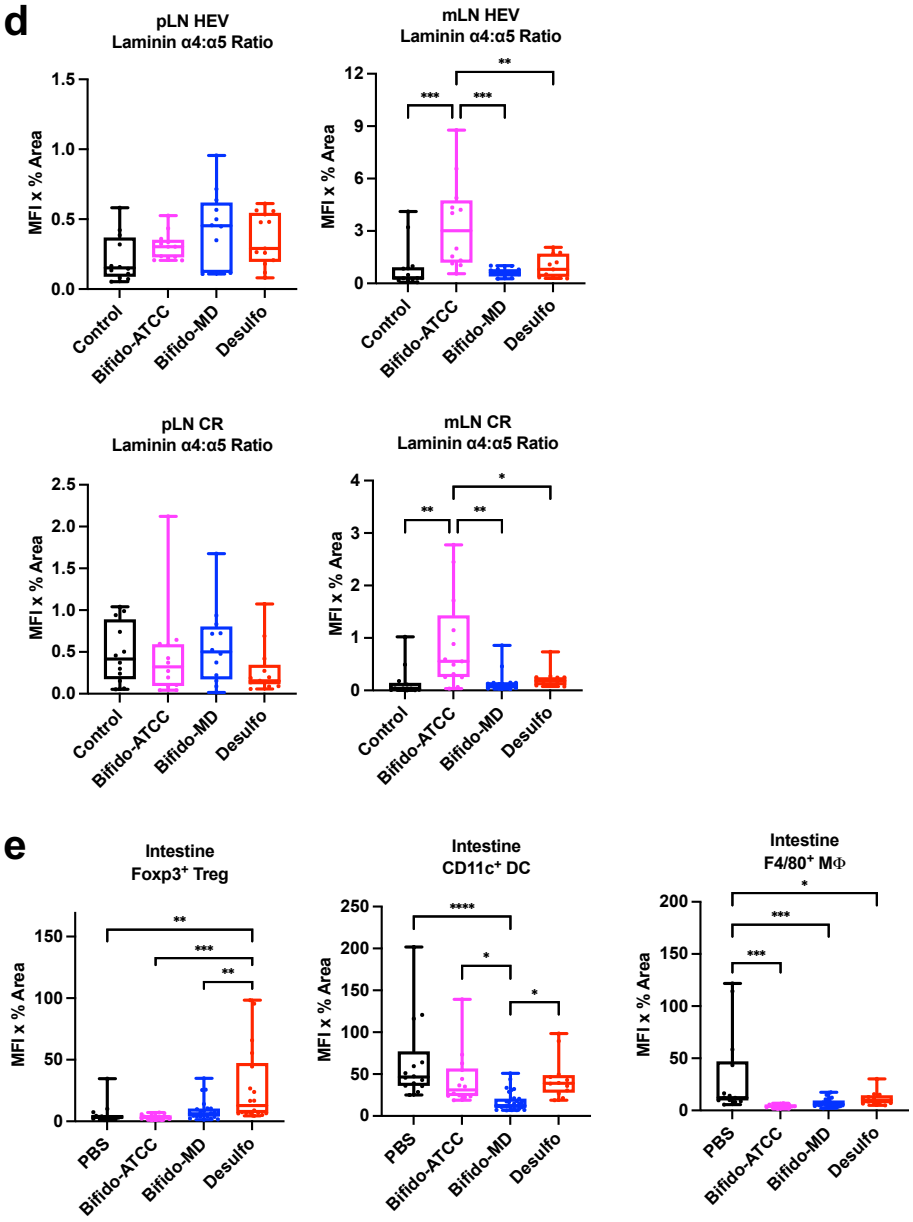
d
pLN HEV
Laminin α4:α5 Ratio
mLN HEV
Laminin α4:α5 Ratio
pLN CR
Laminin α4:α5 Ratio
mLN CR
Laminin α4:α5 Ratio
MFI x % Area
Control
Bifido-ATCC
Bifido-MD
Desulfo
e
Intestine
Foxp3+ Treg
Intestine
CD11c+ DC
Intestine
F4/80+ MΦ
PBS
Bifido-ATCC
Bifido-MD
Desulfo

1341

Fig. 4

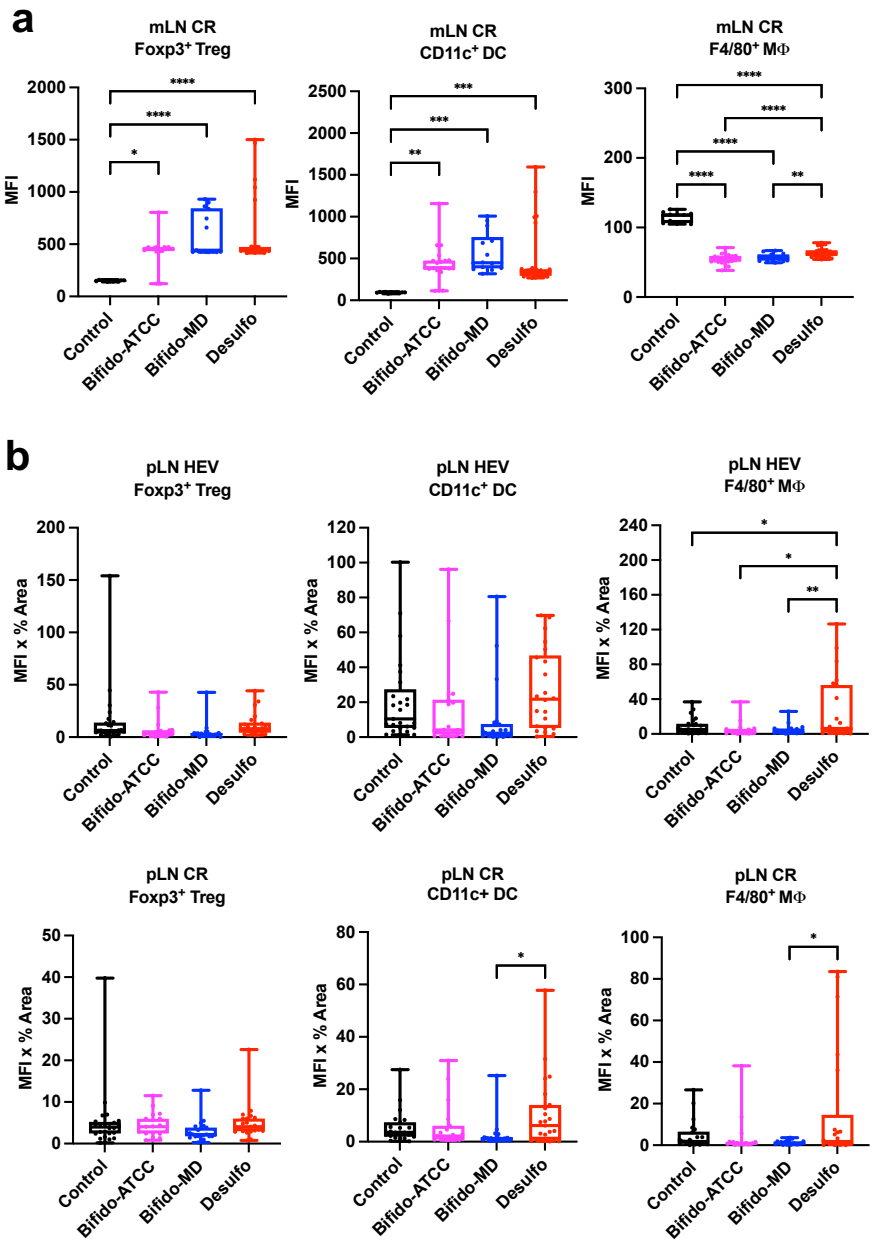
a
mLN CR
Foxp3+ Treg
MFI
2000
1500
1000
500
0
****
****
*
Control
Bifido-ATCC
Bifido-MD
Desulfo
mLN CR
CD11c+ DC
MFI
2500
2000
1500
1000
500
0
***
***
**
Control
Bifido-ATCC
Bifido-MD
Desulfo
mLN CR
F4/80+ MΦ
MFI
300
200
100
0
****
****
****
****
**
Control
Bifido-ATCC
Bifido-MD
Desulfo
b
pLN HEV
Foxp3+ Treg
MFI x % Area
200
150
100
50
0
Control
Bifido-ATCC
Bifido-MD
Desulfo
pLN HEV
CD11c+ DC
MFI x % Area
120
100
80
60
40
20
0
Control
Bifido-ATCC
Bifido-MD
Desulfo
pLN HEV
F4/80+ MΦ
MFI x % Area
240
200
160
120
80
40
0
*
*
**
Control
Bifido-ATCC
Bifido-MD
Desulfo
pLN CR
Foxp3+ Treg
MFI x % Area
50
40
30
20
10
0
Control
Bifido-ATCC
Bifido-MD
Desulfo
pLN CR
CD11c+ DC
MFI x % Area
80
60
40
20
0
*
Control
Bifido-ATCC
Bifido-MD
Desulfo
pLN CR
F4/80+ MΦ
MFI x % Area
100
80
60
40
20
0
*
Control
Bifido-ATCC
Bifido-MD
Desulfo

1342

Fig. 4

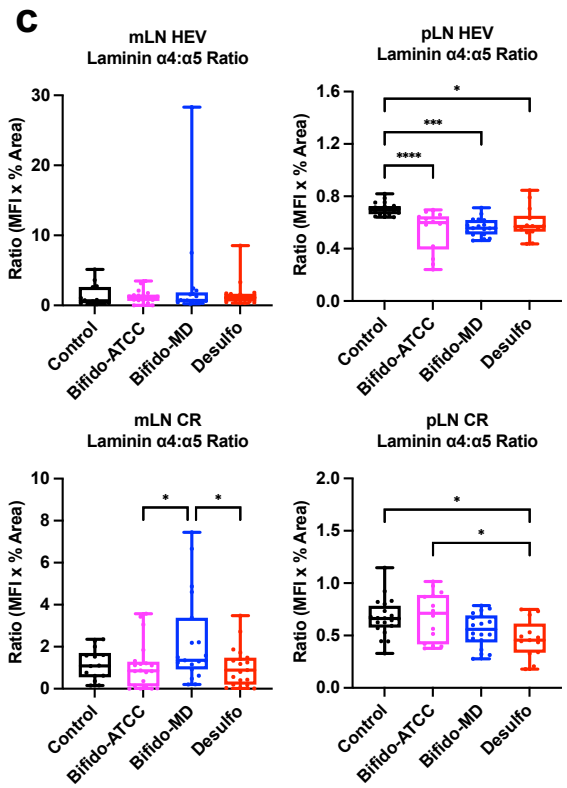
c
mLN HEV
Laminin α4:α5 Ratio
pLN HEV
Laminin α4:α5 Ratio
mLN CR
Laminin α4:α5 Ratio
pLN CR
Laminin α4:α5 Ratio
Ratio (MFI x % Area)
Control
Bifido-ATCC
Bifido-MD
Desulfo

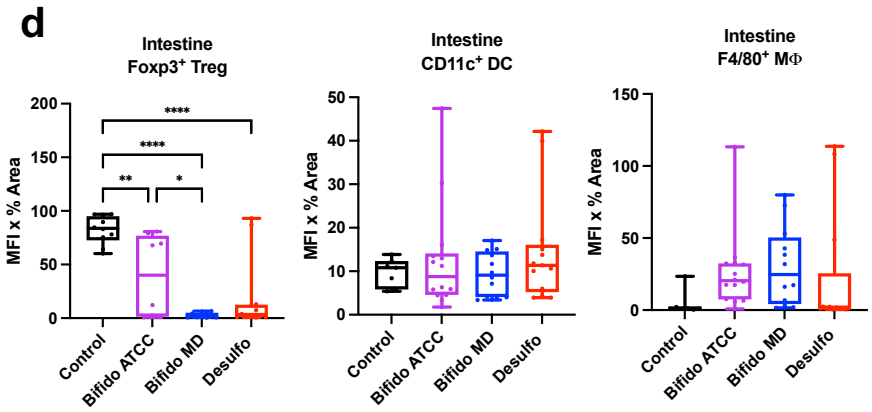
d
Intestine
Foxp3+ Treg
Intestine
CD11c+ DC
Intestine
F4/80+ MΦ
MFI x % Area
Control
Bifido ATCC
Bifido MD
Desulfo

1343

Fig. 5

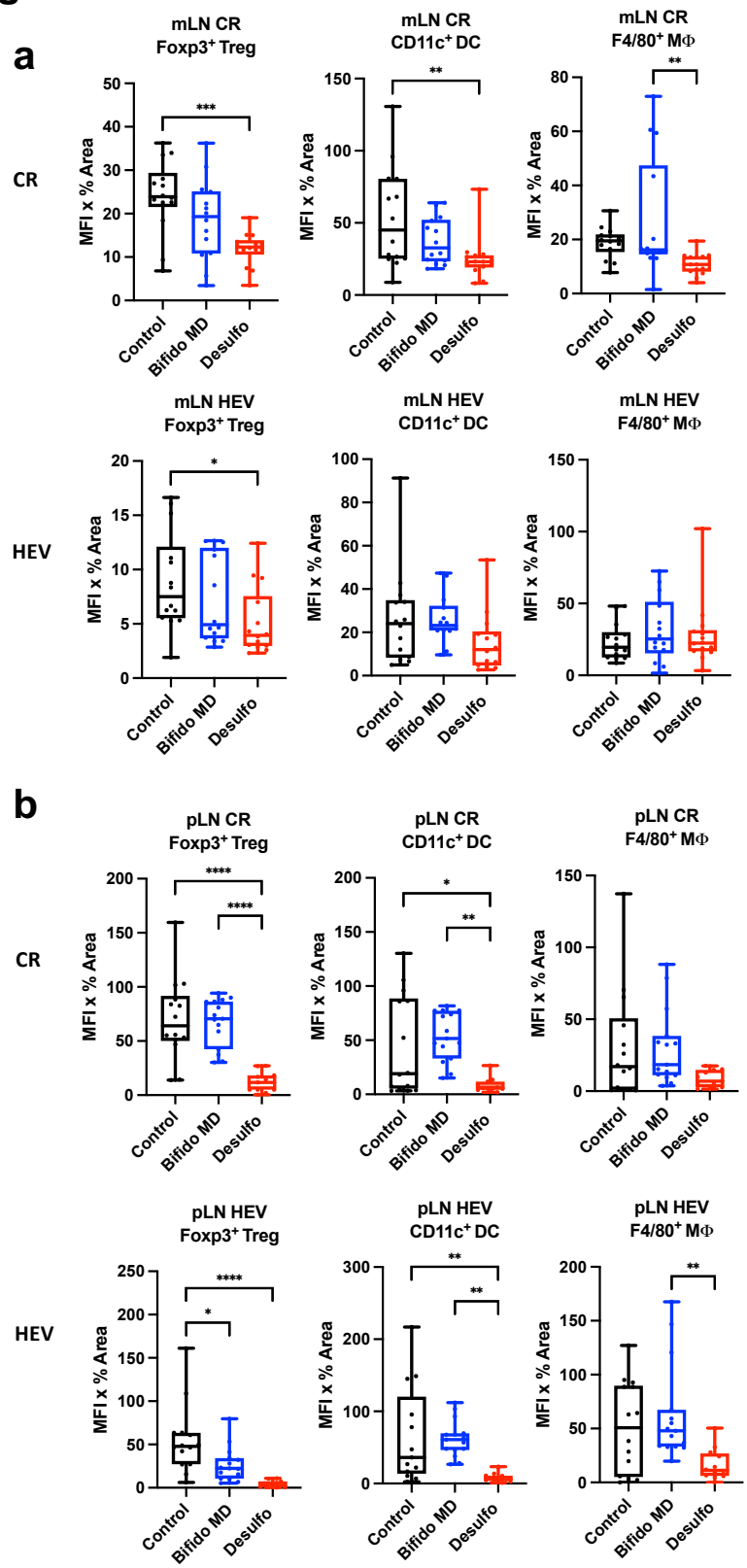
a
CR
HEV
mLN CR Foxp3+ Treg
mLN CR CD11c+ DC
mLN CR F4/80+ MΦ
mLN HEV Foxp3+ Treg
mLN HEV CD11c+ DC
mLN HEV F4/80+ MΦ
b
pLN CR Foxp3+ Treg
pLN CR CD11c+ DC
pLN CR F4/80+ MΦ
pLN HEV Foxp3+ Treg
pLN HEV CD11c+ DC
pLN HEV F4/80+ MΦ
MFI x % Area
Control
Bifido MD
Desulfo

1344

Fig. 5

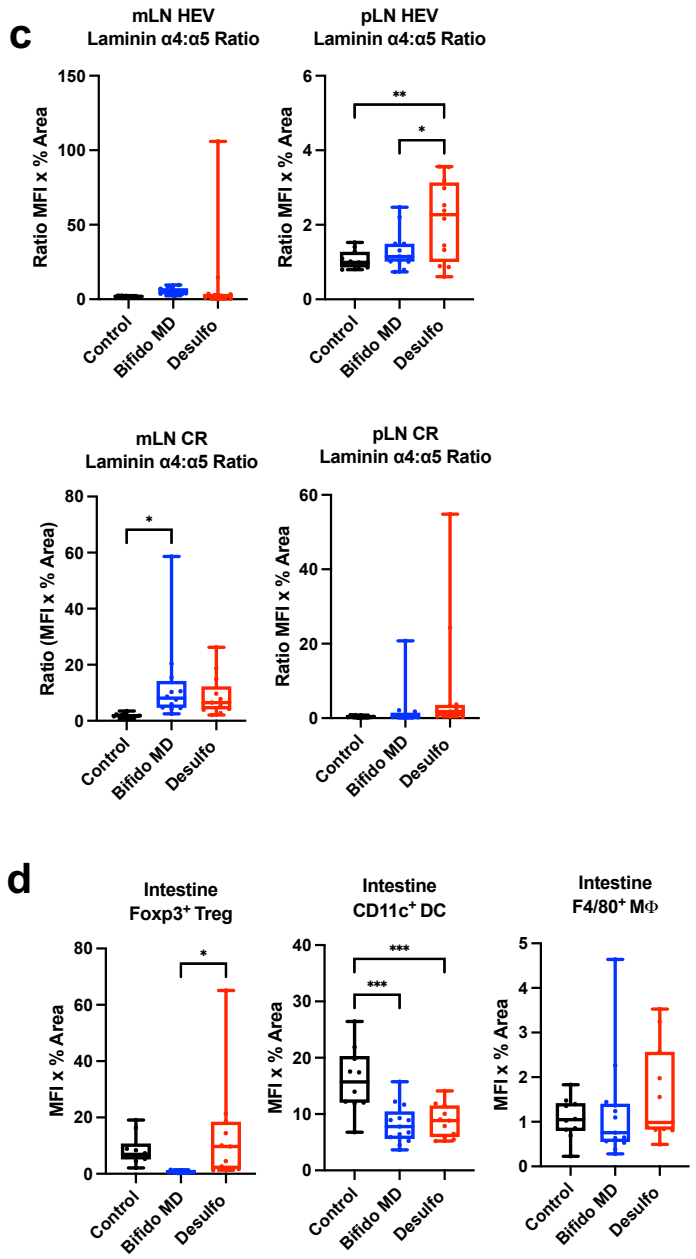
c
mLN HEV
Laminin α4:α5 Ratio
Ratio MFI x % Area
150
100
50
0
Control
Bifido MD
Desulfo
pLN HEV
Laminin α4:α5 Ratio
Ratio MFI x % Area
6
4
2
0
**
*
Control
Bifido MD
Desulfo
mLN CR
Laminin α4:α5 Ratio
Ratio (MFI x % Area)
80
60
40
20
0
*
Control
Bifido MD
Desulfo
pLN CR
Laminin α4:α5 Ratio
Ratio MFI x % Area
60
40
20
0
Control
Bifido MD
Desulfo
d
Intestine
Foxp3+ Treg
MFI x % Area
80
60
40
20
0
*
Control
Bifido MD
Desulfo
Intestine
CD11c+ DC
MFI x % Area
40
30
20
10
0
***
***
Control
Bifido MD
Desulfo
Intestine
F4/80+ MΦ
MFI x % Area
5
4
3
2
1
0
Control
Bifido MD
Desulfo

1345

Fig. 5

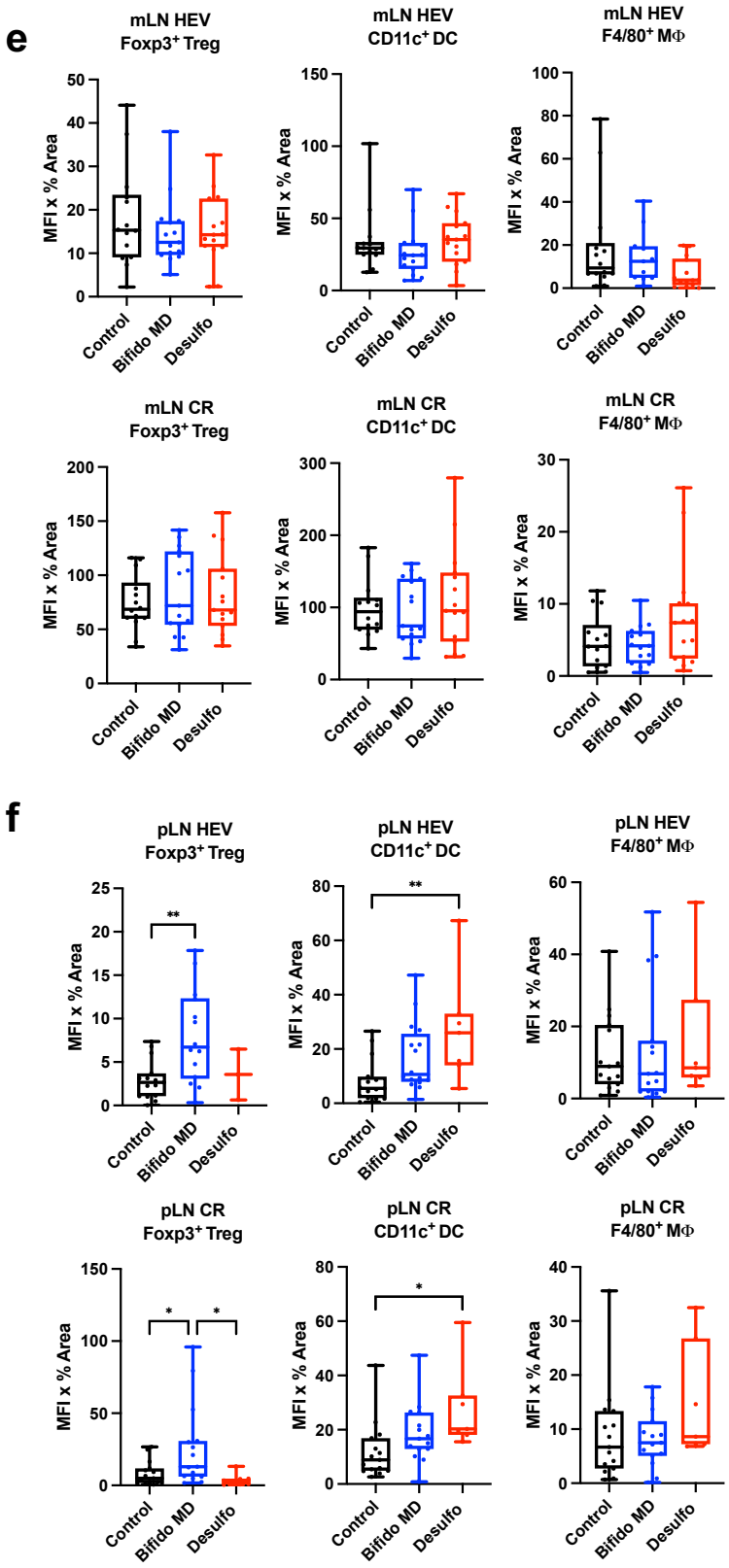
e
mLN HEV
Foxp3+ Treg
mLN HEV
CD11c+ DC
mLN HEV
F4/80+ MΦ
mLN CR
Foxp3+ Treg
mLN CR
CD11c+ DC
mLN CR
F4/80+ MΦ
f
pLN HEV
Foxp3+ Treg
pLN HEV
CD11c+ DC
pLN HEV
F4/80+ MΦ
pLN CR
Foxp3+ Treg
pLN CR
CD11c+ DC
pLN CR
F4/80+ MΦ
MFI x % Area
Control
Bifido MD
Desulfo
**
*

1346

Fig. 5

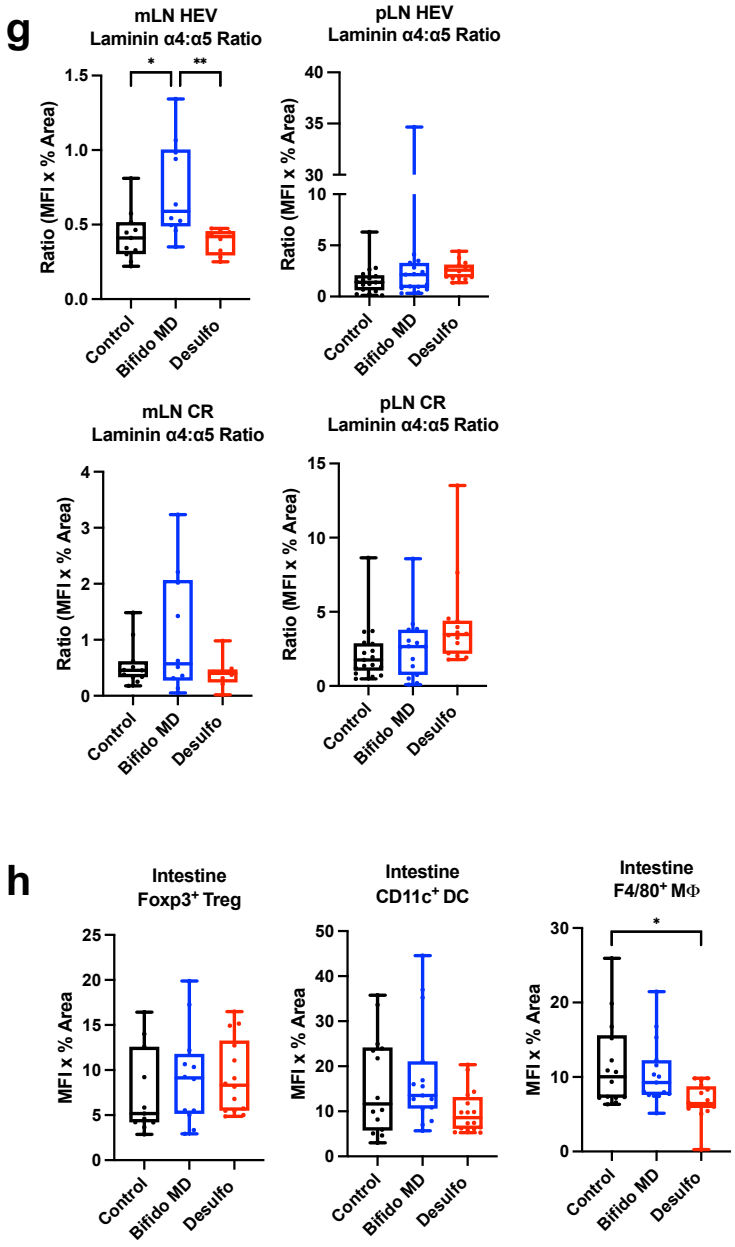
g
mLN HEV
Laminin α4:α5 Ratio
pLN HEV
Laminin α4:α5 Ratio
mLN CR
Laminin α4:α5 Ratio
pLN CR
Laminin α4:α5 Ratio
Ratio (MFI x % Area)
Control
Bifido MD
Desulfo
h
Intestine
Foxp3+ Treg
Intestine
CD11c+ DC
Intestine
F4/80+ MΦ
MFI x % Area

1347

Fig. 6

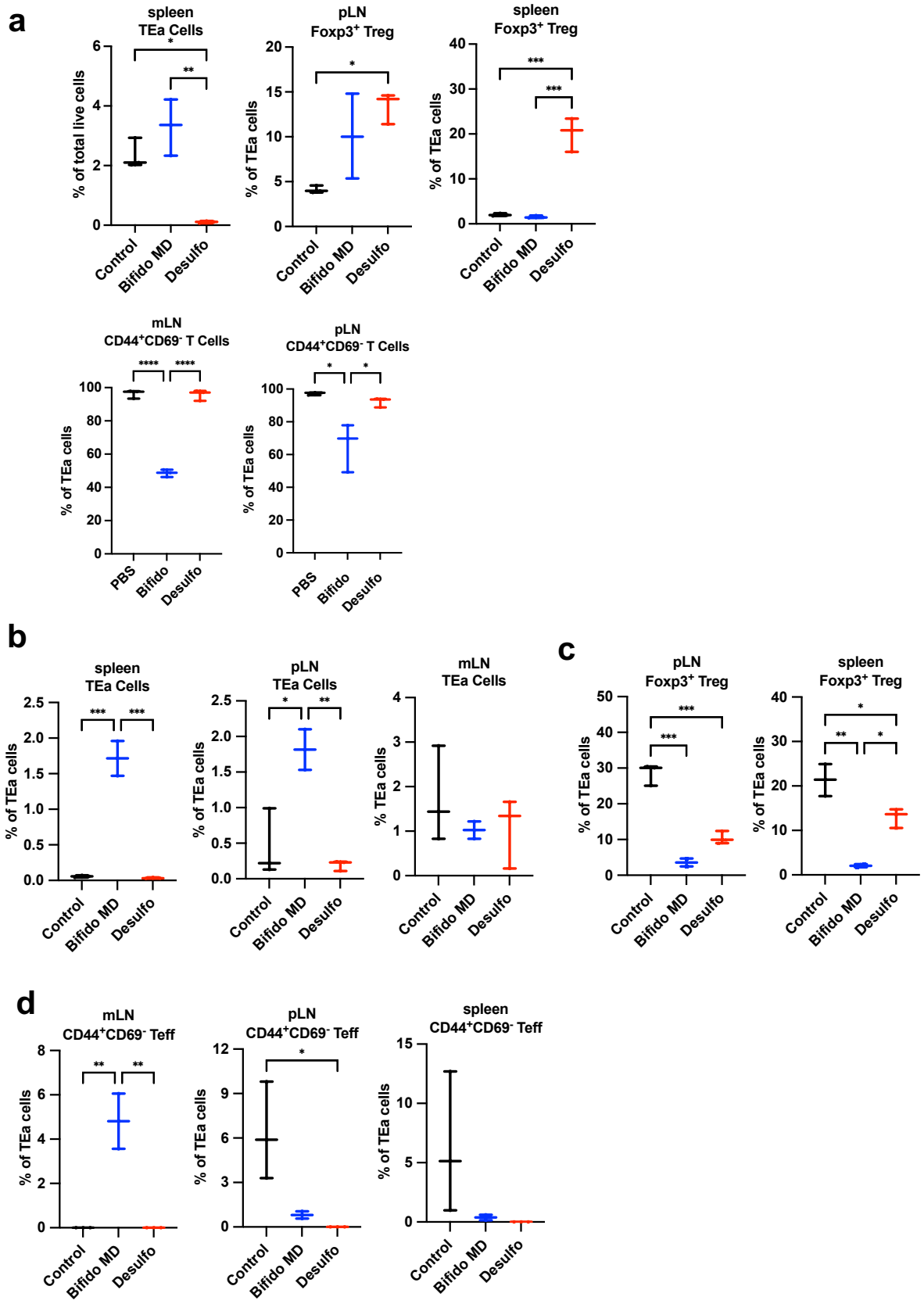
a
spleen
TEa Cells
% of total live cells
pLN
Foxp3+ Treg
% of TEa cells
spleen
Foxp3+ Treg
% of TEa cells
mLN
CD44+CD69- T Cells
% of TEa cells
pLN
CD44+CD69- T Cells
% of TEa cells
Control
Bifido MD
Desulfo
PBS
Bifido
b
spleen
TEa Cells
% of TEa cells
pLN
TEa Cells
% of TEa cells
mLN
TEa Cells
% TEa cells
c
pLN
Foxp3+ Treg
% of TEa cells
spleen
Foxp3+ Treg
% of TEa cells
d
mLN
CD44+CD69- Teff
% of TEa cells
pLN
CD44+CD69- Teff
% of TEa cells
spleen
CD44+CD69- Teff
% of TEa cells

1348

Fig. 6

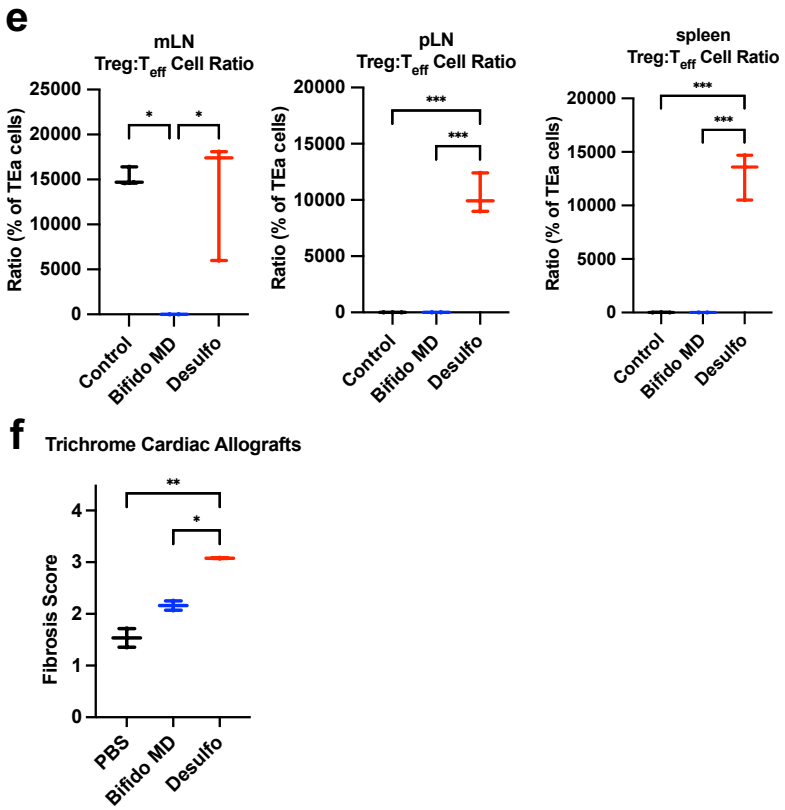
e
mLN
Treg:Teff Cell Ratio
Ratio (% of TEa cells)
25000
20000
15000
10000
5000
0
*
*
Control
Bifido MD
Desulfo
pLN
Treg:Teff Cell Ratio
Ratio (% of TEa cells)
20000
15000
10000
5000
0
***
***
Control
Bifido MD
Desulfo
spleen
Treg:Teff Cell Ratio
Ratio (% of TEa cells)
20000
15000
10000
5000
0
***
***
Control
Bifido MD
Desulfo
f
Trichrome Cardiac Allografts
Fibrosis Score
4
3
2
1
0
**
*
PBS
Bifido MD
Desulfo

1349

Fig. 7

a

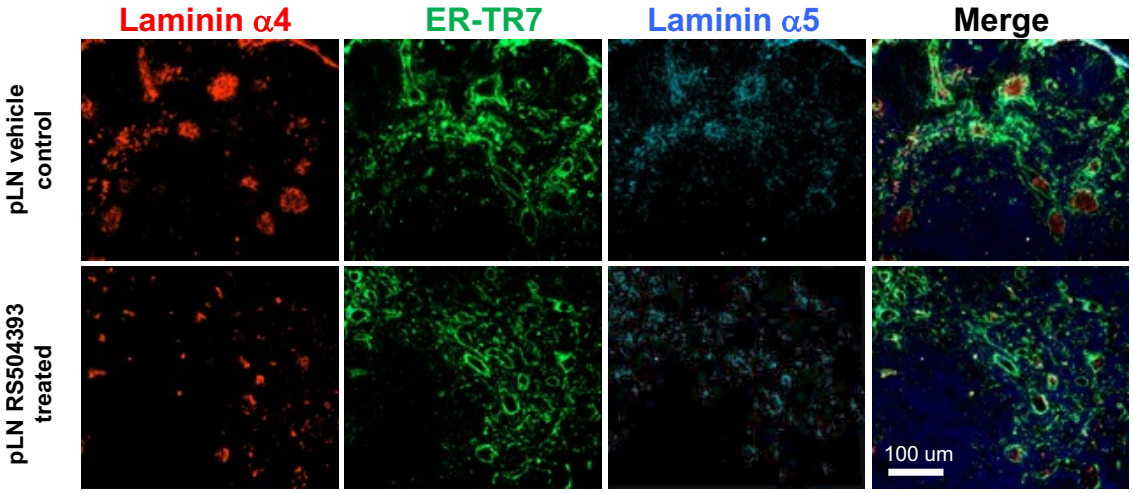
Laminin α4
ER-TR7
Laminin α5
Merge
pLN vehicle control
pLN RS504393 treated
100 um

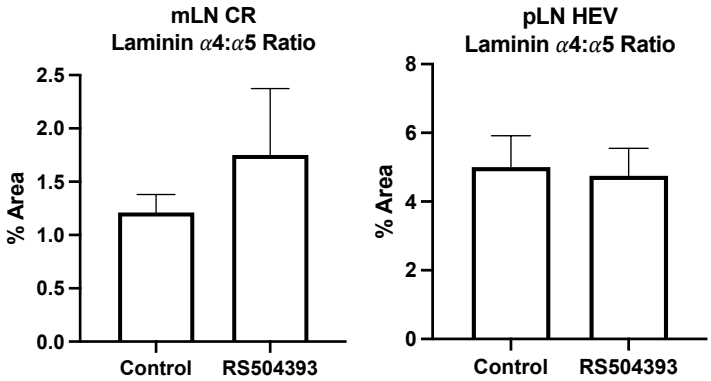
mLN CR
Laminin α4:α5 Ratio
% Area
2.5
2.0
1.5
1.0
0.5
0.0
Control
RS504393
pLN HEV
Laminin α4:α5 Ratio
% Area
8
6
4
2
0
Control
RS504393

b

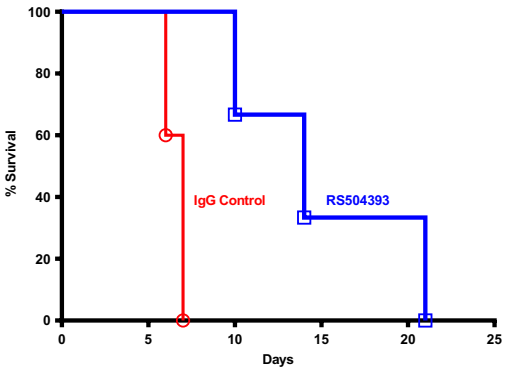
% Survival
100
80
60
40
20
0
IgG Control
RS504393
0
5
10
15
20
25
Days

1350

Fig. 8

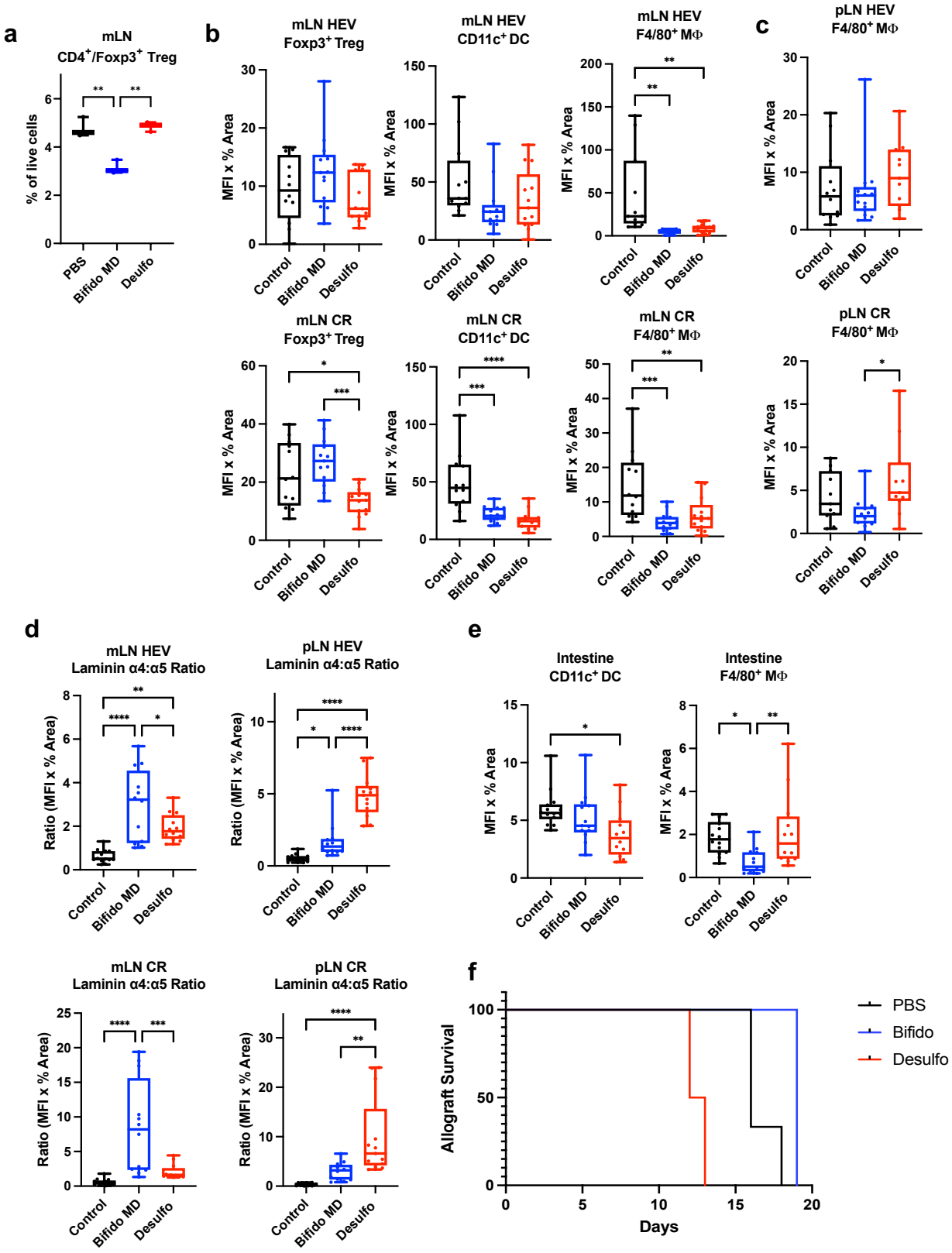
a
mLN
CD4+/Foxp3+ Treg
% of live cells
PBS
Bifido MD
Deulfo
b
mLN HEV
Foxp3+ Treg
mLN HEV
CD11c+ DC
mLN HEV
F4/80+ MΦ
c
pLN HEV
F4/80+ MΦ
mLN CR
Foxp3+ Treg
mLN CR
CD11c+ DC
mLN CR
F4/80+ MΦ
pLN CR
F4/80+ MΦ
MFI x % Area
Control
Bifido MD
Desulfo
d
mLN HEV
Laminin α4:α5 Ratio
pLN HEV
Laminin α4:α5 Ratio
mLN CR
Laminin α4:α5 Ratio
pLN CR
Laminin α4:α5 Ratio
Ratio (MFI x % Area)
e
Intestine
CD11c+ DC
Intestine
F4/80+ MΦ
f
Allograft Survival
Days
PBS
Bifido
Desulfo

1351

Fig. 9

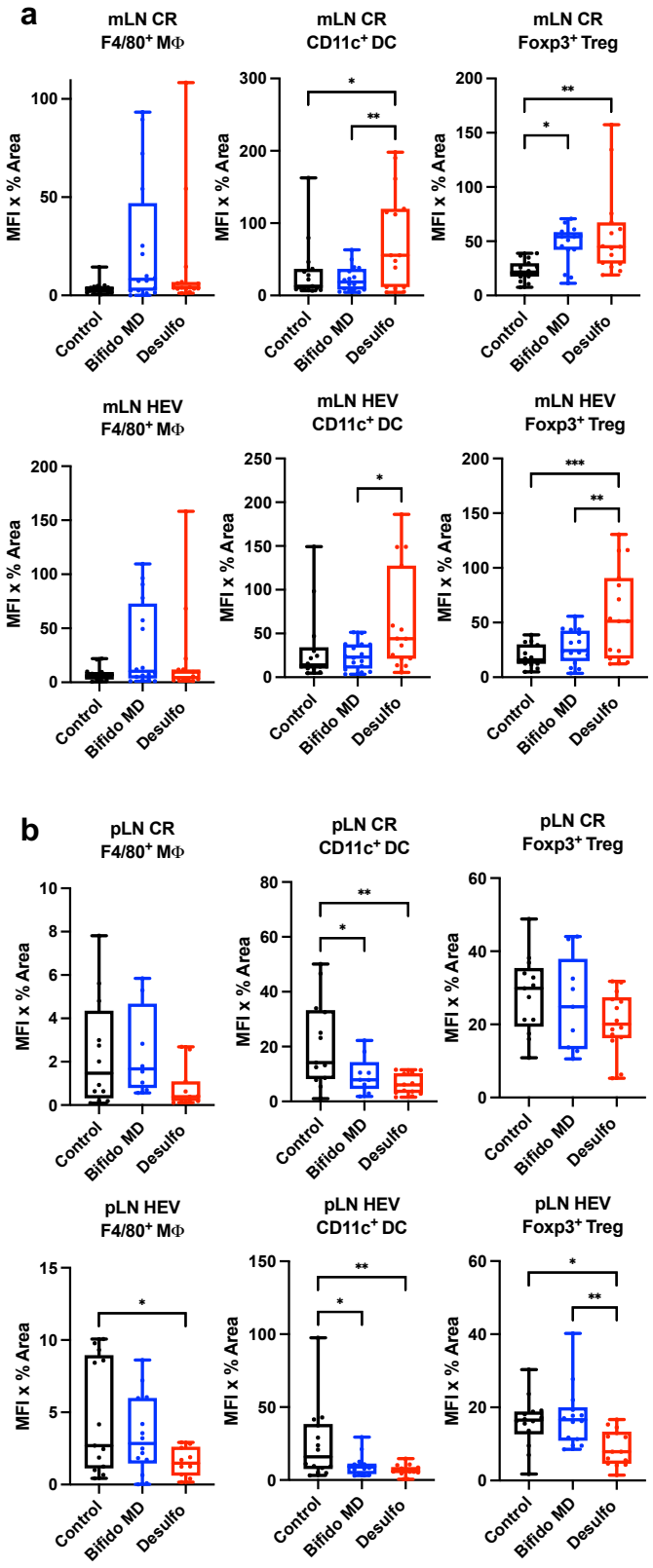
a
mLN CR
F4/80+ MΦ
mLN CR
CD11c+ DC
mLN CR
Foxp3+ Treg
mLN HEV
F4/80+ MΦ
mLN HEV
CD11c+ DC
mLN HEV
Foxp3+ Treg
b
pLN CR
F4/80+ MΦ
pLN CR
CD11c+ DC
pLN CR
Foxp3+ Treg
pLN HEV
F4/80+ MΦ
pLN HEV
CD11c+ DC
pLN HEV
Foxp3+ Treg
MFI x % Area
Control
Bifido MD
Desulfo

1352

Fig. 9

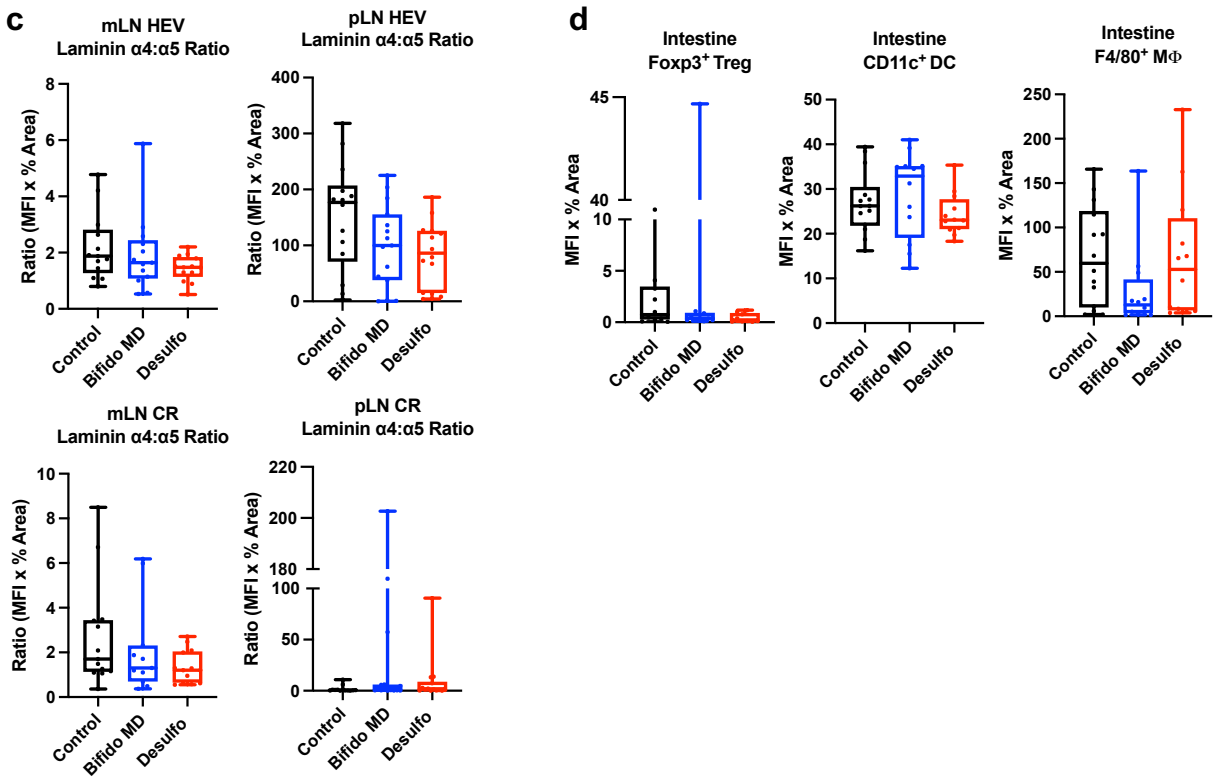
c
mLN HEV
Laminin α4:α5 Ratio
Ratio (MFI x % Area)
pLN HEV
Laminin α4:α5 Ratio
Ratio (MFI x % Area)
mLN CR
Laminin α4:α5 Ratio
Ratio (MFI x % Area)
pLN CR
Laminin α4:α5 Ratio
Ratio (MFI x % Area)
Control
Bifido MD
Desulfo
d
Intestine
Foxp3+ Treg
Intestine
CD11c+ DC
Intestine
F4/80+ MΦ
MFI x % Area
Control
Bifido MD
Desulfo

1353

Fig. 10

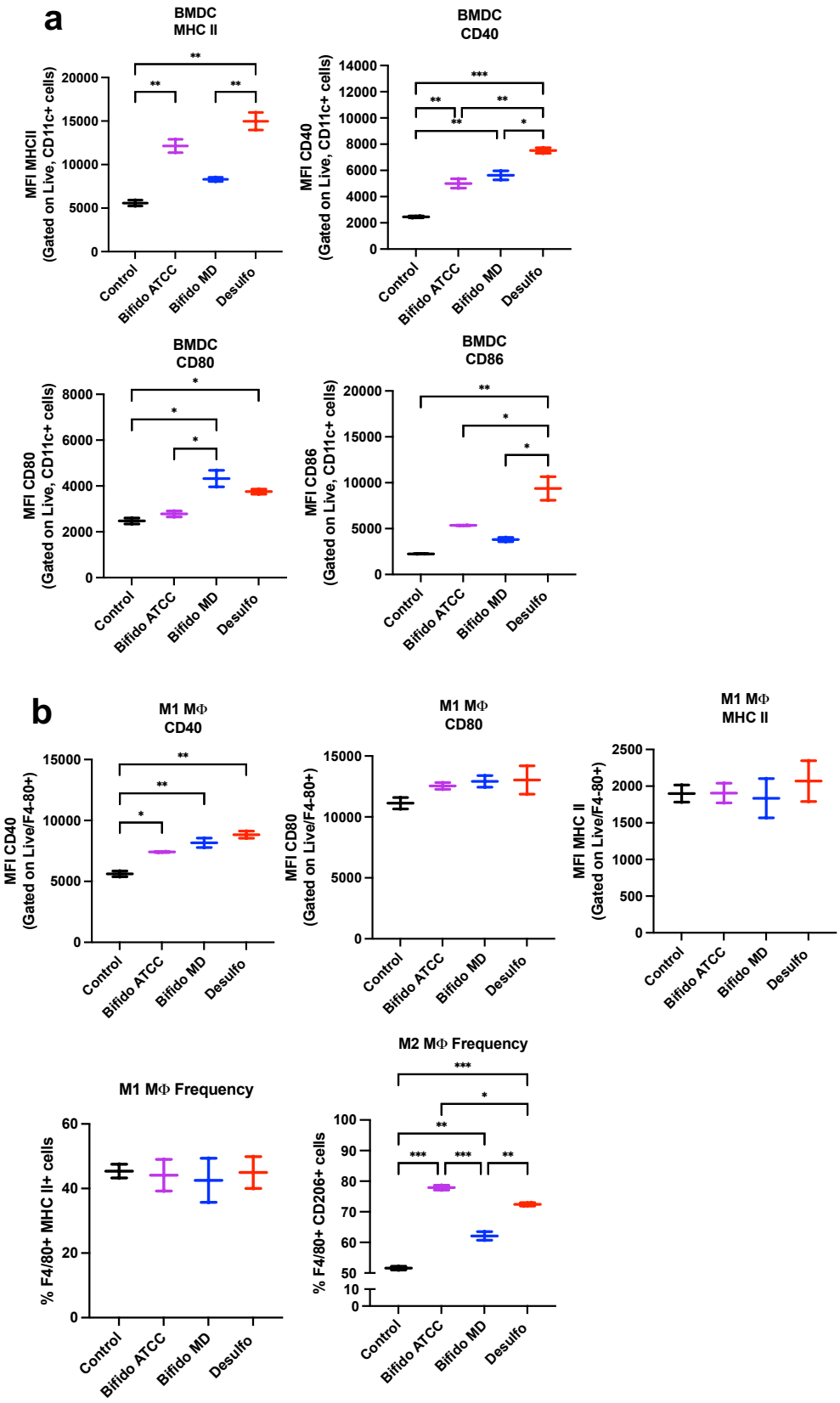
a
BMDC
MHC II
MFI MHCII
(Gated on Live, CD11c+ cells)
BMDC
CD40
MFI CD40
(Gated on Live, CD11c+ cells)
BMDC
CD80
MFI CD80
(Gated on Live, CD11c+ cells)
BMDC
CD86
MFI CD86
(Gated on Live, CD11c+ cells)
Control
Bifido ATCC
Bifido MD
Desulfo
b
M1 MΦ
CD40
MFI CD40
(Gated on Live/F4-80+)
M1 MΦ
CD80
MFI CD80
(Gated on Live/F4-80+)
M1 MΦ
MHC II
MFI MHC II
(Gated on Live/F4-80+)
M1 MΦ Frequency
% F4/80+ MHC II+ cells
M2 MΦ Frequency
% F4/80+ CD206+ cells

1354

Fig. 10

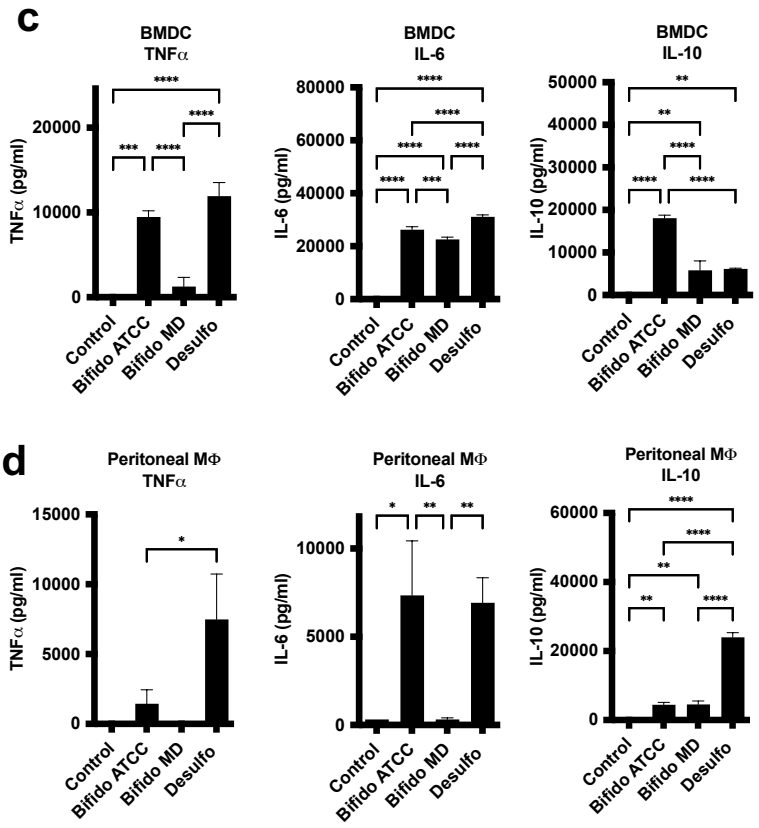
c
BMDC
TNFα
TNFα (pg/ml)
BMDC
IL-6
IL-6 (pg/ml)
BMDC
IL-10
IL-10 (pg/ml)
Control
Bifido ATCC
Bifido MD
Desulfo
d
Peritoneal MΦ
TNFα
TNFα (pg/ml)
Peritoneal MΦ
IL-6
IL-6 (pg/ml)
Peritoneal MΦ
IL-10
IL-10 (pg/ml)

1355

Fig. 11

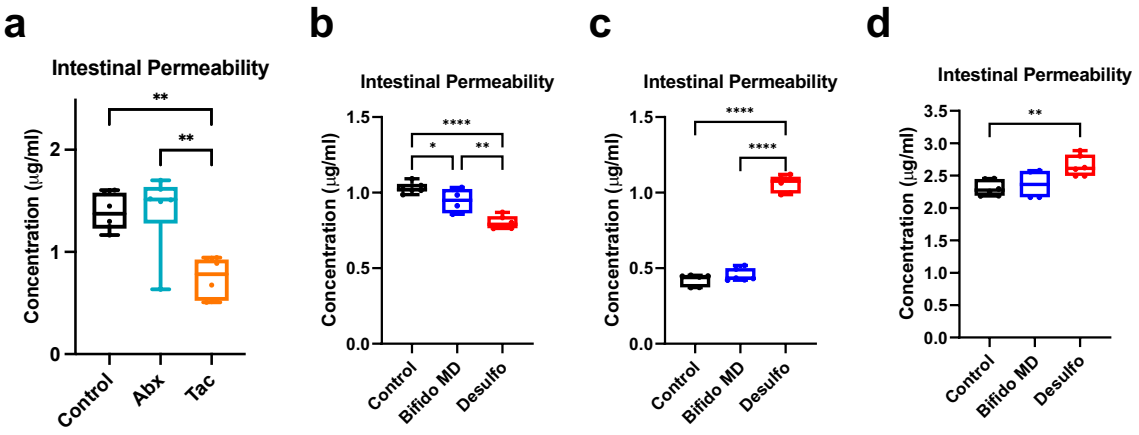
a
Intestinal Permeability
Concentration (μg/ml)
0
1
2
**
**
Control
Abx
Tac
b
Intestinal Permeability
Concentration (μg/ml)
0.0
0.5
1.0
1.5
****
*
**
Control
Bifido MD
Desulfo
c
Intestinal Permeability
Concentration (μg/ml)
0.0
0.5
1.0
1.5
****
****
Control
Bifido MD
Desulfo
d
Intestinal Permeability
Concentration (μg/ml)
0.0
0.5
1.0
1.5
2.0
2.5
3.0
3.5
**
Control
Bifido MD
Desulfo

1356

Fig. 12

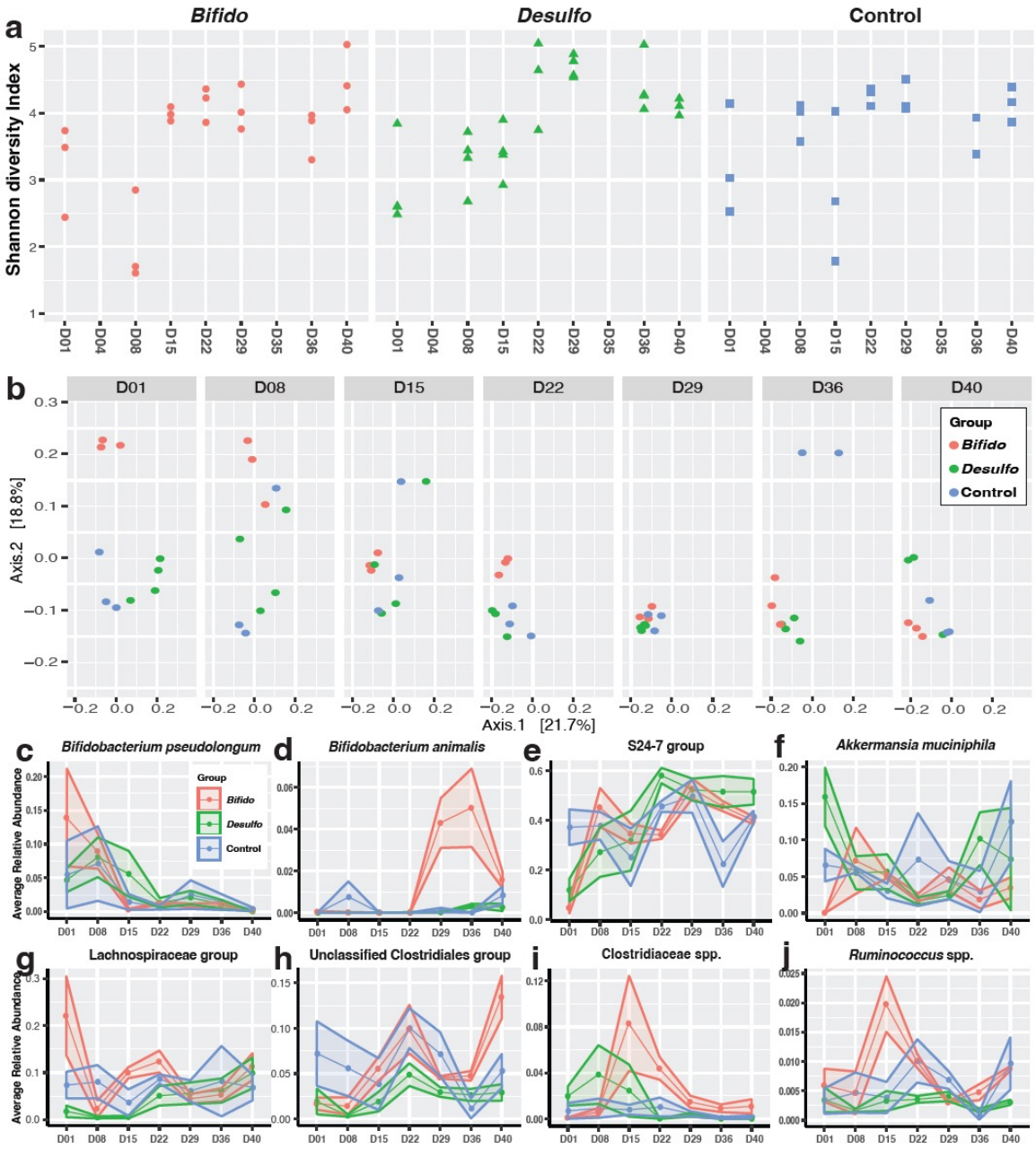
a
Bifido
Desulfo
Control
Shannon diversity Index
D01
D04
D08
D15
D22
D29
D35
D36
D40
b
D01
D08
D15
D22
D29
D36
D40
Group
Bifido
Desulfo
Control
Axis.2 [18.8%]
Axis.1 [21.7%]
c
Bifidobacterium pseudolongum
d
Bifidobacterium animalis
e
S24-7 group
f
Akkermansia muciniphila
g
Lachnospiraceae group
h
Unclassified Clostridiales group
i
Clostridiaceae spp.
j
Ruminococcus spp.
Average Relative Abundance